

POTENTIAL ENERGY SURFACES OF SMALL MOLECULES AND CATIONS:
INSIGHTS FROM COUPLED CLUSTER THEORY

by

LUCAS DANIEL SPEAKMAN

(Under the Direction of Henry F. Schaefer III)

ABSTRACT

Precise thermochemical properties of benzaldehyde, gallium pentahydride, boron pentahydride, aluminum pentahydride, ozone, and silicon dicarbide have been determined through systematic extrapolations of *ab initio* energies within the Coupled Cluster framework of higher order excitation corrections. The discrepancy between experiment and theory regarding benzaldehyde's internal barrier to rotation has been resolved, with a recommended barrier of 7.7 kcal mol⁻¹. Gallium pentahydride may exist at low temperatures, as a weak complex between gallane and molecular hydrogen, with a D_0 of 0.11 kcal mol⁻¹. The deprotonation energies of group thirteen pentahydrides follow an unusual pattern: 326.3 (AlH₅), 331.0 (GaH₅), and 332.4 (BH₅) kcal mol⁻¹. The gap in observed properties usually falls between boron and aluminum, with gallium's properties often very similar to those of aluminum. Several ionization and excitation pathways to the quartet state of ozone radical cation were investigated to aid in synthesis. From the ground state of ozone, vertical ionizations to $^4A_2 O_3^+$, $^4B_2 O_3^+$, and $^4A_1 O_3^+$ are possible at 13.91, 14.39, and 14.90 eV, respectively. Other possible pathways to the quartet states are $^4A_1 O_3^+ \leftarrow ^3A_2 O_3$, $^4A_2 O_3^+ \leftarrow ^3A_2 O_3$, $^4A_1 O_3^+ \leftarrow ^3B_2 O_3$, $^4A_2 O_3^+ \leftarrow ^3B_1 O_3$, $^4B_2 O_3^+ \leftarrow ^3B_1 O_3$, $^4A_1 O_3^+ \leftarrow ^2B_2 O_3^+$, and $^4A_2 O_3^+ \leftarrow ^2B_2 O_3^+$ with vertical IPs of 12.46, 12.85, 12.82,

12.46, 12.65, 1.36, and 1.26 eV, respectively. One of the most accurate potential energy surfaces in literature was developed for SiC₂ by implementing a composite method, *c*-CBS CCSDT. This method includes extrapolation to the complete basis set limit, CCSD(T), with additional CCSDT, relativistic, and core-valence corrections. It yields a barrier to linearity for SiC₂ of 5.45 ± 0.1 kcal mol⁻¹, fundamental vibrational frequencies for the “T-shaped” ground state of 1752, 846, and 15 cm⁻¹, and Δ_fH₀[°](SiC₂) of 152.45 ± 0.20 kcal mol⁻¹.

INDEX WORDS: computational chemistry, Coupled Cluster, potential energy surfaces, benzaldehyde, GaH₅, BH₅, AlH₅, silicon dicarbide

POTENTIAL ENERGY SURFACES OF SMALL MOLECULES AND CATIONS:
INSIGHTS FROM COUPLED CLUSTER THEORY

by

LUCAS DANIEL SPEAKMAN

Bachelor of Arts, Asbury University, 2006

A Dissertation Submitted to the Graduate Faculty of The University of Georgia in Partial
Fulfillment of the Requirements for the Degree

DOCTOR OF PHILOSOPHY

ATHENS, GA

2010

© 2010

Lucas Daniel Speakman

All Rights Reserved

POTENTIAL ENERGY SURFACES OF SMALL MOLECULES AND CATIONS:
INSIGHTS FROM COUPLED CLUSTER THEORY

by

LUCAS DANIEL SPEAKMAN

Major Professor: Henry F. Schaefer III

Committee: Geoffrey D. Smith
Nigel G. Adams

Electronic Version Approved:

Maureen Grasso
Dean of the Graduate School
The University of Georgia
May 2010

DEDICATION

To my wonderful wife, with whom this work would not be possible. I can never tell you how grateful I am for your sacrifices while putting me through graduate school.

To Daniel and Chloe (and hopefully more names someday), I pray that you take my time here during school as an example to follow your own dreams, wherever they might lead you.

ACKNOWLEDGEMENTS

There are so many people to thank who have made Athens, GA home to me, my wife, and my children. First of all, I wish to thank Henry “Fritz” Schaefer III for his invitation to study at his esteemed Center for Computational (Quantum) Chemistry. You have opened up your office, home, and heart to give me a chance to learn about life, religion, and, of course, chemistry.

Linda Rowe, whether you know it or not, you have a nickname: the “CCQC mom”. It is really an appropriate name, since you have watched my sick kids while I attended classes. You always made sure we were taken care; food, van, explaining school policies.

The closest scientific and personal friend I could have is Justin Turney. Our journey started out as a mentor/mentee relationship, but grew into a great friendship. Our Monday breakfasts gave me the right motivation to start our work week.

Of course, CCQC wouldn’t have been nearly as fun if it wasn’t for Frank Picard (SuperTecmo Bowl), Nate Stibrich (finger football), Jeremy Wilke (sports and politics talk), and Andy Simmonett (barbecue and fried cheese).

I would not have been nearly prepared for my graduate work if it were not for the professors of Asbury University: Don Burgess (Physics), Del Mar Searls (Computer Science), Duk Lee (Diff Eq., Complex Analysis), Ken Reitz (math modeling), and Bruce Branan (Organic Chemistry). Two professors made a dramatic impact on my life. Professor David “Doc” Coulliette (Calculus, Applied Math, and Numerical Analysis) taught me that integrity and a heart after Christ are more important than any education you obtained. Professor Richard Reznik

(General and Analytical Chemistry), while on a sabbatical at UGA, briefly met Dr. Schaefer and made the first connection. This connection turned into my first of 3 summers studying at the CC(Q)C followed up by studying at UGA.

I want to thank a few non-scientific people that have made Athens a home: Johnny and Alicia Pachuta (Thursday skiing); Brad Sheffield, Michael Kulick, and Scott Swain (Men's night). Terry Williams, you have single-handedly shown me how to be the spiritual leader of the home, a wonderful husband, and an affectionate father; I thank you and Christie for the guidance you have given us during our small group discussions. The last person I wish to thank is Lance Brooks. I have truly enjoyed getting to know you and working with you for the past few years. I pray that we will continue to work together for the Church and strengthen our friendship.

I would not be here if it was not for my upbringing by my parents and brothers. Mom and Dad, thank you for pushing me to always reach further than what I thought I could reach. Ric, you pioneered the way to Asbury and to post-graduate degree. Sky, you demonstrated the joy of learning my freshman year; Meghan might say you enjoyed it too much! Mark, my twin brother, you will always have a special place in my heart; albeit two minutes older than yours. During the last four years, your faith and trust in the Lord has shown that I need to follow God's plan for my life; not what I think is the most logical or expected next step in my life.

TABLE OF CONTENTS

	Page
ACKNOWLEDGEMENTS	v
LIST OF TABLES	x
LIST OF FIGURES	xiii
CHAPTER	
1 INTRODUCTION AND BACKGROUND MATERIAL.....	1
1.1 QUANTUM MECHANICS.....	1
1.2 COUPLED CLUSTER	2
1.3 FOCAL POINT ANALYSIS.....	3
1.4 PROSPECTUS.....	4
1.5 REFERENCES	6
2 THE MICROWAVE AND INFRARED SPECTROSCOPY OF BENZALDEHYDE: CONFLICT BETWEEN THEORY AND EXPERIMENT DEDUCTIONS.....	9
2.1 ABSTRACT.....	10
2.2 INTRODUCTION	10
2.3 COMPUTATIONAL DETAILS	12
2.4 RESULTS AND DISCUSSION.....	14
2.5 CONCLUSIONS.....	16
2.6 ACKNOWLEDGMENTS	17

2.7 REFERENCES	17
3 DOES GaH ₅ EXIST?	26
3.1 ABSTRACT.....	27
3.2 INTRODUCTION	28
3.3 COMPUTATIONAL DETAILS	31
3.4 RESULTS AND DISCUSSION.....	32
3.5 CONCLUSIONS.....	38
3.6 ACKNOWLEDGEMENTS	38
3.7 REFERENCES	38
4 THE DEPROTONATION ENERGIES OF BH ₅ AND AlH ₅ : COMPARISONS TO GaH ₅	59
4.1 ABSTRACT.....	60
4.2 INTRODUCTION	60
4.3 COMPUTATIONAL DETAILS	62
4.4 RESULTS AND DISCUSSION.....	62
4.5 CONCLUSIONS.....	65
4.6 ACKNOWLEDGEMENTS	65
4.7 REFERENCES	65
5 TOWARD THE OBSERVATION OF QUARTET STATES OF THE OZONE RADICAL CATION: INSIGHTS FROM COUPLED CLUSTER THEORY	77
5.1 ABSTRACT.....	78
5.2 INTRODUCTION	78
5.3 COMPUTATIONAL DETAILS	83

5.4 RESULTS AND DISCUSSION.....	84
5.5 CONCLUSIONS.....	95
5.6 ACKNOWLEDGEMENTS.....	97
5.7 REFERENCES.....	97
6 THE SIC ₂ SAGA CONTINUES: REVISED BARRIER TO LINEARITY, EQUILIBRIUM STRUCTURES, FUNDAMENTAL FREQUENCIES, AND ENTHALPY OF FORMATION.....	114
6.1 ABSTRACT.....	115
6.2 INTRODUCTION.....	116
6.3 COMPUTATIONAL DETAILS.....	120
6.4 RESULTS AND DISCUSSION.....	123
6.5 CONCLUSIONS.....	127
6.6 ACKNOWLEDGEMENTS.....	128
6.7 REFERENCES.....	128
7 CONCLUSIONS.....	143
APPENDIX	
A SUPPLEMENTARY MATERIAL FOR CHAPTER 5.....	145

LIST OF TABLES

	Page
Table 2.1. Previous theoretical predictions of the benzaldehyde rotational barrier (in kcal mol ⁻¹).....	20
Table 2.2. Theoretical rotational barriers for benzaldehyde (in kcal mol ⁻¹).....	21
Table 2.3. Theoretical rotational barriers for phenol (kcal mol ⁻¹).	22
Table 3.1. Total energies (in hartrees) and zero-point vibrational energy (ZPVE) (in kcal mol ⁻¹) for the seven structures of GaH ₅ plus GaH ₃ and H ₂	41
Table 3.2. Relative and ZPVE corrected energies (in kcal mol ⁻¹) with respect to \tilde{X}^1A' GaH ₅ including its dissociation energy.....	42
Table 3.3. Total energies (in hartrees), zero-point vibrational energy (ZPVE), dissociation energies of GaH ₅ , and proton affinities for GaH ₅ , GaH ₄ ⁻ , GaH ₃ , and H ₂ with augmented basis sets (in kcal mol ⁻¹).....	43
Table 3.4. Harmonic vibrational frequencies (in cm ⁻¹) for the ground electronic states of GaH ₅ , GaH ₄ ⁻ , and GaH ₃ at the aug-cc-pVQZ CCSD(T) level of theory.....	44
Table 3.5. Harmonic vibrational frequencies for GaH ₅ transition structures at the cc-pVQZ CCSD(T) level of theory (in cm ⁻¹).....	45
Table 3.6. Comparison of the relative energies (in kcal mol ⁻¹ including ZPVE), H ₂ dissociation energies (D ₀), and proton affinities (PA ₀) of the AH ₄ species.....	46

Table 4.1. BH ₅ Total Energies (in hartrees) with Proton Affinities and ZPVEs (in kcal mol ⁻¹).....	68
Table 4.2. Vibrational Frequencies for BH ₅ and BH ₄ ⁻ (in cm ⁻¹).....	69
Table 4.3. Vibrational Frequencies for AlH ₅ and AlH ₄ ⁻ (in cm ⁻¹).	70
Table 4.4. Total Energies (in hartrees) and ZPVE Values (kcal mol ⁻¹) for BH ₅ , BH ₄ ⁻ , AlH ₅ , and AlH ₄ ⁻	71
Table 4.5. Deprotonation Energies of BH ₅ , AlH ₅ , and GaH ₅ (kcal mol ⁻¹).	72
Table 5.1. Optimized geometries for O ₃ ⁺ states (bond distances in Angstroms; angles in degrees).....	103
Table 5.2. Optimized geometries for O ₃ states (bond distances in Angstroms; angles in degrees).....	104
Table 5.3. Optimized geometries (in Angstroms), harmonic vibrational frequencies (in cm ⁻¹), and ionization potentials (in eV) for O ₂ and O ₂ ⁺	105
Table 5.4. cc-pCV5Z CASSCF CI coefficients (> ±0.23) and corresponding electron configurations.	106
Table 5.5. cc-pCVTZ harmonic vibrational frequencies (in cm ⁻¹), infrared intensities (in km mol ⁻¹) in parentheses, and zero-point vibrational energies (ZPVE) (in eV) for O ₃ and O ₃ ⁺	107
Table 5.6. Comparison of theoretical and experimental excitation energies and ionization potentials (in eV) with respect to the \tilde{X}^1A_1 state of O ₃	108
Table 5.7. Comparison of experimental and theoretical dissociation energies (in eV) for ² A ₁ O ₃ ⁺ and ² B ₂ O ₃ ⁺	109

Table 5.8. Theoretical cc-pCV5Z UCCSD(T) adiabatic (T_e), ZPVE-corrected adiabatic (T_0), and vertical ionization potentials (T_v) in eV.	110
Table 6.1. Bond lengths of SiC ₂ and C ₂ molecules (in Å).	135
Table 6.2. Valence focal point analysis of the barrier to linearity (in kcal mol ⁻¹).	136
Table 6.3. Valence focal point analyses of the heat of formation for path A (in kcal mol ⁻¹).	137
Table 6.4. Valence focal point analyses of the heat of formation for path B (in kcal mol ⁻¹).	138
Table 6.5. Valence focal point analysis of the C ₂ energy split (in kcal mol ⁻¹).	139
Table 6.6. Complete quartic force fields of SiC ₂	140
Table 6.7. Harmonic and anharmonic frequencies of T-shaped SiC ₂ (in cm ⁻¹).	141
Table A.1. Dissociation energies (in eV) for the quartet and doublet states of the ozone radical cation.	146
Table A.2. Theoretical ionization potentials with respect to the ³ A ₂ state of O ₃ (in eV).	147
Table A.3. Theoretical ionization potentials with respect to ³ B ₂ state of O ₃ (in eV).	148
Table A.4. Theoretical ionization potentials with respect to the ³ B ₁ state of O ₃ (in eV).	149
Table A.5. Theoretical ionization potentials with respect to the ² A ₁ and ² B ₂ states of O ₃ ⁺ (in eV).	150
Table A.6. Theoretical ionization potentials with respect to the ¹ A ₁ state of O ₃ (in eV).	151

LIST OF FIGURES

	Page
Figure 1.1. General schematic of a focal point table.	8
Figure 2.1. Structures of benzaldehyde.....	23
Figure 2.1. Structure of phenol	24
Figure 2.3. Benzaldehyde geometrical parameters	25
Figure 3.1. Known equilibrium geometry for CH_5^+	47
Figure 3.2. Predicted geometries for the C_s (I) structure 1 of GaH_5 (Bond lengths given in Å , angles in degrees).....	48
Figure 3.3. Predicted geometries for the C_s (I) structure 1 of GaH_5 with augmented basis functions (Bond lengths given in Å , angles in degrees).	49
Figure 3.4. Predicted geometries for the C_s (II) transition structure 2 of GaH_5 (Bond lengths given in Å , angles in degrees).	50
Figure 3.5. Predicted geometries for the C_{2v} transition structure 3 of GaH_5 (Bond lengths given in Å , angles in degrees).	51
Figure 3.6. Predicted geometries for the C_{3v} second-order saddle-point structure 4 of GaH_5 (Bond lengths given in Å , angles in degrees).....	52
Figure 3.7. Predicted geometries for the C_s (III) transition state 5 of GaH_5 (Bond lengths given in Å , angles in degrees).	53
Figure 3.8. Predicted geometries for the C_{4v} second-order saddle-point structure 6 of GaH_5 (Bond lengths given in Å , angles in degrees).....	54

Figure 3.9. Predicted geometries for the D_{3h} second-order saddle-point structure 7 of GaH ₅ (Bond lengths in given Å).	55
Figure 3.10. Predicted geometries for D_{3h} symmetry GaH ₃ (Bond lengths given in Å).....	56
Figure 3.11. Predicted geometries for D_{3h} symmetry GaH ₃ with augmented basis functions (Bond lengths given in Å).	57
Figure 3.12. Predicted geometries for T_d symmetry GaH ₄ ⁻ with augmented basis functions (Bond lengths given in Å).	58
Figure 4.1. Predicted equilibrium geometries for BH ₅ (bond lengths given in Å, angles in degrees).	73
Figure 4.2. Predicted equilibrium geometries for the BH ₄ ⁻ anion (bond lengths given in Å, angles in degrees).....	74
Figure 4.3. Predicted equilibrium geometries for AlH ₅ (bond lengths given in Å, angles in degrees).	75
Figure 4.4. Predicted equilibrium geometries for the AlH ₄ ⁻ anion (bond lengths given in Å, angles in degrees).....	76
Figure 5.1. Walsh Diagram for XY ₂	111
Figure 5.2. cc-pVTZ CASSCF potential energy curves for O ₃ ⁺ (reference energy is the \tilde{X}^1A_1 state of O ₃	112
Figure 5.3. cc-pVTZ CASSCF potential energy curves for O ₃	113
Figure 6.1. Two-dimensional and three-dimensional potential energy surfaces of SiC ₂ (x,y coordinates in Å, z axis in kcal mol ⁻¹)	142

CHAPTER 1

INTRODUCTION AND BACKGROUND MATERIAL

1.1 QUANTUM MECHANICS

The late nineteenth and early twentieth centuries saw many interesting discoveries in physics and chemistry regarding the particles which make up the macroscopic world. Although classical mechanics accurately predicts the behavior of objects in the visible world, from projectiles and machinery to planetary motion, its failure to correctly describe very small particles was noticed in the 1900s. When physicists used statistical mechanics and the electromagnetic-wave model of light to predict the intensity vs. frequency curve for black body radiation, their results were in complete disagreement with the experimental data in the high-frequency region. In 1900, Max Planck achieved agreement with the observed blackbody-radiation curve by hypothesizing that only certain quantities of light energy could be emitted, in units corresponding to 6.6×10^{-34} J s. This constant, now known as Planck's constant (h), marks the beginning of quantum mechanics. The successful explanation of the photoelectric effect by Einstein confirmed energy quantization of photons. Quantum Mechanics culminated in 1926 with Schrodinger's time-independent equation, $\hat{H}\Psi = E\Psi$, to predict discrete energies of systems where classical mechanics fails.

Computational quantum chemistry simply applies quantum mechanics to problems in chemistry. It is used for interpreting vibrational spectra by frequencies and intensities, determining relative stabilities of molecules; molecular properties and rate constants, analyzing

NMR spectra, mechanisms of chemical reactions, and even protein folding; every branch of chemistry has been influenced by computational quantum chemistry.

1.2 COUPLED CLUSTER

Coupled Cluster (CC) theory¹ has emerged as perhaps the most reliable, yet computationally affordable, method for obtaining approximate solutions to the electronic Schrödinger equation, and for the prediction of molecular properties. The “exponential ansatz” is one of the central equations of coupled cluster theory. The exponentiated cluster operator, \hat{T} , when applied to the reference determinant, Φ_0 , produces a new wavefunction containing cluster functions. Each of these correlates the motion of electrons within specific orbitals:

$$\psi = \left[\left[\varphi_i(\mathbf{x}_1)\varphi_j(\mathbf{x}_2) + f_{ij}(\mathbf{x}_1, \mathbf{x}_2) \right] \varphi_k(\mathbf{x}_3)\varphi_l(\mathbf{x}_4) \right] \quad (1.1)$$

where $f_{ij}(\mathbf{x}_m, \mathbf{x}_n) = \sum_{a>b} t_{ij}^{ab} \varphi_a(\mathbf{x}_m)\varphi_b(\mathbf{x}_n)$ is the cluster function. The cluster operators, \hat{T}_n , are frequently referred to as excitation operators, since the determinants they produce when operating on Φ_0 resemble excited states in Hartree-Fock theory. Truncation of the cluster operator at specific substitution/excitation levels leads to a hierarchy of coupled cluster techniques²⁻⁸

$$\begin{aligned} \hat{T} &\equiv \hat{T}_2 \longrightarrow CCD \\ \hat{T} &\equiv \hat{T}_1 + \hat{T}_2 \longrightarrow CCSD \\ \hat{T} &\equiv \hat{T}_1 + \hat{T}_2 + \hat{T}_3 \longrightarrow CCSDT \end{aligned}$$

where “S”, “D”, and “T” indicate that single-, double-, and triple-excitations, respectively, are included in the wavefunction expansion. With the exponential ansatz, CC is one of the premier methods for computing the correlation energy necessary for accurate molecular predictions. Not

only is CC size-consistent, but it recovers more electron correlation energy than its counterpart, Configuration Interaction (CI), with similar scaling.

1.3 FOCAL POINT ANALYSES

With improved computer technology, higher levels of theory can now be routinely applied to novel chemical systems. It is possible to systematically approach the complete basis set (CBS) limit using carefully constructed families of basis sets, such as Dunning's correlation-consistent polarized valence basis sets (cc-pVXZ).⁹⁻¹¹ Successive members of this family are constructed by adding additional levels of valence and polarization functions to the previous basis set. Each basis set is characterized by the principle number of the highest shell. For example, cc-pVDZ and cc-pVTZ basis sets contract to $3s2p1d$ and $4s3p2d1f$, respectively. While near exponential convergence is observed for Hartree-Fock energies, utilizing a three point fit;^{12,13}

$$a + be^{-cX} \tag{1.2}$$

correlation energies employ a two point functional form,

$$a + bX^{-3} \tag{1.3}$$

where X is the cardinal number of the basis set.¹⁴

The determination of the energy at the CBS limit is vital in the focal-point analysis of Allen and co-workers.¹⁵ The focal-point scheme systematically approaches both the CBS and full configuration interaction (Full CI) limits. Energies are computed at an accurate geometry at the SCF, MP2, CCSD, CCSD(T), CCSDT, CCSDT(Q), and CCSDTQ levels of theory. At each level of theory, computations are performed with the largest possible basis set. The SCF and correlation energies are then extrapolated using eqs 1.2 and 1.3, respectively. Extrapolations for correlation treatments are usually limited to coupled-cluster with singles and doubles method,

augmented by a perturbative triples term [CCSD(T)]. Higher order correlation treatments and other small corrections are included in an additive fashion, see figure 1.1. The extrapolated increments are summed up to yield an estimate of the complete basis set CCSDTQ energy. This approach has been used numerous times with sub-chemical accuracy,¹⁶⁻¹⁹ that is, errors of ± 0.1 kcal mol⁻¹.

By extrapolating the energies at each level of theory to the CBS limit, the error due to incomplete basis set and insufficient correlation treatment can be quantified. With sufficient additional corrections, such as core-valence correlation, relativistic effects, and zero-point vibrational energy, the error, relative to the exact energy within the Born-Oppenheimer approximation, can be reduced to any level desired.

1.4 PROSPECTUS

Although quantum chemistry has been around since 1926, initially it was limited to systems with a few electrons and theory development. It wasn't until the 1970s that computational chemistry became a practical tool for the assignment of spectra and identification of states.²⁰ Aided by advances in computer science and technology, computational chemistry has become a useful tool for every chemist. As it has matured through the decades, most applications fall into three general areas: 1) Development of new theories and approximations for faster, more accurate results, 2) Confirmation/Disproval of experimental results and conclusions; and 3) Collaboration with experimentalists and synthetic chemists. This dissertation encompasses all three situations.

Chapter 2 focuses on scenario two by addressing a discrepancy between theory and experiment relating to the rotational barrier height of benzaldehyde. The experimental result was investigated and found to utilize Pitzer's model.²¹ This model computes the reduced moment

of inertia for a given molecular geometry, and accounts for the effects of an asymmetric top on the internal rotational barrier. Using the reduced moment of inertia and the observed torsional frequency, the rotational barriers were experimentally calculated. This chapter examines the validity of the experimental model and compares to *ab initio* results.

Chapter 3 was prompted by an experimentalist's enquiry whether GaH₅ exists, and if so, could hydrogen scrambling occur? A thorough potential energy surface for hydrogen scrambling and dissociation of this system was investigated. Chapter 4 extends this theoretical characterization to BH₅ and AlH₅ and examines their deprotonation energies.

Collaboration with Professor Frederic Merkt is the reason for chapter 5. He was attempting to synthesize and identify the quartet states of the ozone radical cation and required theoretical data to guide his experiments. Potential energy surfaces for the C_{2v} structures of the singlet and triplet neutral ozone and doublet and quartet states of ozone cation were constructed. All feasible ionizations and excitations are discussed.

The last chapter deals with pushing the limits of CC theory to sub-chemical accuracy for one of the most challenging molecules to computational chemists, SiC₂. In addition to achieving converged predictions of a T-shaped global minimum with correct surface curvature, and determining unassailably whether a low-lying isomer exists, the topography for the large-amplitude pinwheel motion was established. Silicon dicarbide is both basis set and electron correlation treatment sensitive. To overcome these issues, a composite, complete basis set limit CCSDT approach was developed. The potential energy surface contained over 970 energy computations, resulting in one of the most accurate potential energy surface in the literature. Sub-chemical accuracy was reached for the barrier to linearity, heat of formation, and C₂ singlet-triplet energy separation.

1.5 REFERENCES

- ¹ J. Cizek, *J. Chem. Phys.* **45** (11), 4256 (1966).
- ² C. Hampel, K. A. Peterson, and H. J. Werner, *Chem. Phys. Lett.* **190** (1-2), 1 (1992).
- ³ G. E. Scuseria and H. F. Schaefer, *Chem. Phys. Lett.* **152** (4-5), 382 (1988).
- ⁴ C. Sosa, J. Noga, and R. J. Bartlett, *J. Chem. Phys.* **88** (9), 5974 (1988).
- ⁵ A. C. Scheiner, G. E. Scuseria, J. E. Rice, T. J. Lee, and H. F. Schaefer, *J. Chem. Phys.* **87** (9), 5361 (1987).
- ⁶ G. D. Purvis and R. J. Bartlett, *J. Chem. Phys.* **76** (4), 1910 (1982).
- ⁷ J. A. Pople, R. Krishnan, H. B. Schlegel, and J. S. Binkley, *Int. J. Quantum Chem.* **14** (5), 545 (1978).
- ⁸ R. J. Bartlett and G. D. Purvis, *Int. J. Quantum Chem.* **14** (5), 561 (1978).
- ⁹ T. H. Dunning, *J. Chem. Phys.* **90** (2), 1007 (1989).
- ¹⁰ R. A. Kendall, T. H. Dunning, and R. J. Harrison, *J. Chem. Phys.* **96** (9), 6796 (1992).
- ¹¹ D. E. Woon and T. H. Dunning, *J. Chem. Phys.* **98** (2), 1358 (1993).
- ¹² D. Feller, *J. Chem. Phys.* **98** (9), 7059 (1993).
- ¹³ E. F. Valeev, W. D. Allen, R. Hernandez, C. D. Sherrill, and H. F. Schaefer, *J. Chem. Phys.* **118** (19), 8594 (2003).
- ¹⁴ T. Helgaker, W. Klopper, H. Koch, and J. Noga, *J. Chem. Phys.* **106** (23), 9639 (1997).
- ¹⁵ A. L. L. East and W. D. Allen, *J. Chem. Phys.* **99** (6), 4638 (1993).
- ¹⁶ G. S. Tschumper, M. L. Leininger, B. C. Hoffman, E. F. Valeev, H. F. Schaefer, and M. Quack, *J. Chem. Phys.* **116** (2), 690 (2002).
- ¹⁷ N. D. K. Petraco, W. D. Allen, and H. F. Schaefer, *J. Chem. Phys.* **116** (23), 10229 (2002).

- ¹⁸ M. S. Schuurman, S. R. Muir, W. D. Allen, and H. F. Schaefer III, *J. Chem. Phys.* **120** (24), 11586 (2004).
- ¹⁹ J. M. Gonzales, C. Pak, R. S. Cox, W. D. Allen, H. F. Schaefer, A. G. Csaszar, and G. Tarczay, *Chem.-Eur. J.* **9** (10), 2173 (2003).
- ²⁰ S. V. Oneil, H. F. Schaefer, and C. F. Bender, *J. Chem. Phys.* **55** (1), 162 (1971).
- ²¹ K. S. Pitzer, *J. Chem. Phys.* **14**, 239 (1946).

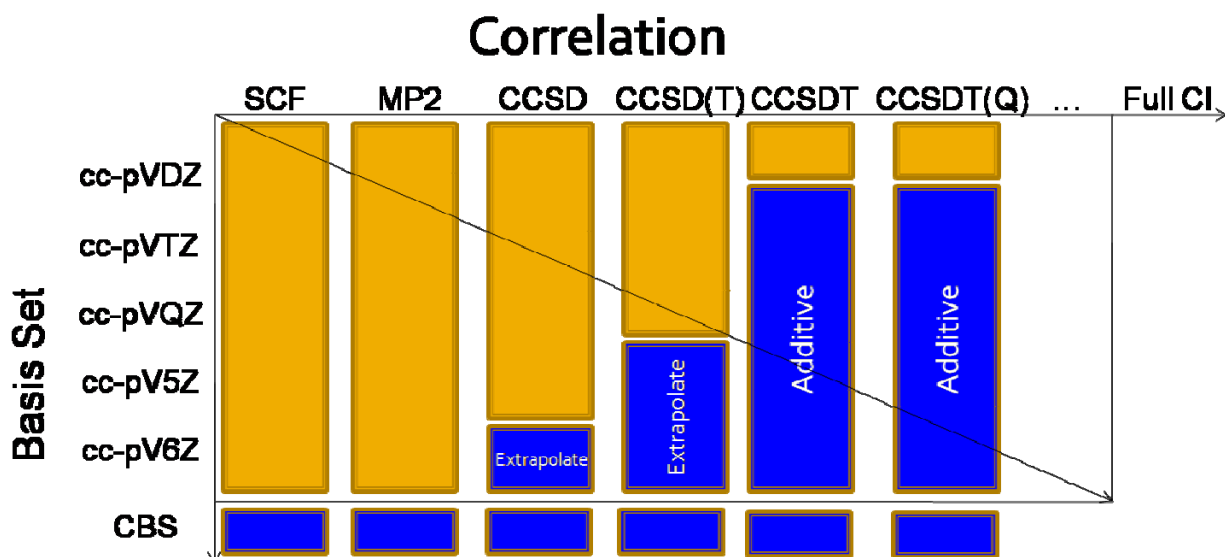


Figure 1.1. General schematic focal point table. The extrapolated and additive increments are summed to yield an approximation to the exact non-relativistic Born-Oppenheimer energy.

CHAPTER 2

THE MICROWAVE AND INFRARED SPECTROSCOPY OF BENZALDEHYDE: CONFLICT BETWEEN THEORY AND EXPERIMENT DEDUCTIONS[†]

[†]Lucas D. Speakman, Brian N. Papas, H. Lee Woodcock, and Henry F. Schaefer III. *J. Chem. Phys.* **120**, 4247 (2004); doi:10.1063/1.1643716. Reprinted here with permission of publisher.

2.1 ABSTRACT

Recently, it has been proposed that *ab initio* calculations cannot accurately treat molecules comprised of a benzene ring with a π -conjugated substituent, for example, benzaldehyde. Theoretical predictions of the benzaldehyde barrier to internal rotation are typically a factor of 2 too high in comparison to the experimental values of 4.67 (infrared) and 4.90 (microwave) kcal mol⁻¹. However, both experiments use Pitzer's 1946 model to compute the reduced moment of inertia and employ the experimentally observed torsional frequency to deduce benzaldehyde's rotational barrier. When Pitzer's model is applied to a system with a nonconjugated functional group, such as phenol, the model and theoretical values are in close agreement. Therefore, we conclude the model may not account for conjugation between the substituent and the π -system of benzene. The experimental values of the benzaldehyde rotational barrier are therefore misleading. The true rotational barrier lies closer to the theoretically extrapolated limit of 7.7 kcal mol⁻¹, based on coupled cluster theory.

2.2 INTRODUCTION

Currently, there is a discrepancy between experimental and theoretical values for rotational barriers of molecules comprised of a benzene ring and a π -conjugated substituent, such as benzaldehyde (Figure 2.1). Meier and Koglin recently argued that the density functional theory (DFT)^{1,2,3} and *ab initio* calculations such as Møller–Plesset theory (MP2)⁴ and Hartree–Fock (HF) yield results that are a factor 2 too high compared to experiments.^{5,6} Meier has used this discrepancy to launch a more general criticism⁷ of DFT. This conflict between theory and experiment rests on the results of three separate experiments.

Miller, Fateley, and Witkowski in 1967 obtained the infrared spectrum of benzaldehyde, from 33 to 400 cm⁻¹, and observed the torsional band at 111 cm⁻¹. This led to a rotational barrier

of $4.66 \text{ kcal mol}^{-1}$.⁸ In 1970 Kakar, Quade, and Kojima reported the torsional frequency of benzaldehyde to be $113.8 \pm 5.0 \text{ cm}^{-1}$ via microwave spectroscopy and then deduced the barrier to internal rotation to be $4.90 \pm 0.43 \text{ kcal mol}^{-1}$.⁹ Fifteen years later, Durig, Bist, Furic, Qui, and Little further explored this rotation barrier by examining the far-infrared spectrum of gaseous benzaldehyde. This resulted in a torsional frequency of 110.85 cm^{-1} and a rotational barrier of $4.67 \text{ kcal mol}^{-1}$.¹⁰

The microwave and infrared spectroscopic results are in close agreement with one another, suggesting that they are accurate measures of the true rotational barrier height for benzaldehyde. All experimental determinations of barrier heights from experiment were based on Pitzer's model,¹¹ which computes the reduced moment of inertia given the molecular geometry and accounts for contributions of an asymmetric top to the internal rotational barrier. Using the reduced moment of inertia and the observed torsional frequency, the rotational barriers were then computed.¹² Pitzer's model has become a standard in evaluating rotational barriers of molecules composed of a rigid frame and an unsymmetrical top, such as benzaldehyde and phenol.

Phenol (Figure 2.2), which is a nonconjugated benzene derivative, is a good test case for determining the accuracy of Pitzer's model as compared to *ab initio* predictions. Berden, Meerts, Schmitt, and Kleinermanns examined phenol via high resolution fluorescence excitation spectroscopy and recorded a rotational barrier of $3.47 \text{ kcal mol}^{-1}$.¹³ Tsuzuki, Houjou, Nawawa, and Hiratani have theoretically computed phenol's rotational barrier height and are in close agreement with experiment with their MP2 barrier of $3.52 \text{ kcal mol}^{-1}$.¹⁴

Due to discrepancies between the experimental and theoretical rotational barriers of benzaldehyde, we decided to undertake the current research. The mutual agreement of phenol's

experimental and theoretical rotational barriers lead us to examine the possibility of a misinterpretation of the benzaldehyde experiments.

2.3 COMPUTATIONAL DETAILS

We employed Dunning's correlation consistent basis sets, denoted cc-pVXZ, for all geometry optimizations and harmonic frequency computations. At the Hartree–Fock level of theory we utilized the cc-pVXZ (X=D,T,Q,5)¹⁵ basis sets. For the second order Møller–Plesset theory (MP2) computations cc-pVXZ (X=D,T,Q) were applied. Potential curves of benzaldehyde were created using cc-pVXZ (X=D,T,Q) HF and cc-pVDZ MP2 computations by performing constrained optimizations of the dihedral angle (C=C–C=O) at 10 degree increments from 0 to 90 and allowing all other parameters to be optimized.

Geometry and harmonic frequency analyses were performed at the cc-pVXZ (X=D,T,Q) HF level for phenol. We obtained potential energy curves for phenol at the cc-pVDZ HF and cc-pVDZ MP2 levels in the same fashion as that of benzaldehyde.

The lowest energy structure of benzaldehyde was found to be the planar conformer with a $\varphi \equiv C = C - C = O$ dihedral angle of zero degrees and all real vibrational frequencies. The highest energy structure occurs for a dihedral angle φ of very close to 90 degrees, referred to as the perpendicular structure, which is a transition state with one imaginary frequency corresponding to rotation of the aldehyde group.

We computed theoretical rotation barriers by subtracting E_{plan} from E_{perp} , to find both the adiabatic and zero point energy (ZPE) corrected classical barrier heights. There exists some ambiguity in the ZPE corrected classical barrier heights. In the planar form, the lowest vibrational frequency was real and was accounted for in the zero point energy (ZPE) correction,

while the lowest frequency in the perpendicular form was imaginary and was not accounted for in the zero point energy correction. It needs to be noted that if this error was corrected for, it would push the theoretical value higher for the rotational barrier height of benzaldehyde.

The MP2/cc-pVQZ optimized geometry (Figure 2.3) (for the cc-pVQZ MP2 geometry optimization, g functions on carbon and oxygen were neglected) was used at all levels of theory for the extrapolation. The HF extrapolated rotational barrier limit was computed from the HF/cc-pVXZ (X=D,T,Q,5) levels of theory. The extrapolated MP2 correction was computed from the MP2/cc-pVXZ (X=D,T,Q,5) levels of theory. The equation

$$A + B * e^{-C * X} \text{ (X=D,T,Q, etc.)}, \quad (2.1)$$

was fit to the Hartree–Fock barrier heights. For the MP2 correction, we performed a two parameter fit to the equation $A + B * X^{-3}$. The final step in the extrapolation was the addition of a cc-pVDZ CCSD(T)^{16,17} correction term that we obtained from the following formula:

$$E_{\text{correction}} = E_{\text{CCSD(T)}} - E_{\text{MP2}}. \quad (2.2)$$

All Hartree–Fock (HF) and MP2 calculations at the cc-pVXZ (X=D,T,Q) level of theory were performed using GAUSSIAN 94.¹⁸ GAUSSIAN 98¹⁹ was employed for cc-pV5Z HF and cc-pVDZ MP2 computations at NERSC while QChem²⁰ was utilized for the cc-pVXZ (X=T,Q) MP2 optimizations. GAUSSIAN 03²¹ was used for the cc-pVTZ MP2 frequencies and cc-pV5Z HF. MOLPRO²² was used for the application of the CCSD(T) method.

A simple computer program was written to compute the reduced moment of inertia for molecules composed of a rigid frame with an attached, unsymmetrical top. The equations used are discussed in detail in Pitzer's 1946 paper.¹¹ Using the reduced moment of inertia, I_r , the rotational barriers were estimated through a series of simple equations developed by Fateley and co-workers,¹²

$$\frac{\nu^2}{F} = V_1 + 4V_2 + 9V_3, \quad (2.3)$$

where $F = 16.852/I_r$, ν =observed torsional frequency (cm^{-1}), $V_1 = V_3 = 0$, and V_2 is the rotational barrier (cm^{-1}).

The latter analysis was done in an attempt to make a direct comparison with Durig¹⁰ and Kakar's⁹ experimental barrier heights and to determine if our theoretical predictions would yield similar results to those obtained via Pitzer's model.

2.4 RESULTS AND DISCUSSION

Meier argues that since benzaldehyde's *ab initio* and density functional theory (DFT) rotational barriers are much higher than the experimental values, they are incorrect (Table 2.1). In fact Meier uses this finding to argue more generally for the failure of DFT.

Using Pitzer's model in an attempt to replicate Kakar and Durig's experimental values resulted in rotational barrier values of 5.01, 4.43, 4.28, 4.28, 4.45, 3.95, and 3.95 for cc-pVXZ (X=D,T,Q,5) HF and cc-pVXZ (X=D,T,Q) MP2, respectively. At each level of theory the optimized geometry and respective torsional frequency were used. Our results are similar to Kakar's 4.90 and Durig's 4.67 kcal mol^{-1} (Table 2.2) rotational barriers. Both Kakar and Durig used Fateley's reduced moment of inertia value to calculate the rotational barrier instead of computing the value themselves. Since the geometry used in Fateley's computation of I_r was not published, this value could not be precisely replicated.

The directly computed quantum mechanical barriers for benzaldehyde are much higher than the experimental 8.63, 7.70, 7.47, 8.44, 8.32, 7.94 (kcal mol^{-1}) for cc-pVXZ (X=D,T,Q) HF and cc-pVXZ (X=D,T,Q) MP2, respectively. Extrapolation resulted in the following rotational barriers: the HF limit (7.98 kcal mol^{-1}), the extrapolated MP2 correction limit ($-0.01 \text{ kcal mol}^{-1}$),

CCSD(T) correction ($-0.31 \text{ kcal mol}^{-1}$) (the T1 diagnostics from the MOLPRO outputs, approximately 0.013, show that the system is qualitatively described by a single-reference configuration, and non-dynamical correlation is not dominant^{23,24}), and a final extrapolated barrier height of $7.66 \text{ kcal mol}^{-1}$. This value, although in disagreement with the experimental deductions, cannot be ignored given the high level of theory and large basis sets employed.

Applications of Pitzer's model to phenol resulted in rotational barriers that were in close agreement (Table 2.3) and displayed only 0.03, 0.01, and 0.03 (kcal mol^{-1}) differences between theoretical computations and Pitzer's model at the cc-pVXZ (X=D,T,Q) HF levels of theory, respectively. Phenol is structurally related to benzaldehyde although one less carbon atom is present and no π -conjugation exists in the asymmetric top of the molecule. Note that the lone pair on the oxygen in phenol delocalizes throughout the benzene ring, forming a slight degree of conjugation in the planar form. However, when phenol rotates, the first lone pair comes out of the benzene ring, and the second lone pair delocalizes in the benzene ring. Thus, the slight conjugation of phenol cancels out in the planar and perpendicular forms and can be ignored. The close agreement between Pitzer's model and the theoretical values confirms a correct implementation of Pitzer's model used in the program and seems to validate Pitzer's model for molecules comprised of a rigid frame with an attached, unsymmetrical top.

In looking at the chemical structures of phenol and benzaldehyde, intuitively, benzaldehyde should have a much higher rotational barrier height. In phenol, as discussed above, the conjugation is apparent in both forms, so stability in phenol is retained and the rotational barrier is low. However, in benzaldehyde the conjugation is present only in the planar form. This leads to a greatly decreased stability as the aldehyde group is rotated and thus experiences a large

rotational barrier. Experimentally, benzaldehyde's barrier height is at most $1.54 \text{ kcal mol}^{-1}$ greater than that of phenol. Clearly this difference is too small.

The discrepancies between theory and experiment lead us to believe there is a problem with the interpretation of the benzaldehyde experiments. Clearly the theoretical and experimental barriers of phenol are in close agreement and help substantiate our claim. Investigating experimental procedures resulted in no likely errors in the spectroscopic methods, since both experiments arrived at comparable torsional frequencies. This leaves only the question how the rotational barrier height was deduced from experiment. The two experimental analyses used Fateley's reduced moment of inertia and their respective observed torsional frequencies and arrived at similar rotational barriers. Therefore, we conclude that Pitzer's model appears to be ill suited for rigid molecules with unsymmetrical tops that demonstrate strong π -conjugation.

Evaluation of the potential curve at 10 degree increments confirms that it fits a potential with only the V_2 term nonzero. This fit has an R -squared value of greater than 0.99. This suggests that only the V_2 term should be needed to describe the barrier.

2.5 CONCLUSIONS

The classic 1946 Pitzer paper which describes how to calculate reduced moments of inertia for molecules with functional groups attached to the main body was not intended to compute rigorous rotational barriers. Pitzer's model applied to phenol results in close agreement between experiment and theory and thus supports Pitzer's model for rotational barriers. However, when applied to π -conjugated-top molecules, such as benzaldehyde, the theory does not work as well. Pitzer's model may not account for the π -conjugated bond in benzaldehyde's top. We therefore conclude that the benzaldehyde experiments should not have used Fateley's reduced

moment of inertia value and, as a direct result, the benzaldehyde experimental rotational barrier height values are too low. The true value of benzaldehyde's rotational barrier height should be closer to the present extrapolated theoretical limit of 7.66 kcal mol⁻¹. Although density functional theory has many known failures, the rotational barrier for benzaldehyde is not one of them.

2.6 ACKNOWLEDGMENTS

We thank the Department of Energy for support within its Combustion and SciDAC programs. We also thank the Department of Energy NERSC computing facility for critical machine access.

2.7 REFERENCES

- ¹ L. J. Sham and W. Kohn, *Phys. Rev. A* **140**, 1133 (1965).
- ² W. Yang and R. G. Parr, *Density-Functional Theory of Atoms and Molecules* (Oxford University Press, New York, 1989).
- ³ W. Koch and M. C. Holthausen, *A Chemist's Guide to Density Functional Theory*, 2nd ed. (Wiley, New York, 2001).
- ⁴ C. Møller and M. S. Plesset, *Phys. Rev.* **46**, 618 (1934).
- ⁵ R. J. Meier and E. Koglin, *Chem. Phys. Lett.* **353**, 239 (2002).
- ⁶ R. J. Meier, *Comput. Mater. Sci.* **27**, 219 (2003).
- ⁷ R. J. Meier, *Faraday Discuss.* **124**, 405 (2003).
- ⁸ F. A. Miller, W. G. Fateley, and R. E. Witkowski, *Spectrochim. Acta, Part A* **23A**, 891 (1967).

- 9 R. K. Kakar, E. A. Rinehart, C. R. Quade, and T. Kojima, *J. Chem. Phys.* **52**, 3803
(1970).
- 10 J. R. Durig, H. D. Bist, K. Furic, J. Qiu, and T. S. Little, *J. Mol. Struct.* **129**, 45 (1985).
- 11 K. S. Pitzer, *J. Chem. Phys.* **14**, 239 (1946).
- 12 W. G. Fatelely, R. K. Harris, F. A. Miller, and R. E. Witkowski, *Spectrochim. Acta* **21**,
231 (1965).
- 13 G. Berden, W. L. Meerts, M. Schmitt, and K. Kleinermans, *J. Chem. Phys.* **104**, 972
(1996).
- 14 S. Tsuzuki, H. Houjou, Y. Nawawa, and K. Hiratani, *J. Phys. Chem. A* **104**, 1332 (2000).
- 15 T. H. Dunning, *J. Chem. Phys.* **90**, 1007 (1989).
- 16 K. Raghavachari, G. W. Trucks, J. A. Pople, and M. Head-Gordon, *Chem. Phys. Lett.*
157, 479 (1989).
- 17 G. E. Scuseria and T. J. Lee, *J. Chem. Phys.* **93**, 5851 (1990).
- 18 M. J. Frisch, G. W. Trucks, H. B. Schlegel *et al.*, GAUSSIAN 94, Revision E.2, Gaussian
Inc., Pittsburgh, PA, 1995.
- 19 M. J. Frisch, G. W. Trucks, H. B. Schlegel *et al.*, GAUSSIAN 98, Revision A.11.4,
Gaussian, Inc., Pittsburgh, PA, 2002.
- 20 J. Kong, C. A. White, A. I. Krylov *et al.*, Q-Chem, Version 2.0, Q-Chem., Inc., Export,
PA, 2000.
- 21 M. J. Frisch, G. W. Trucks, H. B. Schlegel *et al.*, GAUSSIAN 03, Revision B.03,
Gaussian, Inc., Pittsburgh, PA, 2003.
- 22 MOLPRO, a package of *ab initio* programs designed by H.-J. Werner and P. J. Knowles,
version 2002.1, with contributions from R. D. Amos, A. Bernhardsson, A. Berning *et al.*

- ²³ T. J. Lee and P. R. Taylor, *Int. J. Quantum Chem., Quantum Chem. Symp.* **23**, 199 (1989).
- ²⁴ P. R. Taylor, *Lecture Notes in Quantum Chemistry II*, 2nd ed. (Springer-Verlag, Berlin, 1994).

Table 2.1. Previous theoretical predictions of the benzaldehyde rotational barrier (in kcal mol⁻¹).^a

Theoretical	Predicted barrier
STO-3G//STO-3G	5.90
6-311G//3-21G	9.20
3-21G//3-21G	11.30
4-31G//4-21G	9.70
6-31G//3-21G	9.40
6-311G**//6-31G*	8.80
6-31G*//3-21G	9.00
6-31G*//6-31G*	8.90
MP2/3-21G//3-21G	10.00
MP2/6-311G**//6-31G*	8.30
MP2/6-31G*//6-31G*	8.60
ANO-I/SCF	8.40
ANO-I/CAS(8)	6.20
ANO-I/RAS(14)	5.80
ANO-II/SCF	7.80
ANO-II/CAS(8)	5.00
ANO-II/RAS(14)	4.30
D-VWN/TZVP(A2)//D-VWN/TZVP(A2)	10.20
B88-PW91/TZVP(A2)//B88-PW91/TZVP(A2)	9.00
PW91-PW91/TZVP(A2)//PW91-PW91/TZVP(A2)	9.30
B88-P86/TZVP(A2)//B88-P86/TZVP(A2)	9.20
BLYP/TZVP(A2)//BLYP/TZVP(A2)	9.10
FT-97/TZVP~(A2)//FT-97/TZVP(A2)	8.70
HCTH/TZVP(A2)//HCTH/TZVP(A2)	8.50
RCCSD(6-31G*)	7.80
Experiment	Value
Microwave	4.90
Gas-phase IR	4.70

^aData from Meier and Koglin (Ref. 5).

Table 2.2. Theoretical rotational barriers for benzaldehyde (in kcal mol⁻¹).

Basis Set	HF	MP2	Pitzer Model	
			HF	MP2
cc-pVDZ	9.27	9.02	5.01	4.45
cc-pVTZ	8.30	8.23	4.43	3.95
cc-pVQZ	8.05	7.99	4.28	3.95
cc-pV5Z	7.90	7.96 ^a	4.28	

^a The MP2/cc-pV5Z energies were evaluated at the optimized MP2/cc-pVQZ geometries.

Table 2.3. Theoretical rotational barriers for phenol (kcal mol⁻¹).

Basis Set	HF	Pitzer Model (HF)
cc-pVDZ	2.23	2.26
cc-pVTZ	2.19	2.20
cc-pVQZ	2.20	2.17

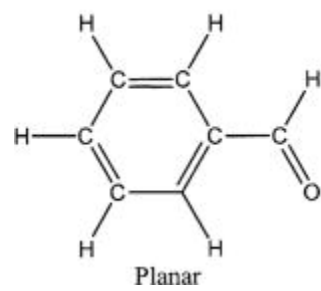
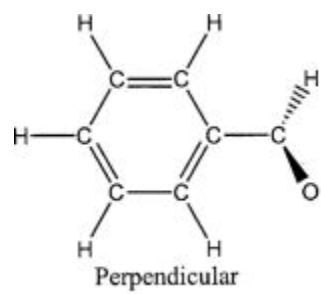


Figure 2.1. Structures of benzaldehyde.

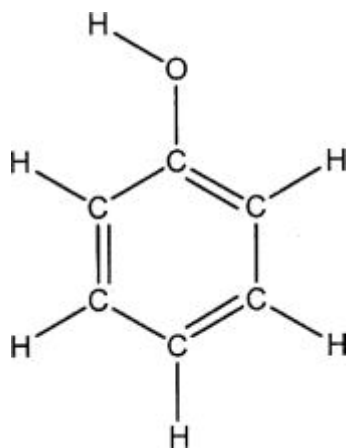


Figure 2.1. Structure of phenol.

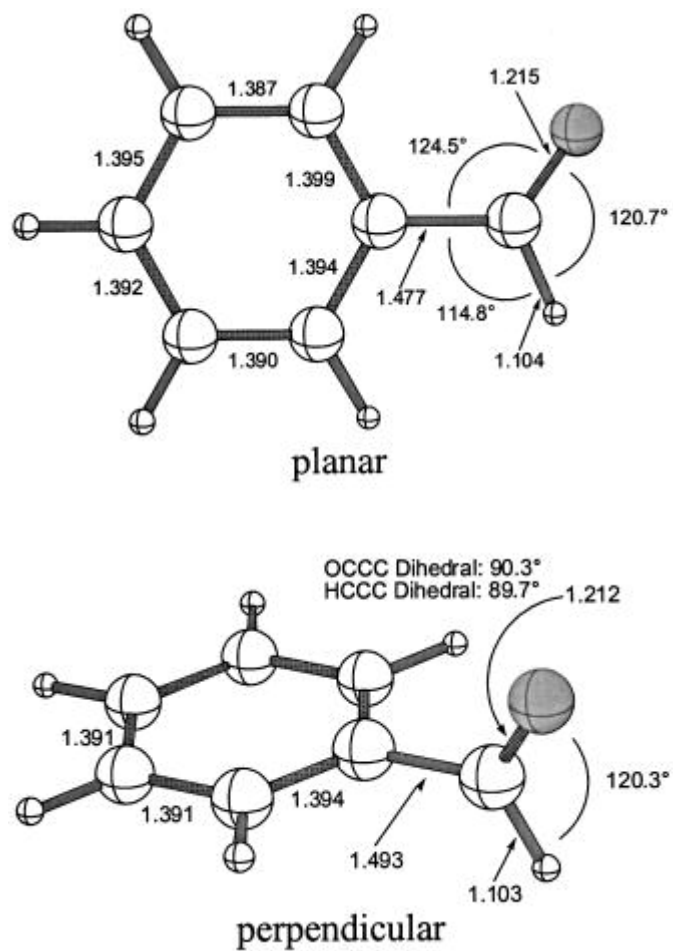


Figure 2.3. Benzaldehyde geometrical parameters. All bond distances in Angstroms.

CHAPTER 3

DOES GaH₅ EXIST? †

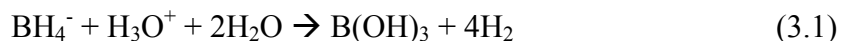
†Lucas D. Speakman, Justin M. Turney, and Henry F. Schaefer III*. *J. Chem. Phys.* **123**, 204303 (2005); doi:10.1063/1.2121588. Reprinted here with permission of publisher

3.1 ABSTRACT

The existence or nonexistence of GaH₅ has been widely discussed [N. M. Mitzel, *Angew. Chem. Int. Ed.* 42, 3856 (2003)]. Seven possible structures for gallium pentahydride have been systematically investigated using *ab initio* electronic structure theory. Structures and vibrational frequencies have been determined employing self-consistent field, coupled cluster including all single and double excitations (CCSD), and CCSD with perturbative triples levels of theory, with at least three correlation-consistent polarized-valence-(cc-pVXZ and aug-cc-pVXZ) type basis sets. The \tilde{X}^1A' state for GaH₅ is predicted to be weakly bound complex 1 between gallane and molecular hydrogen, with C_s symmetry. The dissociation energy corresponding to GaH₅→GaH₃+H₂ is predicted to be $D_e = 2.05 \text{ kcal mol}^{-1}$. The H–H stretching fundamental is predicted to be $\nu = 4060 \text{ cm}^{-1}$, compared to the tentatively assigned experimental feature of Wang and Andrews [*J. Phys. Chem. A* 107, 11371 (2003)] at 4087 cm^{-1} . A second C_s structure 2 with nearly equal energy is predicted to be a transition state, corresponding to a 90° rotation of the H₂ bond. Thus the rotation of the hydrogen molecule is essentially free. However, hydrogen scrambling through the C_{2v} structure 3 seems unlikely, as the activation barrier for scrambling is at least 30 kcal mol^{-1} higher in energy than that for the dissociation of GaH₅ to GaH₃ and H₂. Two additional structures consisting of GaH₃ with a dihydrogen bond perpendicular to gallane (C_{3v} structure 4) and an in-plane dihydrogen bond [$C_s(\text{III})$ structure 5] were also examined. A C_{3v} symmetry second-order saddle point has nearly the same energy as the GaH₃+H₂ dissociation limit, while the $C_s(\text{III})$ structure 5 is a transition structure to the C_{3v} structure. The C_{4v} structure 6 and the D_{3h} structure 7 are much higher in energy than GaH₃+H₂ by 88 and $103 \text{ kcal mol}^{-1}$, respectively.

3.2 INTRODUCTION

Early research on pentahydride type molecules began in 1961 when Davis, Bromels, and Kibby¹ studied the hydrolysis of NaBH_4^- through the general acid reaction:



They observed an inverse hydrogen/deuterium kinetic isotope effect and concluded that a pentacoordinate activated complex may be involved in the rate-determining step of hydrolysis. In the following year, Mesmer and Jolly² experimentally confirmed the existence of a pentacoordinate activated complex, since the hydrolysis of BD_4^- yielded HD, H_2 , and D_2 . Mesmer and Jolly proposed BH_5 as the pentacoordinated complex. Eleven years later, Kreevoy and Hutchins³ suggested a BH_5 intermediate structure similar to the known equilibrium structure of CH_5^+ ; see Figure 3.1. An excellent recent review of the CH_5^+ saga has been given by Borman.⁴ Olah, Westerman, Mo, and Klopman⁵ were the first to theoretically investigate BH_5 in this arrangement. Olah reported that large quantities of H_2 were formed in the nonaqueous solvolysis and proposed hydrogen scrambling in BH_5 prior to dissociation. Since then, there has been much discussion concerning the stability of BH_5 . In 1994, Tague and Andrews⁶ reported the first and only experimental detection of BH_5 via a cryogenic argon matrix study with fundamental frequencies of 2475.2 and 1134.3 cm^{-1} .

Schreiner, Schaefer, and Schleyer^{7,8} thoroughly investigated both BH_5 and AlH_5 to determine their stability and possible hydrogen scrambling effects. The ground state for BH_5 was found to be a C_s structure, a pentahydride molecule comprised of nearly planar borane with dihydrogen out of the plane ($\text{BH}_3 \cdots \text{H}_3$ midpoint distance is 1.5 Å) and parallel to a B-H bond; An analogous structure is found for alane but the $\text{AlH}_3\text{-H}_2$ midpoint distance is 2.3 Å away. The C_s (II) **2** transition structure was nearly degenerate, allowing essentially free rotation of the H_2 σ

molecule. The C_{4v} and D_{3h} saddle-points were reported to have much higher energies, and hydrogen scrambling via the C_{2v} transition state was unlikely (especially for AlH_5), since the latter transition states lie $2.8 \text{ kcal mol}^{-1}$ and $24.6 \text{ kcal mol}^{-1}$, respectively, higher than the dissociation energies of BH_5 and AlH_5 . At room temperature both molecules would dissociate into XH_3 and H_2 ($X = \text{B}$ and Al). However, at absolute zero, BH_5 and AlH_5 complexes would form exothermically, by $1.4 \text{ kcal mol}^{-1}$ and $1.7 \text{ kcal mol}^{-1}$, respectively. The most recent and definitive theoretical work on BH_5 was conducted by Schuurman, Allen, Schleyer, and Schaefer⁹ using cc-p(C)VXZ ($X=2-6$) basis sets, explicitly correlated R_{12} methods, coupled-cluster theory including quadruple excitations (CCSDTQ), and a focal point analysis. Their results confirmed Schreiner's⁷ previous results with a $D_0 = 1.2 \text{ kcal mol}^{-1}$ and barrier height of $4.2 \text{ kcal mol}^{-1}$ to the C_{2v} transition state responsible for hydrogen scrambling.

With BH_5 and AlH_5 systematically investigated for possible hydrogen scrambling through the C_{2v} structure, the question of the existence of gallium pentahydride, GaH_5 , remains. This question has been discussed in a prominent recent review by Mitzel.¹⁰ Recently, Wang and Andrews assigned a GaH_5 fundamental in their infrared matrix isolation spectra¹¹ to their observed feature of 4087 cm^{-1} . They also carried out Density Functional Theory (DFT) computations with the B3LYP/6-311++G(d,p) method and predicted a 4424 cm^{-1} harmonic vibrational frequency for the H_2 stretch.¹² Their DFT geometry for the C_s ground state reports 2.477 \AA for the GaH_3 to H_2 separation, 0.743 \AA for the H_2 bond distance, and 1.577 \AA for the GaH_3 bond lengths.

Although GaH_5 is a recent target for experimental research, the gallane (GaH_3) and the tetrahydridogallate anion (GaH_4^-) have been carefully examined experimentally and theoretically. The first theoretical investigation of GaH_3 was reported in 1970 by Stevenson and

Lipscomb.¹³ They predicted a gallane structure with D_{3h} symmetry with Hartree-Fock (HF) bond distances of 1.551 Å. Since then, Balasubramanian has performed Complete Active Space Self Consistent Field (CASSCF) and Second Order Configuration Interaction (SOC) computations to obtain 1.58 and 1.56 Å Ga-H bond distances, respectively.¹⁴ Duke employed Second Order Møller-Plesset theory (MP2) with the 3-21G* basis set to yield a 1.594 Å Ga-H distance¹⁵ while Schwerdtfeger, Heath, Dolg, and Bennett carried out Quadratic Configuration Interaction (QCI) study to obtain a 1.586 Å Ga-H bond length using a contracted Dunning (15s/11p/6d)/[11s8p/4d] basis set.¹⁶ Since Schwerdtfeger's study, there have been other theoretical studies on gallane.^{17,18} In 1994, Pullumbi, Bouteiller, Manceron, and Mijoule¹⁹ experimentally recorded the infrared (IR) spectrum of GaH₃ in solid argon and also made theoretical predictions with coupled cluster theory, CCSD(T). Experimentally, they recorded IR features at 1923, 759, and 717 cm⁻¹ while their theoretical predictions were 1897, 1891, 759, and 705 cm⁻¹.¹⁹ The most recent experimental and theoretical work was conducted by Wang and Andrews in 2003.¹¹ Their IR matrix isolation study led to experimental fundamentals of 1929, 758, and 719 cm⁻¹ while their DFT work at the B3LYP/6-311++G(d,p) level led to predicted frequencies at 1981, 1977, 763, and 722 cm⁻¹. Their DFT geometry was of D_{3h} symmetry with Ga-H bond distances of 1.567 Å.¹¹

Tetrahydridogallate was first reported experimentally in 1973 by Shirk and Shriver²⁰ through the Raman and IR spectra of GaH₄⁻ salts. They recorded Raman frequencies (from solid KGaH₄) of 1799, 1774, 1724, 830, and 765 cm⁻¹ while their study of NaGaH₄ led to observed IR frequencies of 1760, 1720, and 715 cm⁻¹. Two years later, Kurbakova *et. al.* recorded GaH₄⁻ frequencies of 1752, 1700, 780, and 733 cm⁻¹ from their Raman spectroscopic study of NaGaH₄ in diglyme solution.²¹ The first theoretical study appeared in 1996 by Bühl.²² He performed

SCF and MP2 computations with the 6-31G* basis set to obtain frequencies of 1852 and 1827 cm^{-1} with bond distances of 1.642, 1.629 Å, respectively, in T_d symmetry. The most recent experimental and theoretical work on GaH_4^- is again that of Wang and Andrews.¹¹ Their experiments yielded GaH_4^- frequencies at 1774 and 1766 cm^{-1} while their predicted DFT, B3LYP/6-311++G(d,p), frequencies were 1762, 1684, 782 and 730 cm^{-1} . Wang and Andrew's theoretical geometry displayed T_d symmetry with bond distances of 1.623 Å.¹¹

In the present study the global minimum of GaH_5 along with six other stationary points have been systematically studied using correlated methods available in our laboratory. This study also included GaH_3 and H_2 for the evaluation of dissociation energies. GaH_4^- was also examined to predict the deprotonation energy of GaH_5 .

3.3 COMPUTATIONAL PROCEDURES

Seven possible structures for gallium pentahydride (GaH_5) were optimized and their vibrational frequencies computed. In addition, tetrahydridogallate (GaH_4^-), gallium trihydride (GaH_3), and molecular hydrogen were also structurally optimized.

The three basis sets employed were the correlation consistent polarized valence basis sets developed by Dunning and coworkers^{23,24} denoted cc-pVXZ (X = D, T, Q). Augmented basis sets were used for determining the deprotonation energy of GaH_5 and a more definitive dissociation energy (GaH_5 C_s (I) **1**, GaH_4^- , GaH_3 , and H_2 structures).^{23,24} The largest basis set, aug-cc-pVQZ, consists of 323 contracted Gaussian functions for the GaH_5 structures. Geometries were fully optimized with each basis set and level of theory. Harmonic vibrational frequencies were evaluated using analytic methods when available, and otherwise determined through numerical differentiation of gradients for total energies.

The zeroth-order descriptions for all structures of GaH₅, GaH₄⁻, GaH₃, and H₂ were obtained using single configuration SCF (restricted Hartree-Fock, RHF) wave functions. Correlation effects were included using the coupled cluster method with single and double excitations (CCSD) and CCSD with perturbative triples [CCSD(T)] levels of theory. In the correlated procedures, fourteen core orbitals (28 electrons) were frozen for gallium. The MOLPRO²⁵⁻³³ *ab initio* program package was utilized during this study. All values reported refer to the cc-pVQZ CCSD(T) results unless otherwise stated.

3.4 RESULTS AND DISCUSSION

Tables 3.1, 3.2, and 3.5 present total energies, relative and structure's **1** dissociation energies, and vibrational frequencies for the GaH₅ transition structures, respectively, at the cc-pVXZ (X = D, T, and Q) basis sets. Table 3.3 includes GaH₅, GaH₄⁻, GaH₃, and H₂ total energies, predicted dissociation energies, and GaH₄⁻ proton affinities while Table 3.4 compares the vibrational frequency for GaH₅, GaH₄⁻, and GaH₃. The results in Tables 3.3 and 3.4 were obtained using the aug-cc-pVXZ (X = D, T, and Q) basis sets. Table 3.6 summarizes the state-of-the-art theoretical work for CH₅⁺, SiH₅⁺, GeH₅⁺, BH₅, AlH₅, and GaH₅. Figure 3.1 shows the CH₅⁺ structure while Figures 3.2 through 3.10 display the present theoretical results.

3.4.1 GEOMETRIES

The global minimum for GaH₅ was found to be the C_s (I) **1** structure (Figure 3.2 and Figure 3.3) analogous to BH₅ and AlH₅. Structure **1** consists of a nearly planar gallane attached to a weakly bound molecular hydrogen 2.5 Å (this is the Ga-H₂ midpoint distance) away. This molecular hydrogen is out of the gallane plane, but parallel to one of its Ga-H bond. It is impressive that the σ(H₂) MO interacts with the unoccupied 4p π-orbital of gallane. The three Ga-H bonds for this structure are 0.001 Å longer than those for isolated GaH₃ at the same level of

theory. The dihydrogen bond was determined to be 0.006 Å longer than that for molecular hydrogen, also at the same level of theory.

The second C_s structure **2**, (Figure 3.4), is a transition state with nearly identical geometry to the global minimum, with the exception of rotation of the hydrogen molecule by 90 degrees. This structure has a GaH bond longer by 0.0003 Å than that for gallane and a longer H₂ bond distance by 0.006 Å. The GaH₃-H₂ distance for this structure is 0.024 Å longer than that for the global minimum.

The C_{2v} transition state **3** for hydrogen scrambling (Figure 3.5) has a similar electronic structure to that of the ground state, with three sp² hybridized Ga-H bonds and an empty 4p π orbital. However, instead of the empty 4p π orbital interacting the hydrogen molecule σ -orbital, it interacts with the hydrogen s orbitals on each side with H-Ga-H angles of 36.4 degrees. These three in-plane bond distances are predicted to longer than the isolated GaH bonds in GaH₃ by 0.123, 0.123 and 0.192 Å. The two conventional Ga-H bonds separated by 137.8° were shorter than the GaH₃ bonds by 0.0221 Å.

A second-order saddle point structure **4** with C_{3v} symmetry was also found (Figure 3.6). In this structure, the three Ga-H bond and dihydrogen bonds were identical (to within 0.001 Å) to their corresponding gallane and molecular hydrogen geometries, with the very long Ga...H separation being 8.8 Å. Although Schreiner predicted an analogous very weakly associated bond for BH₅ and AlH₅, the energy of this GaH₅ structure is nearly identical (within 0.001 kcal mol⁻¹) to that of GaH₃ + H₂, unlike BH₅ and AlH₅. Therefore we do not predict **4** to be a significant structure.

The third C_s (III) **5** transition state (Figure 3.7) consists of GaH₃ with H₂ closest to one of the gallane hydrogen atoms at an angle of ~170 degrees of an H...H separation of about 3 Å. The

Ga-H bond lengths and the H-H bond length were nearly identical to their respective isolated GaH₃ and H₂ bond distances.

A sixth gallium pentahydride structure **6** (Figure 3.8) was determined to be a second-order saddle-point with a square pyramidal structure of C_{4v} symmetry. The four identical Ga-H bond lengths were 0.061 Å longer than those for isolated GaH₃. The fifth Ga-H bond is predicted to be shorter than those for GaH₃ by about 0.034 Å.

The seventh GaH₅ structure **7**, another second-order saddle-point state, is a trigonal bipyramidal structure with D_{3h} symmetry (Figure 3.9). The three equatorial Ga-H bonds were 0.054 Å longer than the normal Ga-H gallane bond lengths while the two axial bond distances were also longer, but only by 0.006 Å.

Isolated gallane (GaH₃), Figures 3.10 and 3.11, is predicted to have Ga-H bond distances of 1.585 Å with D_{3h} symmetry. GaH₃ may be characterized as having three sp² hybrid bonds with an empty 4p π -orbital. Our predicted bond distance may be compared with previous theoretical results: 1.551 (SCF)¹³, 1.58 (CASSCF)¹⁴, 1.557 (SOC1)¹⁴, 1.594 (MP2)¹⁵, 1.586 (QCISD)¹⁶, and 1.567 (B3LYP)¹¹. The QCISD bond distance of Schwerdtfeger is in almost perfect agreement with the present research.

3.4.2 ENERGETICS

Total energies for the seven structures of gallium pentahydride, gallane, and molecular hydrogen are given in Table 3.1. Relative energies for the gallium pentahydride structures are given in Table 3.2 along with dissociation energies for the global minimum GaH₅. The augmented basis set computations of dissociation and proton affinities can be found in Table 3.3.

The C_s (I) **1** and C_s (II) **2** structures are nearly degenerate, allowing essentially free rotation of the hydrogen molecule, as shown in Table 3.1. The C_{2v} transition state **3** for

hydrogen scrambling is predicted to lie more than 30 kcal mol⁻¹ above the ground state. The other two structures consisting of loosely associated GaH₃ and H₂ were also higher in energy than **1** by 1.96 (**5**) and 1.27 (**6**) kcal mol⁻¹, respectively. The *C*_{4v} **6** and *D*_{3h} **7** structures were much higher in energy relative to the ground state, by at least 70 kcal mol⁻¹. When zero-point energies are included, the *C*_s (II) **2**, *C*_{3v} **4**, and *C*_s (III) **5** structures become lower in energy than the *C*_s (I) **1** structure. However, the latter structures have imaginary vibrational frequencies, which are not counted in evaluating zero-point vibrational energies.

The *C*_s (I) **1**, *C*_s (II) **2**, and *C*_s (III) **5** structures are predicted to have *D*_e = 1.95, 1.95, and 0.21 kcal mol⁻¹, respectively. When the zero-point corrections are included, these three structures have dissociation energies *D*₀ = -0.06, -0.02, and -0.24 kcal mol⁻¹, respectively. However, at the aug-cc-pVQZ CCSD(T) basis set, has a *D*_e and *D*₀ of 2.05 and 0.11 kcal mol⁻¹. Although these numbers are stable with respect to dissociation, they remain within error of our present method. At very low temperatures, gallium pentahydride might be kinetically stable with respect to dissociation into GaH₃ and H₂. The *C*_{2v} **3**, *C*_{4v} **6**, and *D*_{3h} **7** structures are unlikely candidates for observation since they are predicted to lie 30, 69, and 84 kcal mol⁻¹ above the dissociation energy of gallium pentahydride, respectively.

The proton affinity is predicted to be 331.0 kcal mol⁻¹ which is similar to the proton affinities for BH₄⁻ (333.5 kcal mol⁻¹) and AlH₄⁻ (328.7 kcal mol⁻¹).

3.4.3 VIBRATIONAL FREQUENCIES

Prior experimental work is available with which to compare the theoretically predicted vibrational frequencies for GaH₃ and GaH₄⁻ (Table 3.4). Pullumbi *et. al.*¹⁹ performed IR matrix isolation experiments on gallane, while Shirk and Shriver²⁰ and Kurbakova *et. al.*²¹ carried out

vibrational analyses of tetrahydrogallate salts. The theoretically predicted and experimentally determined frequencies are in close agreement, as shown in Table 3.4.

For GaH₅, the predicted harmonic vibrational frequency for the H₂ stretching is 230 cm⁻¹ higher than Wang and Andrews' assignment. However, the experimental H₂ anharmonicity correction accounts for this difference. The general equation for a harmonic frequency evaluation is

$$\nu = G(\nu) = \omega_e \left(\nu + \frac{1}{2}\right) - \omega_e x_e \left(\nu + \frac{1}{2}\right)^2 + \omega_e y_e \left(\nu + \frac{1}{2}\right)^3 + \omega_e z_e \left(\nu + \frac{1}{2}\right)^4 + \dots \quad (3.1)$$

Setting $\nu = 1$ and $\nu = 0$ and taking their difference

$$G(1) - G(0) \cong \omega_e - 2\omega_e x_e + \frac{26}{8}\omega_e y_e \quad (3.2)$$

Then using the following experimental data, $\omega_e = 4401.2 \text{ cm}^{-1}$ ³⁴, $\omega_e x_e = 121.3$ ³⁴, and $\omega_e y_e = 0.81$ ³⁴ yields the experimental fundamental frequency for molecular hydrogen to be $\nu = 4161 \text{ cm}^{-1}$.³⁵

If we apply the same anharmonic correction to our own H₂ computations with aug-cc-pVQZ CCSD(T) level of theory, $\omega_e = 4399 \text{ cm}^{-1}$, we predict fundamental frequency of H₂ to be 4157 cm⁻¹, which is very close to the experimental value. If the same experimental anharmonic correction is applicable to GaH₅, then the theoretical value should be much closer to experiment. The theoretical frequency for the GaH₅ molecular hydrogen stretching frequency including this anharmonic correction is 4063 cm⁻¹, only 24 cm⁻¹ lower than the Wang and Andrews¹¹ assigned frequency for the H₂GaH₃ complex.

Table 3.5 reports the harmonic vibrational frequencies of the GaH₅ transition structures. An analysis of the imaginary vibrational frequencies of the six GaH₅ structures was conducted. As expected, the C_{2v} **3** structure's imaginary frequency corresponds to the normal mode for

hydrogen scrambling. The imaginary vibrational mode of this third structure corresponds to the breaking of the H_a-H_b bond and the formation of another bond between H_b-H_c, resulting in hydrogen scrambling. The C_s (II) structure **2** has a single imaginary frequency which corresponds to the molecular hydrogen bond rotating about the GaH₃ plane.

Both imaginary vibrational frequencies for the C_{3v} structure **4** relate to molecular hydrogen rotating about GaH₃, while maintaining the long (8 Å) GaH₃···H₂ separation. The third C_s (III) structure **5** appears to be a transition state to the C_{3v} **4** structure with its imaginary frequency pulling the molecular hydrogen out of the plane and perpendicular to the GaH₃ portion of the molecule.

The higher energy structures, C_{4v} **6** and D_{3h} **7**, are predicted to have degenerate imaginary frequencies. For the C_{4v} structure **6**, the first imaginary component corresponds to motion toward C_s (I) **1**, while the second connects to the C_{2v} structure **3**. The degenerate imaginary frequency associated with the D_{3h} structure **7** relates to the two axial hydrogen atoms moving away from the rest of the molecule.

The search for group III and IV pentahydrides may now be extended to include gallium pentahydride, as shown in Table 3.6. Some general trends occur throughout the pentahydride series: rotation of the H₂ around the gallium 4pπ-orbital is unrestricted, and all molecules show a barrier to hydrogen scrambling by a C_{2v} **3** structure (except for CH₅⁺). The C_{4v} **6** and D_{3h} **7** structures are always higher in energy, and the C_{3v} structure **4** dissociates for BH₅ and GaH₅.

3.5 CONCLUSIONS

Gallium pentahydride may exist as a weak complex between gallane and molecular hydrogen at very low temperatures. The C_s (I) **1** and C_s (II) **2** structures are nearly degenerate, allowing free hydrogen rotation of the H_2 bond. Both structures **1** and **2** are predicted to have dissociation energies $D_e = 1.95 \text{ kcal mol}^{-1}$ for the process $\text{GaH}_5 \rightarrow \text{GaH}_3 + \text{H}_2$. Hydrogen scrambling is unlikely to occur since the C_{2v} symmetry transition state **3** is predicted to lie 30 kcal mol^{-1} above the energy required for dissociation of GaH_5 . The H_2 fundamental vibrational frequency in structure **1** ($\text{GaH}_3 \cdots \text{H}_2$) is predicted to be $\nu = 4063 \text{ cm}^{-1}$, compared to a proposed experimental GaH_5 feature at 4087 cm^{-1} .

3.6 ACKNOWLEDGEMENTS

LDS acknowledges the Center for Computational Chemistry for the opportunity to conduct this research. The authors would also like to thank Dr. Yukio Yamaguchi for very helpful discussions and suggestions. This research was supported by the U.S. National Science Foundation, Grant CHE-0451445.

3.6 REFERENCES

- ¹ R. E. Davis, E. Bromels, and L. L. Kibby, *J. Am. Chem. Soc.* **84**, 885 (1961).
- ² R. E. Mesmer and W. L. Jolly, *J. Am. Chem. Soc.* **84**, 2039 (1962).
- ³ M. M. Kreevoy and J. E. C. Hutchins, *J. Am. Chem. Soc.* **94**, 6371 (1972).
- ⁴ S. Borman, July 25, 2005 *Chemical & Engineering News*, pages 45-48. See also B. Redlich, S. Schlemmer, and D. Marx, *Science* (2005).
- ⁵ G. A. Olah, P. W. Westerman, Y. K. Mo, and G. Klopman, *J. Am. Chem. Soc.* **94**, 7859 (1972).
- ⁶ T. J. Tague and L. Andrews, *J. Am. Chem. Soc.* **116**, 4970 (1994).

- 7 P. R. Schreiner, H. F. Schaefer, and P. R. Schleyer, *J. Chem. Phys.* **101**, 7625 (1994).
- 8 P. R. Schreiner, H. F. Schaefer, and P. R. Schleyer, *J. Chem. Phys.* **103**, 5565 (1995).
- 9 M. S. Schuurman, W. D. Allen, P. R. Schleyer, and H. F. Schaefer, *J. Chem. Phys.* **122**,
104302 (2005).
- 10 N. M. Mitzel, *Angew. Chem. Int. Ed.* **42**, 3856 (2003).
- 11 X. Wang and L. Andrews, *J. Phys. Chem. A* **107**, 11371 (2003).
- 12 L. Andrews and X. Wang, *J. Phys. Chem. A* **108**, 4202 (2004).
- 13 P. E. Stevenson and W. N. Lipscomb, *J. Chem. Phys.* **52**, 5343 (1970).
- 14 K. Balasubramanian, *Chem. Phys. Lett.* **164**, 231 (1989).
- 15 B. Duke, *J. Molec. Struct.* **208**, 197 (1990).
- 16 P. Schwerdtfeger, G. A. Heath, M. Dolg, and M. A. Bennett, *J. Am. Chem. Soc.* **114**,
7518 (1992).
- 17 Y. Cheung, N. L. Ma, and W. Li, *J. Molec. Struct.* **283**, 169 (1993).
- 18 K. A. Grencewicz and D. W. Ball, *J. Phys. Chem.* **100**, 5672 (1996).
- 19 P. Pullumbi, Y. Bouteiller, L. Manceron, and C. Mijoule, *Chem. Phys.* **185**, 25 (1994).
- 20 A. E. Shirk and D. F. Shriver, *J. Am. Chem. Soc.* **95**, 5904 (1973).
- 21 A. P. Kurbakova, L. A. Leites, V. V. Gavrilenko, Y. N. Karaksin, and L. I. Zakharkin,
Spect. Acta **31A**, 281 (1975).
- 22 M. Buhl, *Magn. Reson. Chem.* **34**, 782 (1996).
- 23 T. H. Dunning Jr., *J. Chem. Phys.* **90**, 1007 (1989).
- 24 A. K. Wilson, D. E. Woon, K. A. Peterson, and T. H. Dunning, *J. Chem. Phys.* **110**, 7667
(1999).

- 25 R. D. Amos, A. Bernhardsson, A. Berning, P. Celani, D. L. Cooper, M. J. O. Deegan, A.
J. Dobbyn, F. Eckert, C. Hampel, G. Hetzer, P. J. Knowles, T. Korona, R. Lindh, A. W.
Lloyd, S. J. McNicholas, F. R. Manby, W. Meyer, M. E. Mura, A. Nicklass, P. Palmieri,
R. Pitzer, G. Rauhut, M. Schutz, U. Schumann, H. Stoll, A. J. Stone, R. Tarroni, T.
Thorsteinsson, and H. J. Werner, *MOLPRO* (2002).
- 26 M. J. O. Deegan and P. J. Knowles, *Chem. Phys. Lett.* **227**, 321 (1994).
- 27 C. Hampel, K. A. Peterson, and H. J. Werner, *Chem. Phys. Lett.* **190**, 1 (1992).
- 28 C. Hampel and H. J. Werner, *J. Chem. Phys.* **104**, 6286 (1996).
- 29 R. Lindh, *Theor. Chim. Acta* **85**, 423 (1993).
- 30 R. Lindh, U. Ryu, and B. Liu, *J. Chem. Phys.* **95**, 5889 (1991).
- 31 G. Rauhut, A. E. Azhary, F. Eckert, U. Schumann, and H. J. Werner, *Spectrochim. Acta A*
55, 651 (1999).
- 32 M. Schutz, *J. Chem. Phys.* **113**, 9986 (2000).
- 33 M. Schutz and H. J. Werner, *Chem. Phys. Lett.* **318**, 370 (2000).
- 34 K. P. Huber and G. Herzberg, *Molecular Spectra and Molecular Structure IV. Constants*
of Diatomic Molecules. (Van Nostrand Reinhold Company Inc., New York, 1979).
- 35 D. K. Veirs and G. M. Rosenblatt, *J. Mol. Spec.* **121**, 401 (1987).
- 36 S. G. Lias, J. E. Bartmess, J. F. Liebmann, J. L. Holmes, R. D. Levin, and W. G. Mallard,
J. Phys. Chem. Ref. Data **17**, 1 (1988).
- 37 J. C. Traeger and R. G. Loughlin, *J. Am. Chem. Soc.* **103**, 3647 (1981).

Table 3.1. Total energies (in hartrees) and zero-point vibrational energy (ZPVE) (in kcal mol⁻¹) for the seven structures of GaH₅ plus GaH₃ and H₂.

Level of Theory	C _s (I) 1	C _s (II) 2	C _{2v} 3	C _{3v} 4	C _s (III) 5	C _{4v} 6	D _{3h} 7	GaH ₃	H ₂
Imaginary	0	1	1	2	1	2	2		
cc-pVDZ SCF	-1926.057779	-1926.057779	-1925.995307	-1926.057043	-1926.057117	-1925.908564	-1925.867299	-1924.928304	-1.128746
ZPVE	19.80	19.80	21.55	18.64	18.64	18.26	17.34	12.09	6.55
cc-pVTZ SCF	-1926.135007	-1926.135006	-1926.071861	-1926.134338	-1926.134425	-1925.983961	-1925.941597	-1925.001356	-1.132990
ZPVE	19.73	19.74	21.48	18.60	18.60	18.22	17.25	12.04	6.56
cc-pVQZ SCF	-1926.139498	-1926.139497	-1926.076446	-1926.138740	-1926.138823	-1925.988358	-1925.946084	-1925.005254	-1.133495
ZPVE	19.75	19.75	21.52	18.62	18.62	18.25	17.27	12.07	6.55
cc-pVDZ CCSD	-1926.193376	-1926.193377	-1926.144426	-1926.191278	-1926.191500	-1926.074992	-1926.049702	-1925.027611	-1.163673
ZPVE	19.78	19.73	20.78	17.88	17.87	16.98	16.49	11.61	6.26
cc-pVTZ CCSD	-1926.290538	-1926.290538	-1926.240841	-1926.288115	-1926.288403	-1926.172239	-1926.143562	-1925.115784	-1.172337
ZPVE	19.83	19.79	20.65	17.90	18.11	17.53	16.16	11.59	6.30
cc-pVQZ CCSD	-1926.300434	-1926.300434	-1926.251060	-1926.297722	-1926.298014	-1926.182635	-1926.154097	-1925.123931	-1.173796
ZPVE	19.85	19.81	20.67	17.90	17.90	17.45	16.02	11.61	6.29
cc-pVDZ CCSD(T)	-1926.194750	-1926.194750	-1926.147395	-1926.192473	-1926.192720	-1926.080165	-1926.056313	-1925.028806	-1.163673
ZPVE	19.78	19.74	20.68	17.84	17.83	16.75	16.29	11.57	6.26
cc-pVTZ CCSD(T)	-1926.292540	-1926.292540	-1926.244831	-1926.289786	-1926.290115	-1926.179062	-1926.152011	-1925.117455	-1.172337
ZPVE	19.85	19.81	20.54	17.86	18.30	17.30	15.87	11.55	6.30
cc-pVQZ CCSD(T)	-1926.302707	-1926.302707	-1926.255441	-1926.299591	-1926.299934	-1926.190058	-1926.163187	-1925.125800	-1.173796
ZPVE	19.87	19.84	20.55	17.86	18.07	17.21	15.94	11.57	6.29

Table 3.2. Relative and ZPVE corrected energies (in kcal mol⁻¹) with respect to \tilde{X}^1A' GaH₅ including its dissociation energy. The number of imaginary frequencies per structure are also included at the cc-pVQZ CCSD(T) level of theory.

Basis Set	Theory	C _s (I) 1	C _s (II) 2	C _{2v} 3	C _{3v} 4	C _s (III) 5	C _{4v} 6	D _{3h} 7	D _e	D ₀
Imaginary		0	1	1	2	1	2	2		
cc-pVDZ	SCF	0.00	0.00	39.20	0.46	0.42	93.63	119.53	0.46	
	ZPVE	0.00	0.00	40.96	-0.69	-0.74	92.10	117.07		-0.70
cc-pVTZ	SCF	0.00	0.00	39.62	0.42	0.37	94.78	121.37	0.41	
	ZPVE	0.00	0.00	41.37	-0.71	-0.77	93.27	118.88		-0.72
cc-pVQZ	SCF	0.00	0.00	39.57	0.48	0.42	94.84	121.37	0.47	
	ZPVE	0.00	0.00	41.33	-0.65	-0.71	93.34	118.89		-0.66
cc-pVDZ	CCSD	0.00	0.00	30.72	1.32	1.18	74.29	90.16	1.31	
	ZPVE	0.00	-0.05	31.72	-0.59	-0.73	71.49	86.87		-0.59
cc-pVTZ	CCSD	0.00	0.00	31.19	1.52	1.34	74.23	92.23	1.52	
	ZPVE	0.00	-0.04	32.01	-0.41	-0.38	71.93	88.55		-0.42
cc-pVQZ	CCSD	0.00	0.00	30.98	1.70	1.52	73.92	91.83	1.70	
	ZPVE	0.00	-0.04	31.81	-0.24	-0.43	71.52	88.00		-0.25
cc-pVDZ	CCSD(T)	0.00	0.00	29.72	1.43	1.27	71.90	86.87	1.43	
	ZPVE	0.00	-0.05	30.62	-0.52	-0.68	68.87	83.38		-0.52
cc-pVTZ	CCSD(T)	0.00	0.00	29.94	1.73	1.52	71.21	88.18	1.72	
	ZPVE	0.00	-0.04	30.63	-0.26	-0.02	68.66	84.20		-0.27
cc-pVQZ	CCSD(T)	0.00	0.00	29.66	1.96	1.74	70.69	87.55	1.95	
	ZPVE	0.00	-0.03	30.34	-0.05	-0.06	68.03	83.62		-0.06

Table 3.3. Total energies (in hartrees), zero-point vibrational energy (ZPVE), dissociation energies of GaH₅, and proton affinities for GaH₅, GaH₄⁻, GaH₃, and H₂ with augmented basis sets (in kcal mol⁻¹).

Level of Theory		GaH ₅	GaH ₄ ⁻	GaH ₃	H ₂	D _e	D ₀	PA _e	PA ₀
aug-cc-pVDZ	SCF	-1926.058800	-1925.522668	-1924.929172	-1.128826	0.50		336.43	
	ZPVE	19.75	15.39	12.06	6.52		-0.67		332.06
aug-cc-pVTZ	SCF	-1926.135460	-1925.596668	-1925.001622	-1.133056	0.49		338.10	
	ZPVE	19.72	15.38	12.03	6.56		-0.64		333.76
aug-cc-pVQZ	SCF	-1926.139560	-1925.600635	-1925.005293	-1.133509	0.48		338.18	
	ZPVE	19.75	15.44	12.07	6.55		-0.65		333.88
aug-cc-pVDZ	CCSD	-1926.200633	-1925.667147	-1925.033044	-1.164899	1.69		334.77	
	ZPVE	19.62	14.79	11.51	6.21		-0.21		329.94
aug-cc-pVTZ	CCSD	-1926.293119	-1925.756624	-1925.117676	-1.172636	1.76		336.66	
	ZPVE	19.77	14.84	11.55	6.29		-0.16		331.73
aug-cc-pVQZ	CCSD	-1926.301126	-1925.764604	-1925.124419	-1.173867	1.78		336.67	
	ZPVE	0.00	14.94	11.59	6.29		19.66		351.61
aug-cc-pVDZ	CCSD(T)	-1926.202297	-1925.669715	-1925.034425	-1.164899	1.87		334.20	
	ZPVE	19.62	14.73	11.47	6.21		-0.08		329.31
aug-cc-pVTZ	CCSD(T)	-1926.295302	-1925.759962	-1925.119459	-1.172636	2.01		335.93	
	ZPVE	19.79	14.78	11.51	6.29		0.03		330.93
aug-cc-pVQZ	CCSD(T)	-1926.303469	-1925.768184	-1925.126328	-1.173867	2.05		335.90	
	ZPVE	0.00	14.87	11.55	6.29		19.89		350.77

Table 3.4. Harmonic vibrational frequencies (in cm^{-1}) for the ground electronic states of GaH_5 , GaH_4^- , and GaH_3 at the aug-cc-pVQZ CCSD(T) level of theory. Experimental results are fundamental frequencies.

Species	GaH_5			GaH_4^-				GaH_3				
		QZ CCSD(T)	Exp ¹¹		QZ CCSD(T)	Exp ¹¹	Exp ²⁰	Exp ²¹	QZ CCSD(T)	Exp ¹⁹	Exp ¹¹	
Vibrational frequencies	a'	4303	4087	a_1	1743	1774	1760	1752	a_1'	1962	1923	1929
	a'	1961		e	764			780	a_2''	703	717	719
	a'	1947		t_2	1654	1766	1720	1700	e'	1953		
	a'	755		t_2	723		715	733	e'	759	759	758
	a'	705										
	a'	626										
	a'	317										
	a'	252										
	a''	1951										
	a''	755										
	a''	326										
	a''	110										

Table 3.5. Harmonic vibrational frequencies for GaH₅ transition structures at the cc-pVQZ CCSD(T) level of theory (in cm⁻¹).

<i>C_s</i> (II) 2	<i>C_{2v}</i> 3	<i>C_{3v}</i> 4	<i>C_s</i> (III) 5	<i>C_{4v}</i> 6	<i>D_{3h}</i> 7
38 <i>i</i>	1618 <i>i</i>	48 <i>i</i>	31 <i>i</i>	946 <i>i</i>	665 <i>i</i>
245	573	16 <i>i</i>	22	946 <i>i</i>	665 <i>i</i>
311	664	36	78	269	154
322	686	36	146	538	481
611	731	50	155	629	482
705	1109	703	703	630	727
755	1294	760	759	1000	727
755	1468	760	760	1681	1618
1949	1818	1953	1954	1714	1669
1949	1976	1953	1955	1714	1705
1961	2021	1962	1963	1800	1705
4071	2036	4163	4155	2063	1881

Table 3.6. Comparison of the relative energies (in kcal mol⁻¹ including ZPVE), H₂ dissociation energies (D₀), and proton affinities (PA₀) of the AH₄ species.

Geometry		CH ₅ ⁺ ^a	SiH ₅ ⁺ ^b	GeH ₅ ⁺ ^c	BH ₅ ^d	AlH ₅ ^d	GaH ₅ ^e
C _s (I)	1	0.0	0.0	0.0	0.0	0.0	0.0
C _s (II)	2	0.0	0.0	0.0	0.0	0.0	0.0
C _{2v}	3	0.2	26.9	32.7	4.2 ^f	24.6	30.3
C _{3v}	4	31.5 ^g	8.8	7.5	0.2 ^h	0.9 ⁱ	-0.1
C _{4v}	6	3.5 ^g	60.6	83.8 ^j	22.8	71.9 ^k	68.0
D _{3h}	7	11.5 ^g	82.6	48.3 ^j	45.3	84.0 ^k	83.6
D _e ^l							2.1 ^m
D ₀ ^l		42.0 ^g	10.3	10.0	1.4 ^f	1.7	0.1 ^m
PA ₀ ⁿ		130.5	153.2	156.4	333.5 ^o	328.7	331.0 ^l

^a TZ2P+f CCSD(T)//TZ2P CCSD(T), unless otherwise specified.
^b TZ2P CCSD, unless otherwise specified.
^c TZ2P+f CCSD, unless otherwise specified.
^d TZ2P(f,d) CCSD(T)//TZ2P CCSD(T), unless otherwise specified.
^e cc-pVQZ CCSD(T); this research.
^f cc-pVQZ CCSD(T) (Ref. 6).
^g QCISD(T)/6-311++G(3df,3pd)//MP2(fu)/6-311++G(2df,2pd). Experimental D₀ = 45.3 kcal mol⁻¹: ΔH_f of CH₅⁺ = 216.0 kcal mol⁻¹ (Ref. 36).
ΔH_f of CH₃⁺ = 261.3 kcal mol⁻¹ (Ref. 37).
^h Dissociates at higher levels.
ⁱ TZ2P CCSD(T).
^j DZP SCF.
^k DZP CCSD.
^l AH₅⁽⁺⁾ --> AH₃⁽⁺⁾ + H₂.
^m aug-cc-pVQZ CCSD(T); this research.
ⁿ AH₄⁽⁻⁾ + H⁺ --> AH₅⁽⁺⁾.
^o TZ(3d1f1g,2p1d) CCSD(T)/TZ(3d1f,2p1d) CCSD(T),

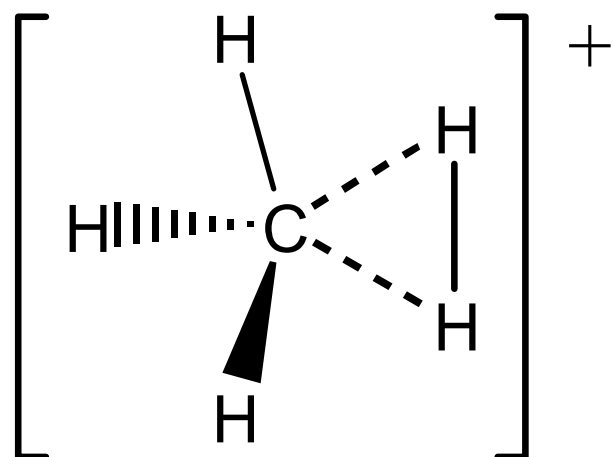


Figure 3.1. Known equilibrium geometry for CH_5^+ .

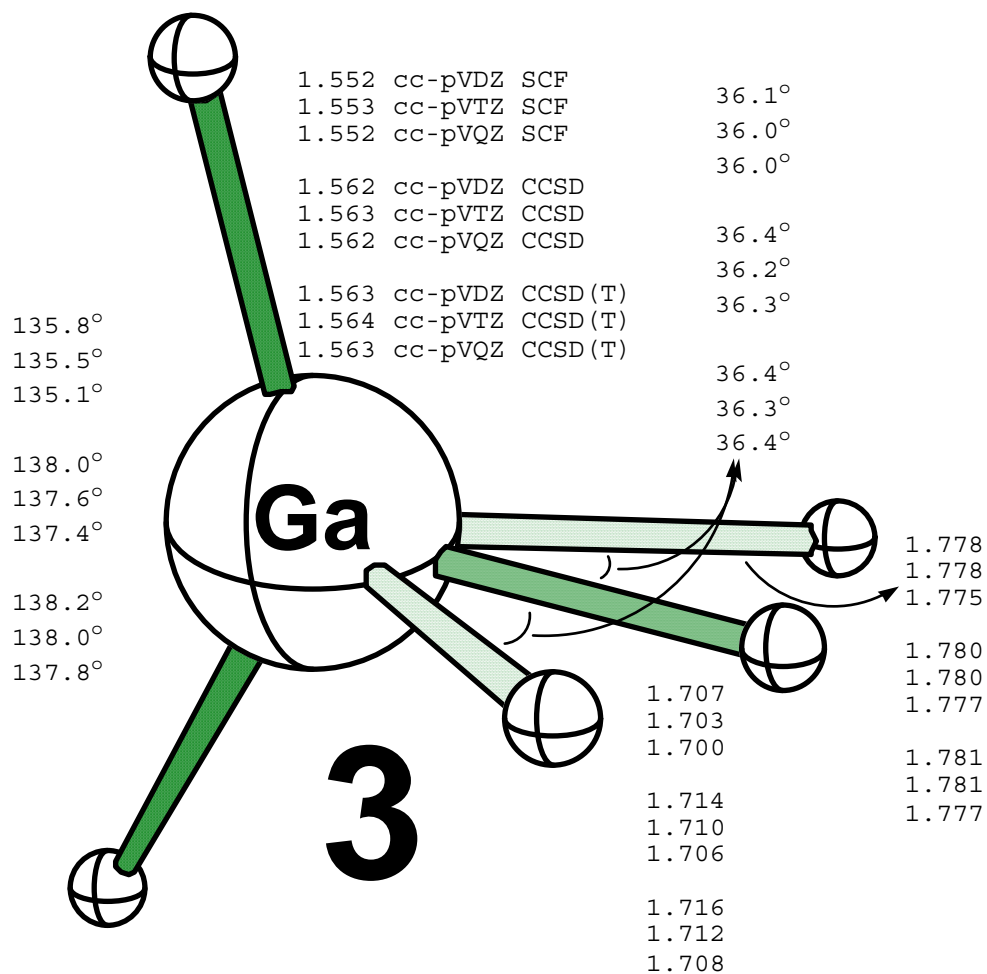


Figure 3.5. Predicted geometries for the C_{2v} transition structure **3** of GaH_5 (Bond lengths given in \AA , angles in degrees).

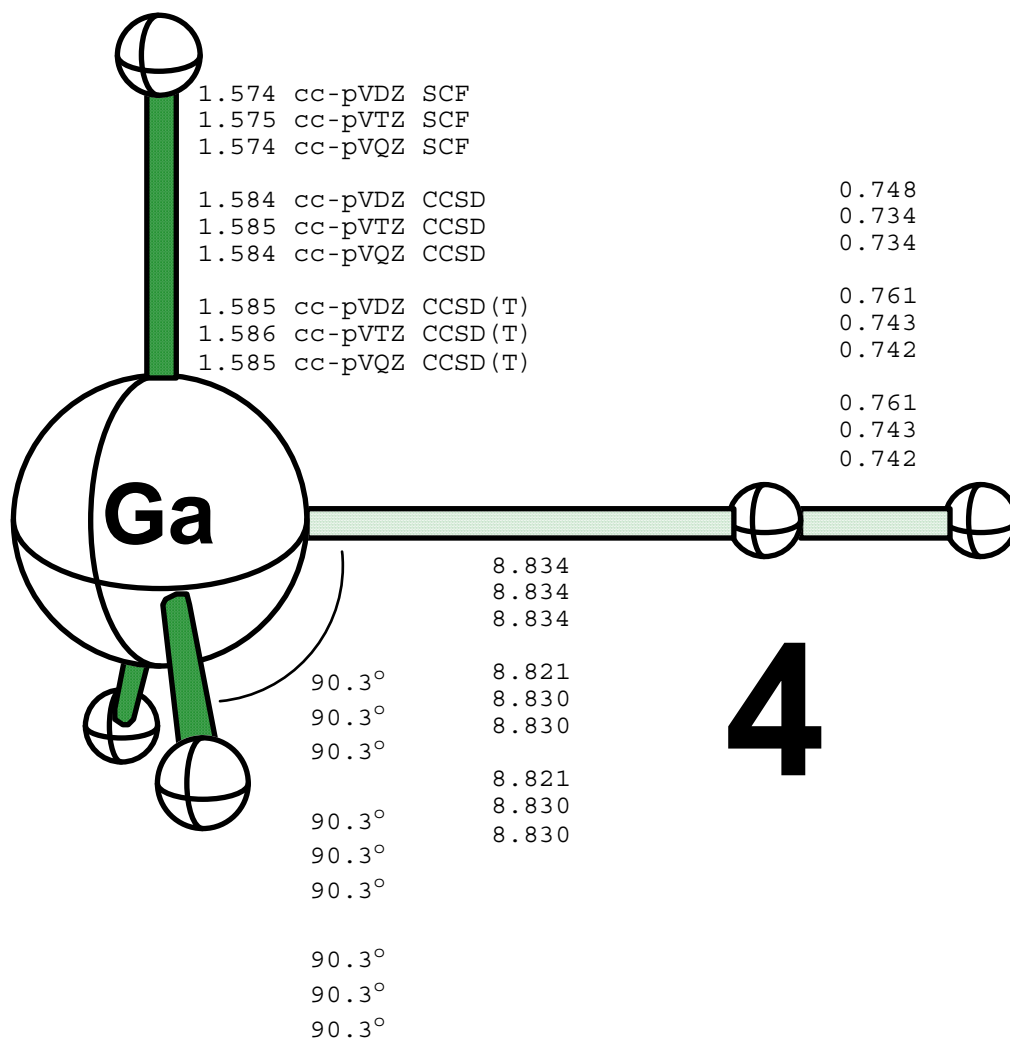


Figure 3.6. Predicted geometries for the C_{3v} second-order saddle-point structure **4** of GaH_5 (Bond lengths given in \AA , angles in degrees).

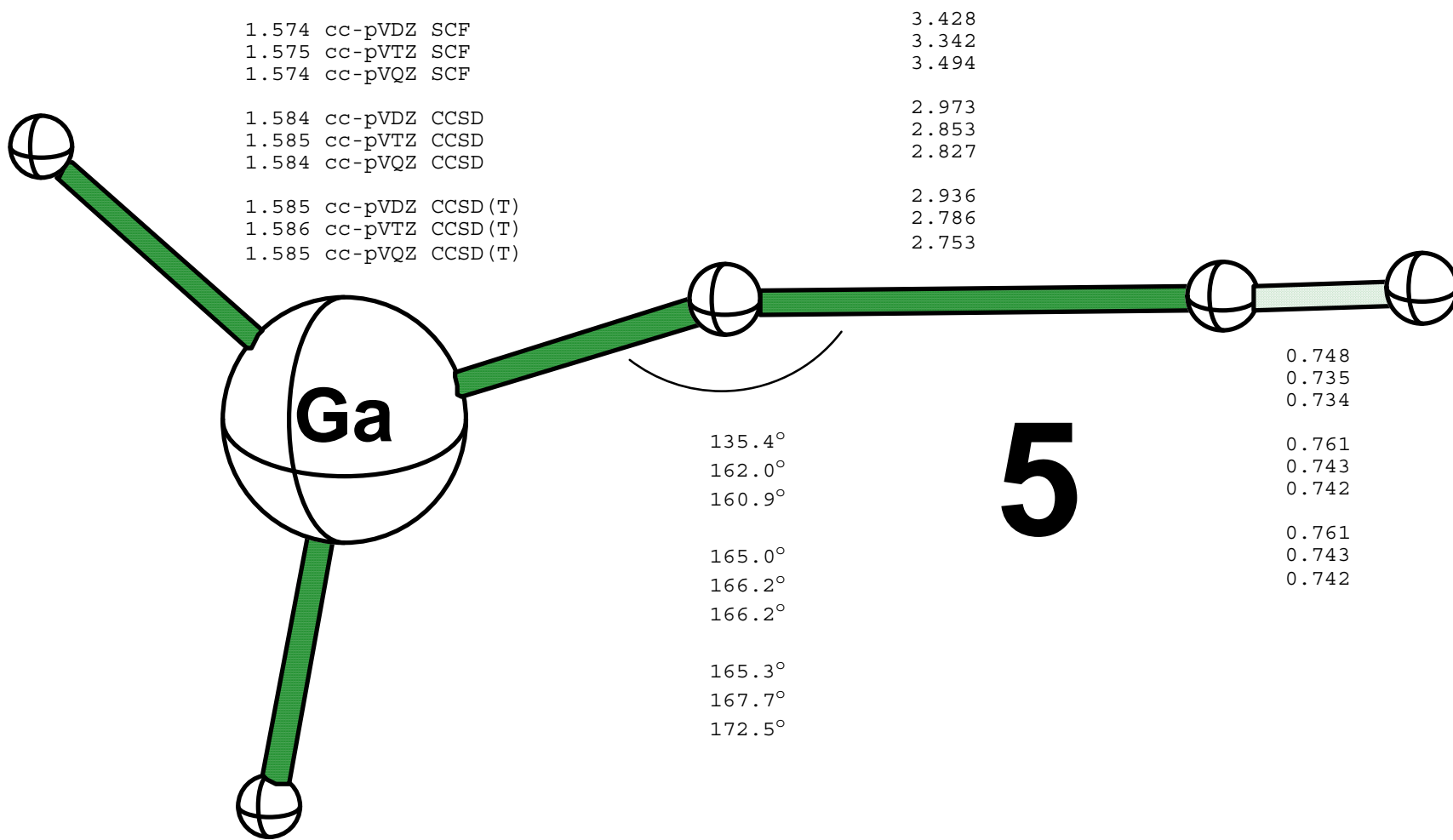


Figure 3.7. Predicted geometries for the C_s (III) transition state **5** of GaH_5 (Bond lengths given in \AA , angles in degrees).

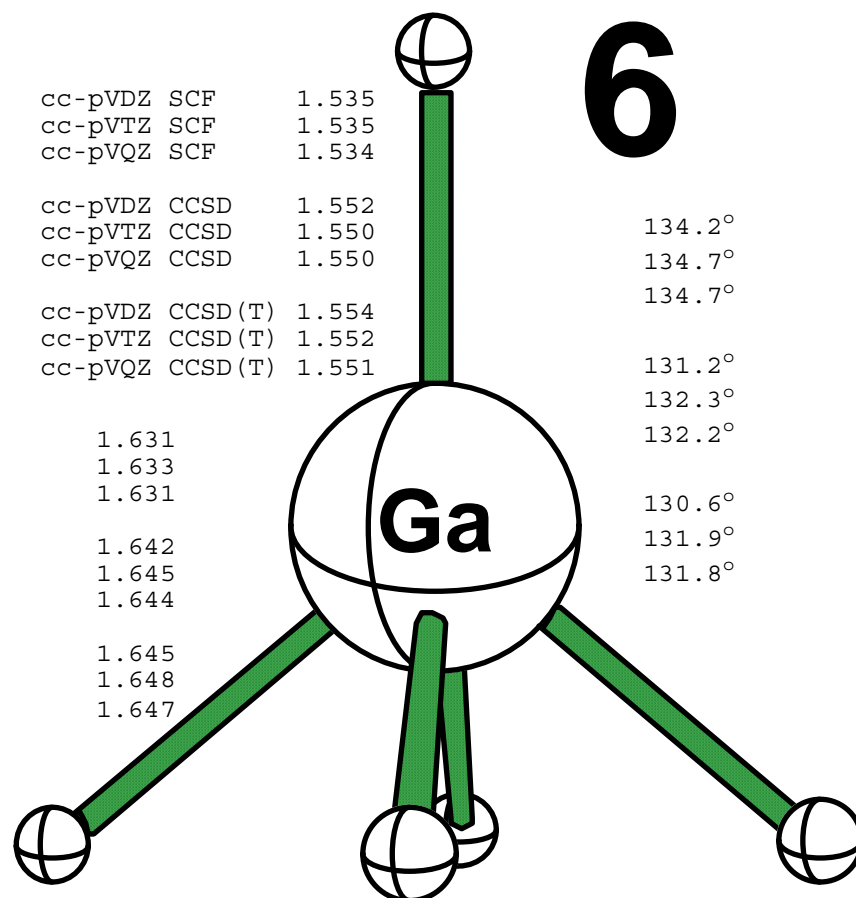


Figure 3.8. Predicted geometries for the C_{4v} second-order saddle-point structure **6** of GaH_5 (Bond lengths given in \AA , angles in degrees).

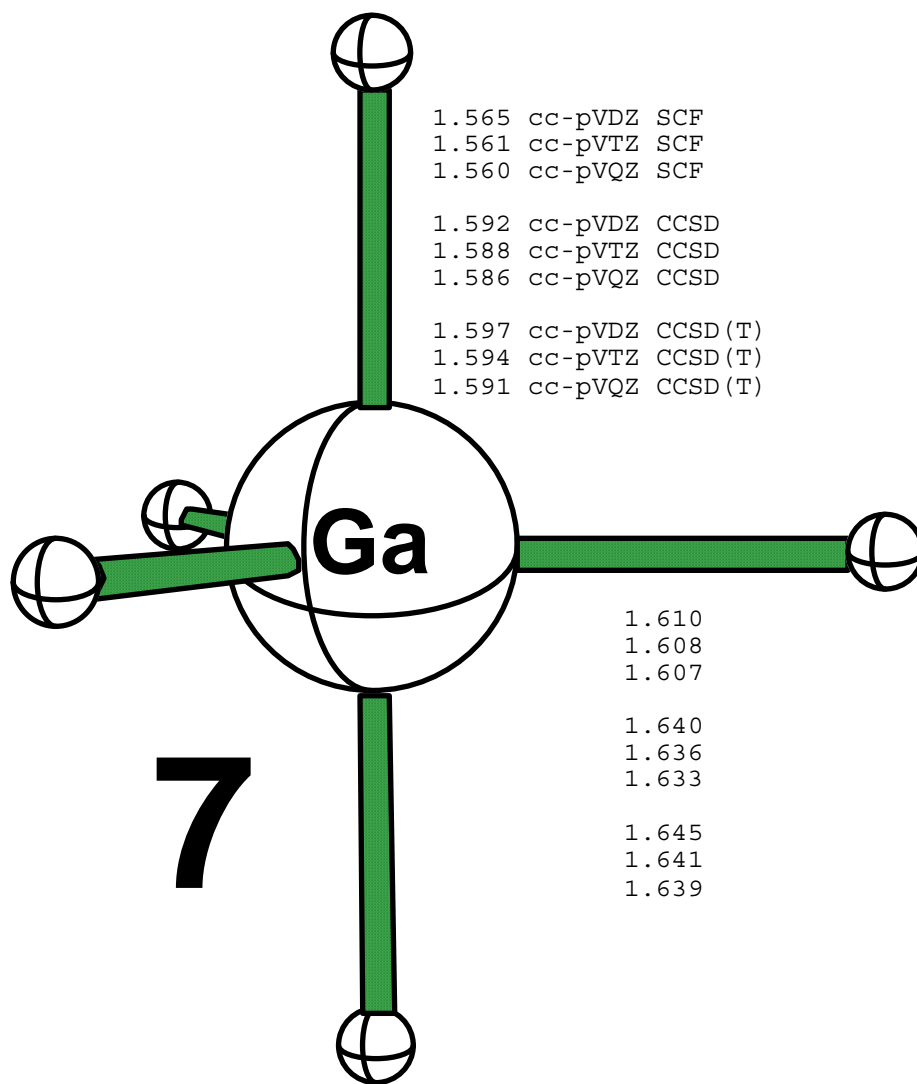


Figure 3.9. Predicted geometries for the D_{3h} second-order saddle-point structure **7** of GaH_5 (Bond lengths in given \AA).

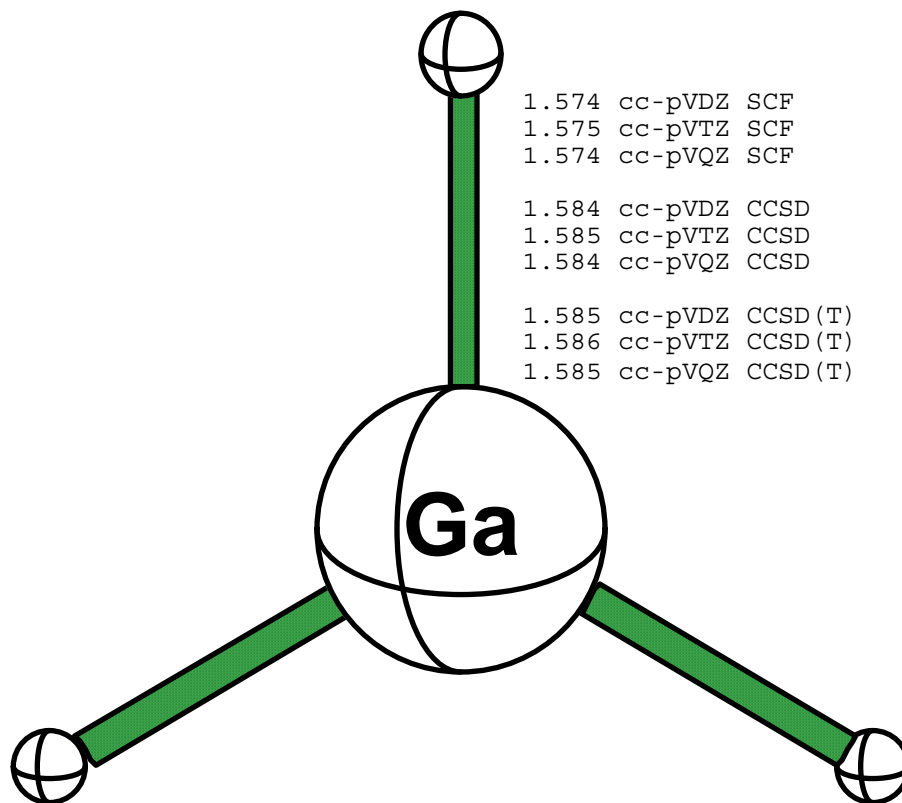


Figure 3.10. Predicted geometries for D_{3h} symmetry GaH_3 (Bond lengths given in \AA).

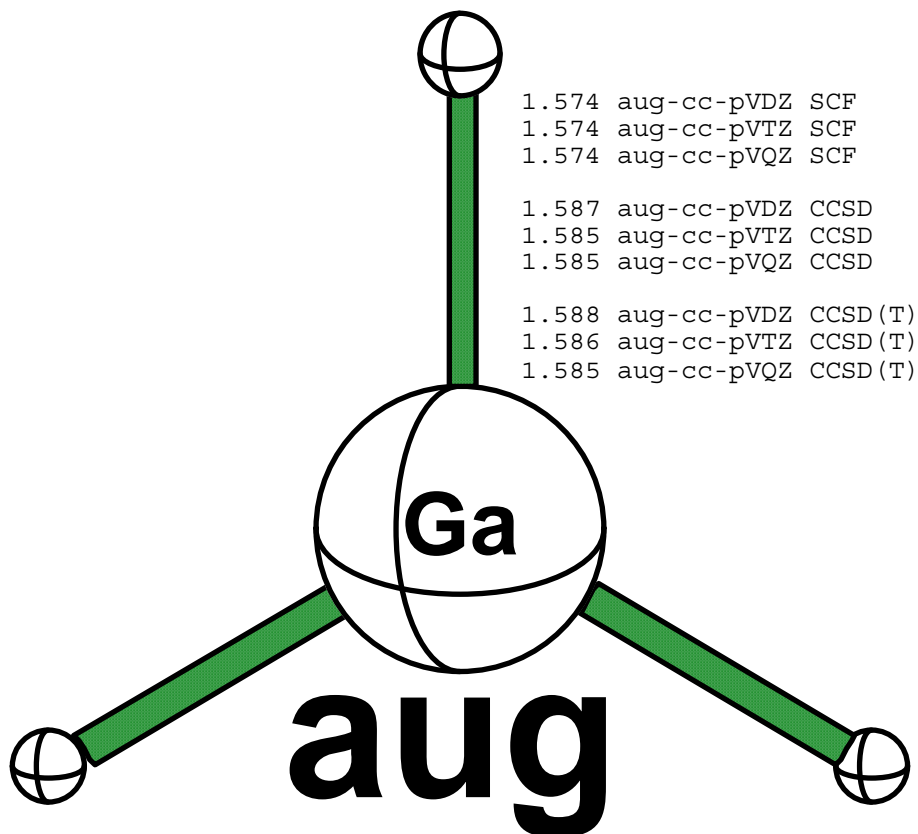


Figure 3.11. Predicted geometries for D_{3h} symmetry GaH_3 with augmented basis functions (Bond lengths given in \AA).

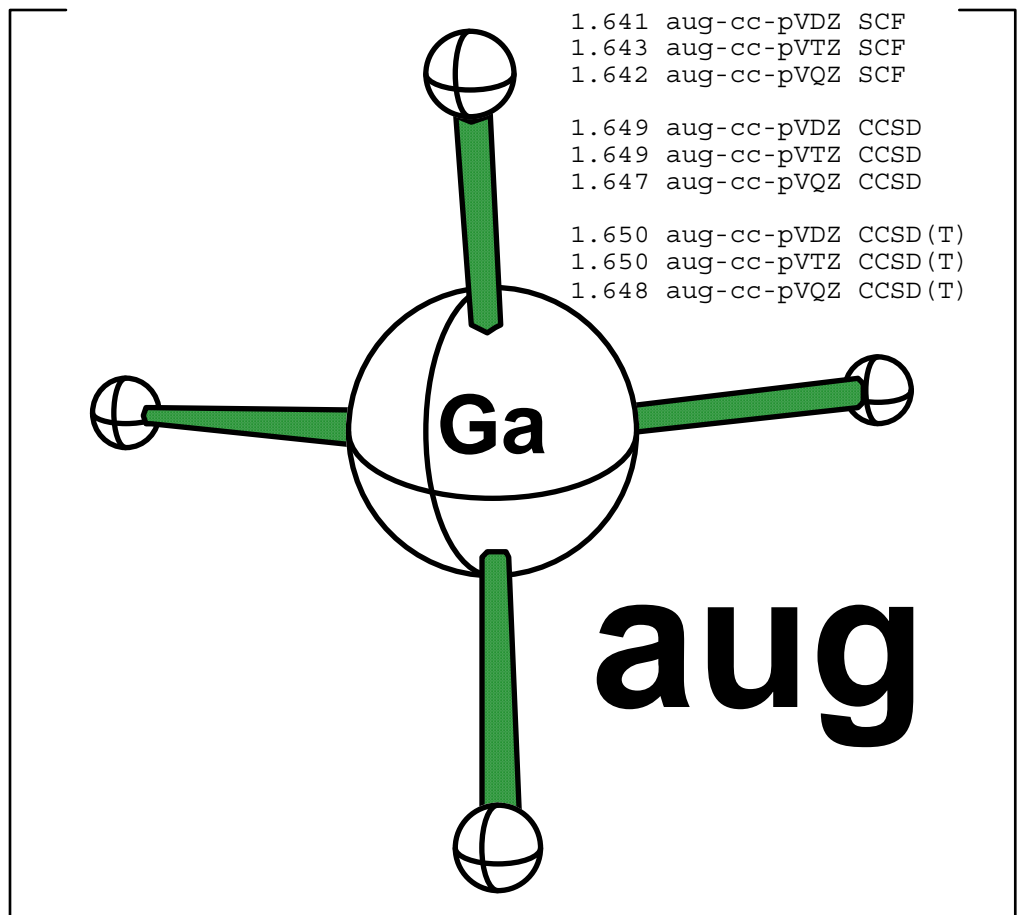


Figure 3.12. Predicted geometries for T_d symmetry GaH_4^- with augmented basis functions (Bond lengths given in \AA).

CHAPTER 4

THE DEPROTONATION ENERGIES OF BH_5 AND AlH_5 :

COMPARISONS TO GaH_5^\dagger

† Lucas D. Speakman, Justin M. Turney, and Henry F. Schaefer III. *Chem. Phys.* 331, 396 (2007); doi:10.1016/j.chemphys.2006.11.008. Reprinted here with permission of publisher.

4.1 ABSTRACT

Hypercoordinate boron is most unusual, leading to considerable theoretical and experimental research on the parent BH_5 molecule. The deprotonation energies of BH_5 and the related molecules AlH_5 and GaH_5 have been of particular interest. Here the energy differences for $\text{XH}_5 \rightarrow \text{XH}_4^- + \text{H}$ ($\text{X}=\text{B}$ and Al) are computed to be $332.4 \text{ kcal mol}^{-1}$ and $326.3 \text{ kcal mol}^{-1}$, respectively, with an aug-cc-pVQZ basis set at the CCSD(T) level of theory. Vibrational frequencies for BH_4^- and AlH_4^- are also reported as 1098, 1210, 2263, and 2284 cm^{-1} and 760, 779, 1658, and 1745 cm^{-1} , respectively, again at the CCSD(T) aug-cc-pVQZ level of theory. Comparisons with the valence isoelectronic GaH_5 molecule are made.

4.2 INTRODUCTION

Hypercoordinate is a theme of long-standing interest in chemistry¹. In particular, the synthesis of pentavalent compounds of Group 13 elements (B, Al, Ga, ...) has been a very challenging problem². The theoretical and experimental demonstration of the existence of BH_5 has been a long and arduous task since it was proposed in the early 1960s. This long search for BH_5 appears to have been successfully concluded with the recent experiments of Tague and Andrews³.

The first high level theoretical study⁴ of BH_5 appeared in 1994. That research systematically investigated multiple BH_5 structures including BH_4^- and reported the deprotonation energy of BH_5 . More recently (2005), the theoretical studies of BH_5 reached subchemical accuracy ($0.1 \text{ kcal mol}^{-1}$) in their analysis⁵ of the BH_5 stability with respect to dissociation and possible hydrogen scrambling effects through the C_{2v} structure. The results from references 4 and 5 confirm the viability of BH_5 . Perhaps most importantly, Schuurman's high

level of theory application on the C_s structure provides agreement with the two vibrational stretching modes assigned by Tague and Andrews³.

The most recent theoretical study of BH_4^- (deprotonated BH_5) is that of Dixon and Gutowski⁶. They report an aug-cc-pVTZ CCSD(T) bond distance of 1.240 Å for tetrahedral symmetry. Their harmonic vibrational frequencies were 2261, 2240, 1185, and 1086 cm^{-1} , predicted with the aug-cc-pVDZ basis set and the CCSD(T) level of theory.

Schreiner, Schaefer, and Schleyer⁷ continued their study of pentacoordinate systems with AlH_5 by examining six possible structures and predicting the global minimum to be a weak complex between alane (AlH_3) and dihydrogen with C_s symmetry, analogous to that of BH_5 ^{4,5} and GaH_5 ⁸. Moc, Bober, and Panek's⁹ recent theoretical study confirms the Schreiner *et al.* predictions. Andrews and Wang¹⁰ and Wang, Andrews, Tam, DeRose, and Fajardo¹¹ both report an experimental H-H stretching mode for AlH_5 at 4062 cm^{-1} , which agrees with Schreiner's predicted frequency⁷ of 4082 cm^{-1} . Andrews and Wang performed additional MP2/6-311++G(3df,3pd) computations on AlH_5 and predicted the H-H stretching mode to be 4424 cm^{-1} with no anharmonic correction. It is interesting to note that Andrews and Wang predict an imaginary frequency in their computations. This mode corresponds to the H_2 rotation of Schreiner *et al.*'s⁷ second C_s structure to the C_s minimum.

There have been several theoretical and experimental investigations of the AlH_4^- anion. Shirk and Shriver¹² observed 1757, 772, 1678, and 766 cm^{-1} through the Raman and IR spectra of AlH_4^- salts. Pullumbi, Bouteiller, and Manceron¹³ predicted harmonic frequencies of 1760, 1679, 810, and 776 cm^{-1} at the CCSD(T) level of theory and observed 1609, 767, and 750 cm^{-1} in their matrix isolation experiments. Schreiner *et al.*⁷ also investigated AlH_4^- and predicted the vibrational frequencies to be 1679, 1594, 772, and 748 cm^{-1} and a bond distance of 1.639 Å at

the TZ2P CCSD(T) levels of theory. Wang *et al.*¹¹ observed two infrared absorptions, 1609 and 766 cm⁻¹, from coideposition of laser-ablated atoms with Ar/H₂ at 3.5 K. Their B3LYP/6-311++G** DFT computations predicted vibrational frequencies of 1735, 1649, 783, and 763 cm⁻¹ and bond distances of 1.644 Å.

This brief report comments on the work of Schreiner⁴ and extends the deprotonation energies of BH₅ and AlH₅ to the aug-cc-pVQZ CCSD(T) level of theory.

4.3 COMPUTATIONAL DETAILS

Geometries for boron pentahydride and tetrahydridoborate were optimized using coupled cluster theory including all single and double excitations (CCSD)¹⁴⁻¹⁷ and CCSD with the effects of connected triple excitations included perturbatively [CCSD(T)]¹⁸⁻²⁰. At the correlated levels the boron 1s-like core orbital and aluminum 1s, 2s, and 2p-like core orbitals were frozen. Dunning's augmented correlation-consistent polarized-valence basis sets, aug-cc-pVXZ^{21,22} (X = D, T, Q) were employed. The largest basis set, aug-cc-pVQZ, consists of 310 and 314 contracted gaussian functions for BH₅ and AlH₅, respectively. Zero-point vibration energy (ZPVE) corrections were included at all levels. The average atomic mass was used for Boron and Aluminum. All computations utilized the MOLPRO *ab initio* package²³⁻³¹.

The deprotonation energy of BH₅, equivalent to the negative of the proton affinity (PA) of BH₄⁻, was evaluated as the energy difference for the reaction BH₄⁻ + H⁺ → BH₅. Unless otherwise stated, all values reported here refer to our most reliable method, the aug-cc-pVQZ CCSD(T) level of theory.

4.4 RESULTS AND DISCUSSION

Table 4.1 reproduces Schreiner's previous theoretical values and the corresponding proton affinities. Tables 4.2 and 4.3 report the present work for the harmonic vibrational

frequencies for the boron and aluminum compounds, respectively. Table 4.4 shows the total energies and ZPVE values for all four molecules, while Table 4.5 displays the deprotonation energies for BH_5 , AlH_5 , and GaH_5 . Figures 4.1, 4.2, 4.3, and 4.4 depict the optimized structures for BH_5 , BH_4^- , AlH_5 , and AlH_4^- , respectively.

4.4.1 AN OVERSIGHT

In the 1994 paper, Schreiner, Schaefer, and Schleyer (SSS) reported total energies and ZPVE for BH_5 and BH_4^- and the deprotonation energy as $345.8 \text{ kcal mol}^{-1}$ at the $\text{TZ}(3d1f1g,2p1d)$ CCSD(T) level of theory. The first two columns in Table 4.1 contains SSS's total energies (in hartrees) and ZPVE (in kcal mol^{-1}) for BH_5 and BH_4^- while the last three columns are all possible PAs from his data. The first PA column is the adiabatic value while the last two columns are ZPVE corrected with the DZP SCF and TZP SCF methods, respectively. SSS computed the ZPVE of BH_5 at the TZ2P CCSD(T) level, but for BH_4^- they report ZPVE values for DZP SCF and TZ2P SCF. The reported SSS value of $345.8 \text{ kcal mol}^{-1}$ is in error and should be corrected to $338.5 \text{ kcal mol}^{-1}$ at the $\text{TZ}(3d1f1g,2p1d)$ CCSD(T) level of theory including the TZ2P SCF ZPVE correction. This error was inadvertently transferred to Schreiner, Schaefer, and Schleyer's paper⁷ describing AlH_5 .

4.4.2 GEOMETRIES

The optimized C_s boron pentahydride structure consists of a nearly planar BH_3 entity attached to a hydrogen molecule 1.42 \AA (this the B H_2 midpoint distance) away. This molecular hydrogen is out of the borane plane, but parallel to one of its B-H bonds. Our BH_5 structure agrees well with Schuurman's⁵ recent work and the earlier research of SSS. The optimized structure for AlH_5 is similar to that of BH_5 , with molecular hydrogen 2.22 \AA away from the AlH_3 moiety.

The anionic structures are of T_d symmetry with r_e (B-H) and r_e (Al-H) being 1.237 Å and 1.644 Å, respectively. As expected, our lower level BH_4^- aug-cc-pVTZ CCSD(T) result is qualitatively similar to that of Dixon⁶.

4.4.3 VIBRATIONAL FREQUENCIES

Harmonic vibrational frequencies are reported for BH_4^- and BH_5 in Table 4.2. Both optimized structures are minima, confirmed by the absence of imaginary vibrational frequencies. Again, we are in agreement with Dixon's⁶ assignment of the aug-cc-pVDZ CCSD(T) vibrational frequencies. Only four frequencies are reported since $\nu_2(t)$, $\nu_3(e)$, and $\nu_4(t)$ are triply, doubly, and triply degenerate modes, respectively. For a more complete BH_5 vibrational analysis the reader is directed to Schuurman's⁵ paper.

The aluminum pentahydride and AlH_4^- vibrational frequencies are shown in Table 4.3. Both structures are minima with no imaginary frequencies. Our predicted H-H harmonic stretching mode of AlH_5 is 190 cm^{-1} above the observed fundamental frequency of Wang, Andrews, Tam, DeRose, and Fajardo¹¹. If we apply a simple anharmonic correction of -240 cm^{-1} (see Speakman, Turney, and Schaefer⁸ for details), our predicted hydrogen stretching mode is 4012 cm^{-1} , 50 cm^{-1} less than the observed frequency.

4.4.4 ENERGETICS

The deprotonation energies of BH_5 and AlH_5 have now been extended via the aug-cc-pVQZ CCSD(T) method, as shown in Table 4.5. We predict a value of 332.4 kcal mol^{-1} for BH_5 , which is 1.1 kcal mol^{-1} less than Schreiner's corrected proton affinity, and 326.3 kcal mol^{-1} for AlH_5 .

4.5 CONCLUSIONS

The best previous deprotonation energy of BH_5 is $345.8 \text{ kcal mol}^{-1}$. The latter value has now been simply corrected to $333.5 \text{ kcal mol}^{-1}$. That value has been superceded in the present research by the more reliable aug-cc-pVQZ CCSD(T) level of theory, yielding $332.4 \text{ kcal mol}^{-1}$. We also report vibrational frequencies of 1098, 1210, 2263, and 2284 cm^{-1} for BH_4^- .

We have also improved the theoretical geometries and harmonic vibrational frequencies for AlH_5 and AlH_4^- predicting the H-H stretching mode of AlH_5 to be 4012 cm^{-1} , comparable to Wang *et al.*'s observed frequency¹¹. Our predicted AlH_4^- harmonic frequencies also agree well with Shirk and Shriver's experiments¹².

It is of special interest to compare the BH_5 , AlH_5 , and GaH_5 deprotonation energies in Table 4. 5. All three compounds have similar dissociation energies around $330 \text{ kcal mol}^{-1}$. The deprotonation energies for Group 3 pentacoordinate systems show the trend $\text{BH}_5 > \text{GaH}_5 > \text{AlH}_5$. The actual results are 332.4 (BH_5), 326.3 (AlH_5), and 331.0 (GaH_5). This pattern is a bit unusual, since the gap in observed properties usually falls between boron and aluminum with the gallium properties often very similar to those for aluminum.

4.6 ACKNOWLEDGEMENTS

This research was supported by the U. S. National Science Foundation, Grant CHE-045144.

4.7 REFERENCES

- ¹ J. I. Musher, *Angew. Chem. Int. Ed.* **8**, 54 (1969).
- ² N. M. Mitzel, *Angew. Chem. Int. Ed.* **42**, 3856 (2003).
- ³ T. J. Tague and L. Andrews, *J. Am. Chem. Soc.* **116**, 4970 (1994).
- ⁴ P. R. Schreiner, H. F. Schaefer, and P. R. Schleyer, *J. Chem. Phys.* **101**, 7625 (1994).

- 5 M. S. Schuurman, W. D. Allen, P. R. Schleyer, and H. F. Schaefer, *J. Chem. Phys.* **122**,
104302 (2005).
- 6 D. A. Dixon and M. Gutowski, *J. Phys. Chem. A* **109**, 5129 (2005).
- 7 P. R. Schreiner, H. F. Schaefer, and P. R. Schleyer, *J. Chem. Phys.* **103**, 5565 (1995).
- 8 L. D. Speakman, J. M. Turney, and H. F. Schaefer, *J. Chem. Phys.* **123**, 204303 (2005).
- 9 J. Moc, K. Bober, and J. Panek, *J. Mol. Model.* **12**, 93 (2005).
- 10 L. Andrews and X. Wang, *J. Phys. Chem. A* **108**, 4202 (2004).
- 11 X. Wang, L. Andrews, S. Tam, M. DeRose, and M. Fajardo, *J. Am. Chem. Soc.* **125**, 9218
(2003).
- 12 A. E. Shirk and D. F. Shriver, *J. Am. Chem. Soc.* **95**, 5904 (1973).
- 13 P. Pullumbi, Y. Bouteiller, and L. Manceron, *J. Chem. Phys.* **101**, 3610 (1994).
- 14 G. D. Purvis and R. J. Bartlett, *J. Chem. Phys.* **76**, 1910 (1982).
- 15 A. C. Scheiner, G. E. Scuseria, T. J. Lee, J. E. Rice, and H. F. Schaefer, *J. Chem. Phys.*
87, 5391 (1987).
- 16 G. E. Scuseria, C. L. Janssen, and H. F. Schaefer, *J. Chem. Phys.* **89**, 7382 (1988).
- 17 G. E. Scuseria, A. C. Scheiner, T. J. Lee, J. E. Rice, and H. F. Schaefer, *J. Chem. Phys.*
86, 2881 (1987).
- 18 K. Raghavachari, G. W. Trucks, J. A. Pople, and M. Head-Gordon, *Chem. Phys. Lett.*
157, 479 (1989).
- 19 G. E. Scuseria, *Chem. Phys. Lett.* **176**, 27 (1991).
- 20 G. E. Scuseria and T. J. Lee, *J. Chem. Phys.* **93**, 5851 (1990).
- 21 T. H. Dunning, *J. Chem. Phys.* **90**, 1007 (1989).
- 22 R. A. Kendall, T. H. Dunning, and R. J. Harrison, *J. Chem. Phys.* **96**, 6769 (1992).

- 23 R. D. Amos, A. Bernhardsson, A. Berning, P. Celani, D. L. Cooper, M. J. O. Deegan, A.
J. Dobbyn, F. Eckert, C. Hampel, G. Hetzer, P. J. Knowles, T. Korona, R. Lindh, A. W.
Lloyd, S. J. McNicholas, F. R. Manby, W. Meyer, M. E. Mura, A. Nicklass, P. Palmieri,
R. M. Pitzer, G. Rauhut, M. Schutz, U. Schumann, H. Stoll, A. J. Stone, R. Tarroni, T.
Thorsteinsson, and H. J. Werner, MOLPRO (2002).
- 24 M. J. O. Deegan and P. J. Knowles, *Chem. Phys. Lett.* **227**, 321 (1994).
- 25 C. Hampel, K. A. Peterson, and H. J. Werner, *Chem. Phys. Lett.* **190**, 1 (1992).
- 26 C. Hampel and H. J. Werner, *J. Chem. Phys.* **104**, 6286 (1996).
- 27 R. Lindh, *Theor. Chim. Acta* **85**, 423 (1993).
- 28 R. Lindh, U. Ryu, and B. Liu, *J. Chem. Phys.* **95**, 5889 (1991).
- 29 G. Rauhut, A. E. Azhary, F. Eckert, U. Schumann, and H. J. Werner, *Spectrochim. Acta A*
55, 651 (1999).
- 30 M. Schutz, *J. Chem. Phys.* **113**, 9986 (2000).
- 31 M. Schutz and H. J. Werner, *Chem. Phys. Lett.* **318**, 370 (2000).

Table 4.1. BH₅ Total Energies (in hartrees) with Proton Affinities and ZPVEs in kcal mol⁻¹.

Level of Theory	C _s BH ₅	T _d BH ₄ ⁻	PA (in kcal mol ⁻¹)		
			No ZPVE	ZPVE 1 ^b	ZPVE 2 ^c
DZP SCF	-27.52376	-26.97056	347.14	344.44	344.54
ZPVE ^a 1	22.40	19.70			
TZ2P SCF	-27.52900	-26.98656	340.39	337.69	337.79
ZPVE ^a 2	22.30	19.70			
DZP CISD	-27.66704	-27.12073	342.81	340.11	340.21
DZP CISD+Q	-27.67572	-27.13044	342.17	339.47	339.57
TZ2P CISD	-27.69080	-27.15564	335.82	333.12	333.22
TZ2P CISD+Q	-27.70146	-27.16789	334.82	332.12	332.22
DZP CCSD	-27.67359	-27.12781	342.48	339.78	339.88
TZ2P CCSD	-27.70041	-27.16447	336.31	333.61	333.71
DZP CCSD(T)	-27.67509	-27.13053	341.72	339.02	339.12
TZ2P CCSD(T)	-27.70450	-27.16909	335.98	333.28	333.38
ZPVE	26.50				
TZ(3d1f,2p1d) CCSD(T)	-27.72052	-27.18523	335.90	333.20	333.30
TZ(3d1f1g,2p1d) CCSD(T)	-27.72309	-27.18752	336.08	333.38	333.48

^a ZPVE energies scaled by 0.91.

^b The DZP SCF ZPVE correction is -2.70 kcal mol⁻¹. This correction factor is applied to each level of theory in this column.

^c The TZ2P SCF ZPVE correction is -2.60 kcal mol⁻¹. This correction factor is applied to each level of theory in this column.

Table 4.2. Vibrational Frequencies for BH₅ and BH₄⁻ (in cm⁻¹).

Molecule	Symmetry	CCSD			CCSD(T)			Prior ^b	Expt. ^c
		DZ ^a	TZ	QZ	DZ	TZ	QZ		
BH ₄ ⁻	ω ₁ (a)	2270	2275	2284	2260	2266	2284	2261	
	ω ₄ (t)	2245	2258	2263	2239	2254	2263	2240	
	ω ₆ (e)	1193	1212	1210	1185	1203	1210	1185	
	ω ₉ (t)	1096	1100	1098	1086	1087	1098	1086	
BH ₅	ω ₁ (a')	3728	3691	3685	3654	3603	3594	3322	
	ω ₂ (a')	2613	2627	2631	2601	2615	2619	2513	v ₂ = 2475
	ω ₃ (a')	2520	2532	2536	2508	2519	2523	2444	
	ω ₄ (a')	1575	1691	1714	1620	1742	1767		
	ω ₅ (a')	1189	1210	1211	1184	1204	1205	1182	
	ω ₆ (a')	1174	1195	1196	1167	1189	1190	1171	v ₆ = 1134
	ω ₇ (a')	899	938	945	909	955	966		
	ω ₈ (a')	659	717	731	702	756	766		
	ω ₉ (a'')	2649	2667	2671	2640	2659	2663	2555	v ₉ = 2544
	ω ₁₀ (a'')	1178	1197	1197	1172	1190	1191	1170	
	ω ₁₁ (a'')	992	1020	1022	995	1021	1023	1015	
	ω ₁₂ (a'')	187	183	184	201	200	203		

^a Abbreviation for aug-cc-pVXZ (X = D, T, Q).

^b Prior theoretical work for BH₄⁻ is Dixon and Gutowski⁶.
Prior theoretical work for BH₅ by Schuurman *et al.*⁵. (anharmonically corrected)

^c Experimental results from Tague and Andrews³ for BH₅.

Table 4.3. Vibrational Frequencies for AlH_5 and AlH_4^- (in cm^{-1}).

Molecule	Symmetry	CCSD			CCSD(T)			Prior Theoretical			Experimental Fundamental, ν		
		DZ ^a	TZ	QZ	DZ	TZ	QZ	Ref. 7	Ref. 11	Ref. 13	Ref. 11	Ref. 12	Ref. 13
AlH_4^-	$\omega_1(a)$	1708	1735	1750	1703	1730	1745	1679	1735	1760		1757	
	$\omega_4(t)$	1623	1648	1660	1620	1645	1658	1594	1649	1679	1609	1678	1609
	$\omega_6(e)$	773	784	786	768	777	779	772	783	810	766	772	767
	$\omega_9(t)$	754	760	765	750	756	760	748	763	776		766	750
AlH_5	$\omega_1(a')$	4250	4273	4270	4238	4256	4252	4082	4380			4062	
	$\omega_2(a')$	1911	1937	1953	1906	1932	1947	1852	1985				
	$\omega_3(a')$	1908	1933	1948	1902	1926	1941	1848	1982				
	$\omega_4(a')$	785	791	803	781	794	814		817				
	$\omega_5(a')$	783	783	791	779	778	786	761	809				
	$\omega_6(a')$	703	726	726	716	722	722	691	774				
	$\omega_7(a')$	367	378	386	374	387	395	351	390				
	$\omega_8(a')$	287	307	316	301	329	339	268	312				
	$\omega_9(a'')$	1912	1938	1954	1907	1932	1948	1853	1989				
	$\omega_{10}(a'')$	732	753	772	729	765	778	758	741				
	$\omega_{11}(a'')$	373	390	398	381	400	409	368	402				
	$\omega_{12}(a'')$	125	113	110	125	113	111	49					

^a Abbreviation for aug-cc-pVXZ (X = D, T, Q).

Table 4.4. Total Energies (in hartrees) and ZPVE Values (kcal mol⁻¹) for BH₅, BH₄⁻, AlH₅, and AlH₄⁻.

Level of Theory		C_s BH ₅	T_d BH ₄ ⁻	C_s AlH ₅	T_d AlH ₄ ⁻
aug-cc-pVDZ	CCSD	-27.681290	-27.150202	-244.907248	-244.380205
	ZPVE	27.68	20.99	20.03	14.88
aug-cc-pVTZ	CCSD	-27.715549	-27.180351	-244.940227	-244.410915
	ZPVE	28.12	21.12	20.32	15.08
aug-cc-pVQZ	CCSD	-27.723429	-27.187768	-244.948568	-244.419117
	ZPVE	28.19	21.14	20.47	15.18
aug-cc-pVDZ	CCSD(T)	-27.684822	-27.154512	-244.908891	-244.382569
	ZPVE	27.67	20.88	20.03	14.82
aug-cc-pVTZ	CCSD(T)	-27.720502	-27.186224	-244.942439	-244.414032
	ZPVE	28.10	21.01	20.33	15.02
aug-cc-pVQZ	CCSD(T)	-27.728729	-27.187768	-244.950945	-244.422455
	ZPVE	28.17	21.14	20.49	15.12

Table 4.5. Deprotonation Energies of BH₅, AlH₅, and GaH₅ (kcal mol⁻¹).

Level of Theory	BH ₅ ^a		AlH ₅ ^a		GaH ₅ ^b	
	PA _e	PA ₀	PA _e	PA ₀	PA _e	PA ₀
aug-cc-pVDZ CCSD	333.26	326.57	330.72	325.57	334.77	329.94
aug-cc-pVTZ CCSD	335.84	328.85	332.15	326.91	336.66	331.73
aug-cc-pVQZ CCSD	336.13	329.08	332.24	326.94	336.67	331.61
aug-cc-pVDZ CCSD(T)	332.77	325.99	330.27	325.06	334.20	329.31
aug-cc-pVTZ CCSD(T)	335.26	328.18	331.58	326.27	335.93	330.93
aug-cc-pVQZ CCSD(T)	339.46	332.43	331.63	326.26	335.90	330.99

^a Current Research

^b Reference 8

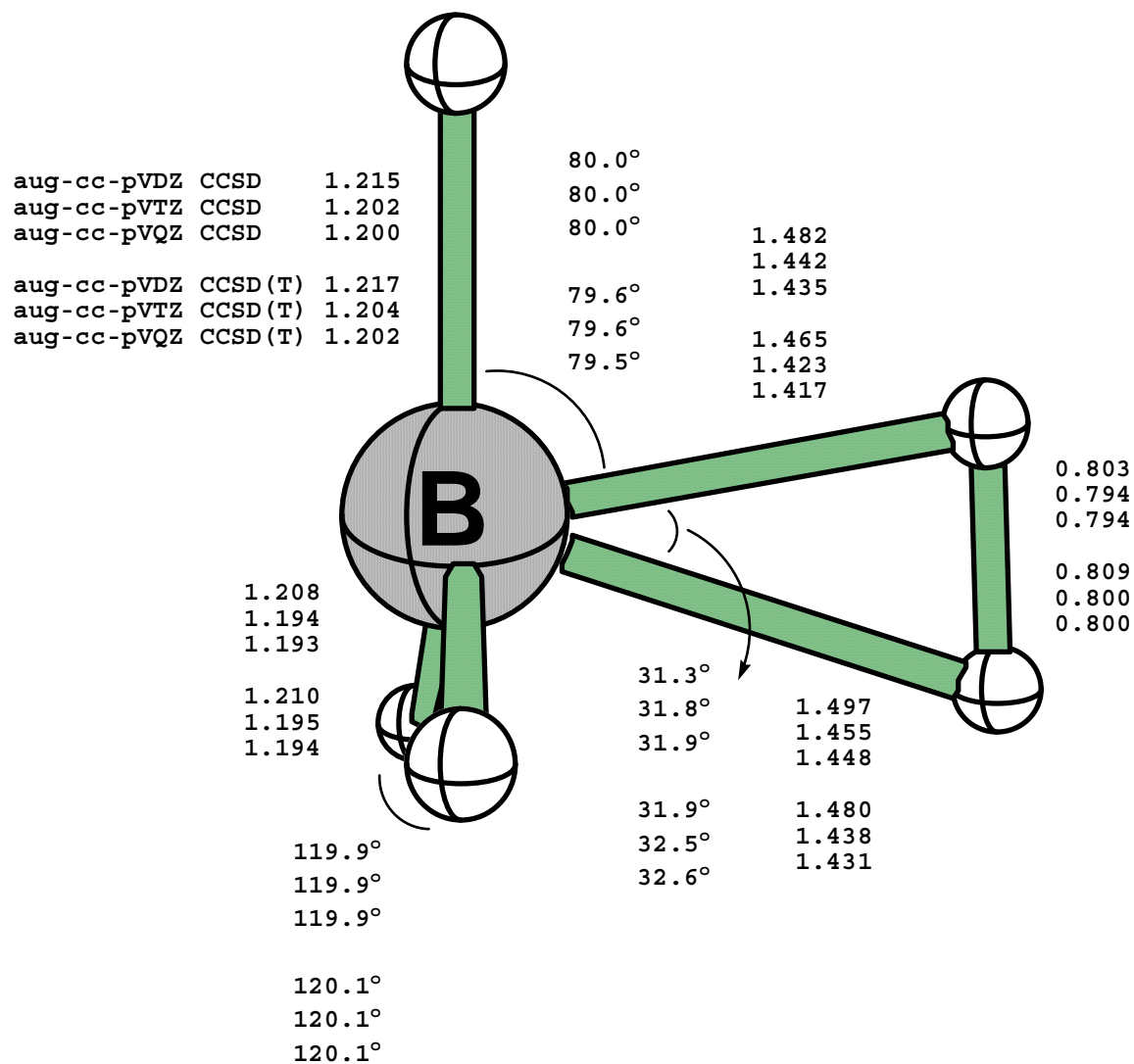


Figure 4.1. Predicted equilibrium geometries for BH₅ (bond lengths given in Å, angles in degrees).

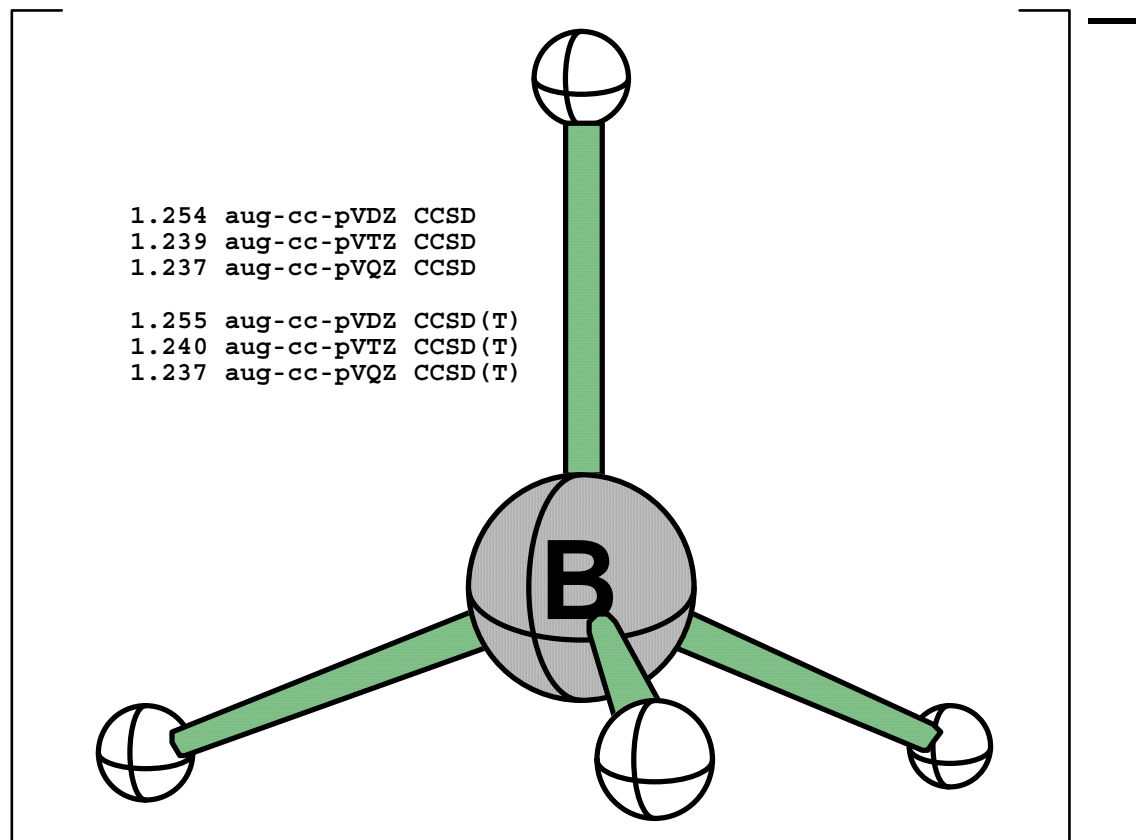


Figure 4.2. Predicted equilibrium geometries for the BH_4^- anion (bond lengths given in \AA , angles in degrees).

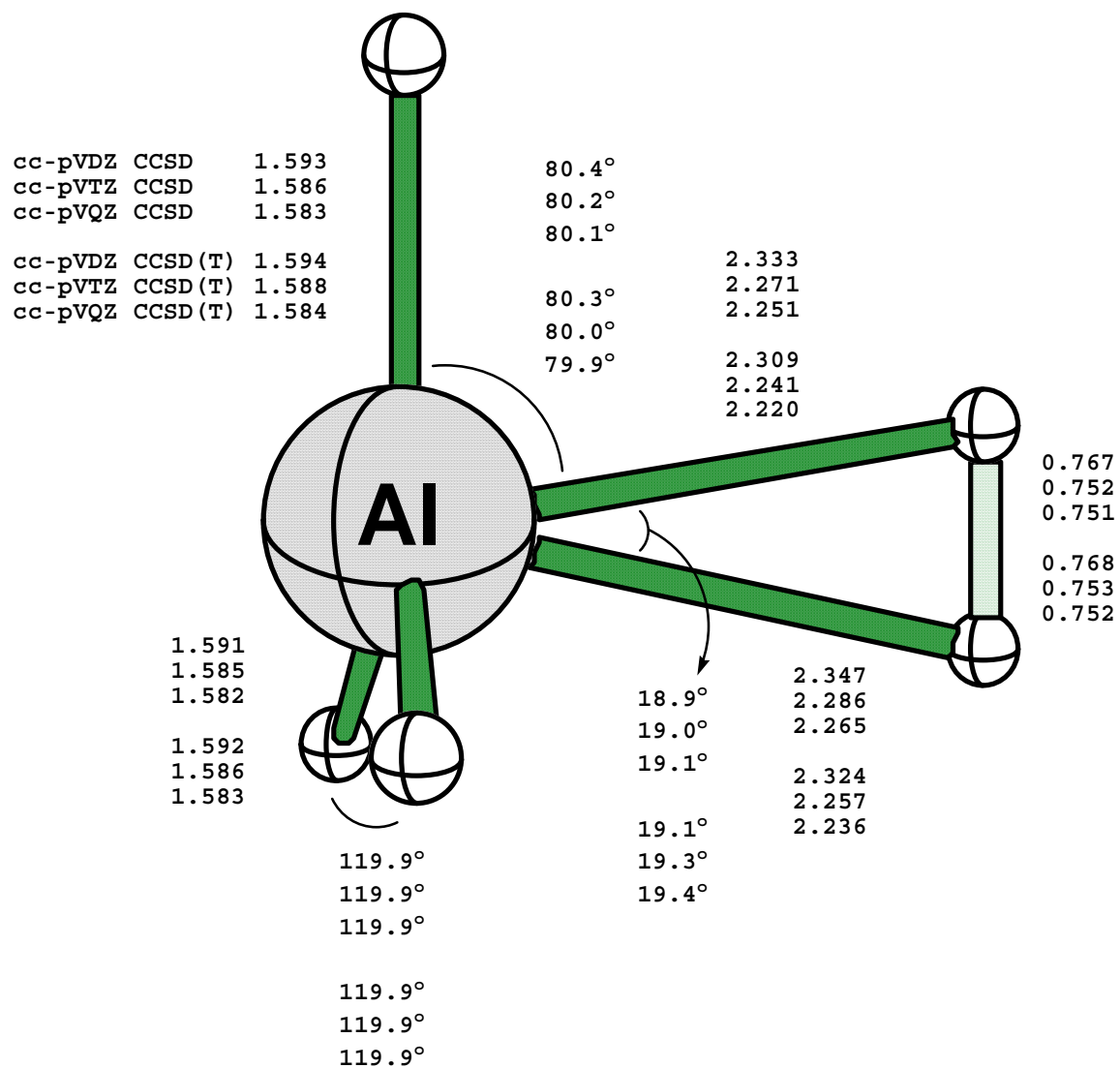


Figure 4.3. Predicted equilibrium geometries for AlH_5 (bond lengths given in \AA , angles in degrees).

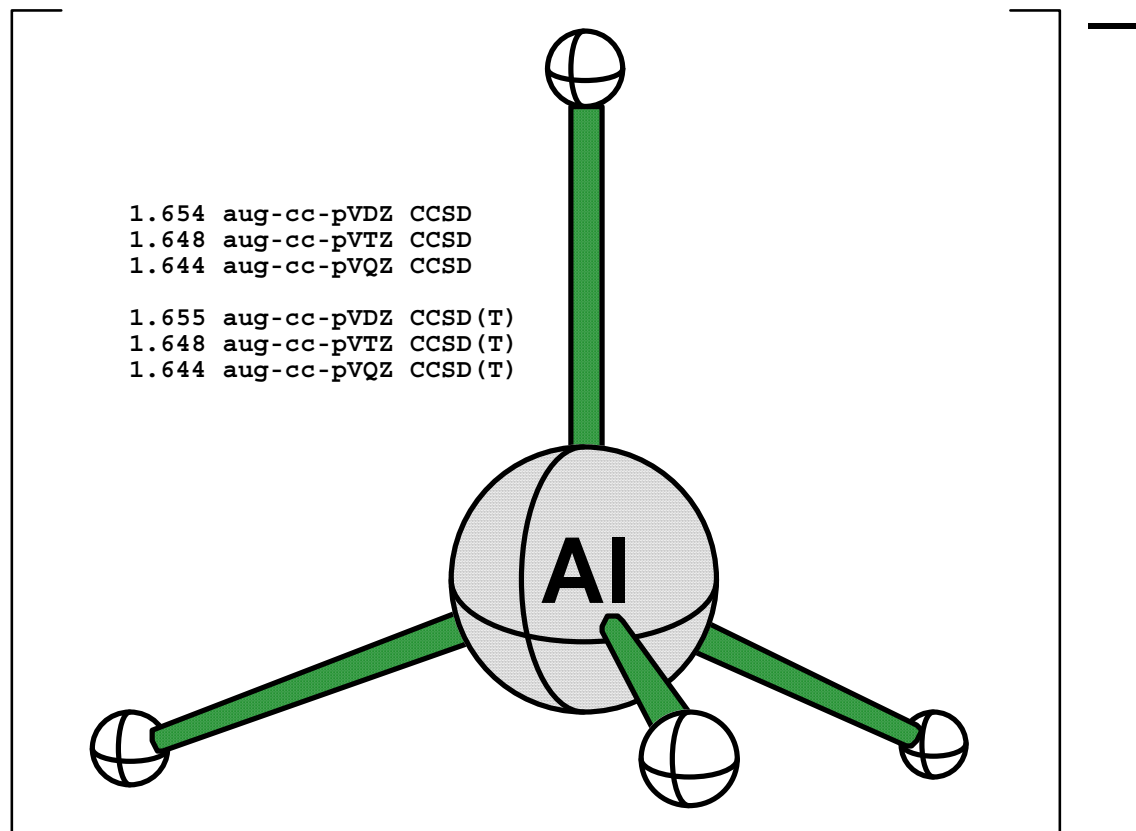


Figure 4.4. Predicted equilibrium geometries for the AlH_4^- anion (bond lengths given in \AA , angles in degrees).

CHAPTER 5

TOWARD THE OBSERVATION OF QUARTET STATES OF THE OZONE RADICAL CATION: INSIGHTS FROM COUPLED CLUSTER THEORY[†]

[†]Lucas D. Speakman, Justin M. Turney, and Henry F. Schaefer III. *J. Chem. Phys.* **128**, 214302 (2008); doi:10.1063/1.2924128. Reprinted here with permission of publisher.

5.1 ABSTRACT

Since the discovery of ozone depletion, the doublet electronic states of the ozone radical cation have received much attention in experimental and theoretical investigations, while the low-lying quartet states have not. In the present research viable pathways to the quartet states from the lowest three triplet states of ozone, 3A_2 , 3B_2 , and 3B_1 , and excitations from the 2A_1 and 2B_2 states of the ozone radical cation have been studied in detail. The potential energy surfaces, structural optimizations, and vibrational frequencies for several states of ozone and its radical cation have been thoroughly investigated using the Complete Active Space Self-Consistent Field (CASSCF), unrestricted coupled cluster theory from a restricted open-shell Hartree-Fock reference including all single and double excitations (UCCSD), UCCSD method with the effects of connected triple excitations included perturbatively [UCCSD(T)], and unrestricted coupled cluster including all single, double, and triple excitations with the effects of connected quadruple excitations included perturbatively [UCCSDT(Q)]. These methods used Dunning's correlation-consistent polarized core-valence basis sets, cc-pCVXZ (X=D, T, Q, and 5). The most feasible pathways (symmetry and spin allowed transitions) to the quartet states are $^4A_1 \leftarrow ^3A_2$; $^4A_2 \leftarrow ^3A_2$; $^4A_1 \leftarrow ^3B_2$; $^4A_2 \leftarrow ^3B_1$; $^4B_2 \leftarrow ^3B_1$; $^4A_2 \leftarrow ^1A_1$; $^4B_2 \leftarrow ^1A_1$; and $^4A_1 \leftarrow ^1A_1$ with vertical IPs of 12.46; 12.85; 12.82; 12.46; 12.65; 13.43; 13.93; and 14.90 eV, respectively.

5.2 INTRODUCTION

Ozone plays a vital role in our stratosphere by absorbing ultraviolet radiation.^{1,2} Neutral ozone has been well characterized both experimentally and theoretically, but the ozone radical cation was largely ignored until the recent discovery of depleted ozone.³ Since the recognition of ozone depletion, scientists have investigated possible pathways for ozone's creation and destruction, for which reliable experimental and theoretical results are needed to obtain a

comprehensive understanding. However, in the pursuit of the cationic states of ozone, the quartet states have been almost completely ignored by theoretical and experimental chemists. This paper aims to theoretically characterize the quartet states of O_3^+ and to consider possible avenues of excitation from neutral triplet electronic states of ozone for laboratory detection.

Ozone has a long experimental history, dating back at least to the classic 1880 paper by Chappuis.⁴ Since then, a breadth of theoretical and experimental research has been performed on ozone, leading to several recent review articles.⁵⁻⁸ Many theoretical methods fail to satisfactorily describe $\tilde{X}^1A_1 O_3$, because it is best described by a two configuration reference wave function and the treatment of dynamical electron correlation. Although ground state ozone is a multireference problem, the work of Watts, Bartlett, and Stanton⁹⁻¹¹ has shown that the inclusion of iterative or perturbative triple excitations in single reference coupled cluster methods can yield accurate results for molecular geometry and vibrational frequencies. In 1970 Tanaka and Morino¹² experimentally deduced r_0 and θ_0 to be 1.272 Å and 116.8°, followed in 1977 by Depannemaecher and Bellet¹³ with a 1.278 Å bond length and 116.8° bond angle. Barbe and his coworkers recently updated their spectroscopic constants for ozone from earlier work to the values^{14,15} 1133, 715, and 1087 cm^{-1} for ω_1 , ω_2 , and ω_3 , respectively. The \tilde{X}^1A_1 state of O_3 is included as a reference point for all electronic excitation and ionization processes in the present research.

The lowest triplet states of ozone also exhibit some theoretical challenges. It is clear from recent review articles⁵⁻⁸ that multireference methods agree with experiment for adiabatic excitation energies to the lowest neutral triplet states of ozone, while single reference methods do not. For example, Borowski, Fulcher, Malmqvist, and Roos¹⁶ used multi-configuration second-order perturbation theory (CASPT2) with an atomic natural orbital (4s3p3d1f) contracted basis

set to order the triplet states of ozone: 3A_2 , 3B_2 , 3B_1 lying 1.16, 1.34, and 1.35 eV above the ground state, respectively. Meanwhile, recent experiments¹⁷⁻²⁰ confirm this order with excitation energies of 1.184 ± 0.002 , 1.29 ± 0.03 , and 1.45 ± 0.03 eV for 3A_2 , 3B_2 , and 3B_1 , respectively. Watts and Bartlett²¹ computed CCSD(T)/cc-pVTZ//CCSDT-3/cc-pVTZ adiabatic excitation energies of 1.08, 1.16, 1.46 eV with CCSDT-3 for the 3B_2 , 3A_2 , and 3B_1 states, assigning 3B_2 as the lowest excited triplet state instead of 3A_2 . However, they mention that basis set considerations could affect their predicted order. Since the 3A_2 and 3B_2 states are so close in energy, possible excitation from the ozone ground state should be investigated to examine whether higher order coupled cluster methods will assign 3A_2 as the lowest triplet state.

Since 1966 there have been many experimental techniques used to detect the ozone radical cation: photoelectron spectroscopy,²²⁻²⁷ photoionization mass spectrometry,^{28,29} photofragment spectroscopy,³⁰ electron impact ionization,³¹ pulsed-field-ionization zero-kinetic-energy photoelectron (PFI-ZEKE),³² and threshold photoelectron spectroscopy.³³ The initial photoelectron spectroscopic studies indicated that the three lowest doublet electronic states, 2A_2 , 2A_1 , and 2B_2 , were within one eV of each other and the two lowest states were nearly degenerate. In 1984, Katsumata, Shiromaru, and Kimura²⁶ were able to assign 2A_2 as the highest of the three O_3^+ doublet states but were unable to identify either 2A_1 or 2B_2 as the electronic ground state. Due to the nearly degenerate 2A_1 and 2B_2 energy levels, it was not until 2005 when Willitsch, Innocenti, Dyke, and Merkt³² conducted a PFI-ZEKE experiment to establish the adiabatic O_3^+ ground state as 2A_1 , lying only 3.12 kcal mol⁻¹ below the 2B_2 state.

While experimentalists have endeavored for forty years to label the nearly degenerate low-lying doublet states of O_3^+ , theoretical chemists have also struggled since 1975 to make reliable predictions concerning the lowest three states. Hay, Dunning, and Goddard³⁴ used a

generalized valence bond configuration interaction (GVB-CI) procedure with a DZ basis set ($9s5p/4s2p$) to predict the vertical ionization potentials to the 2A_1 , 2B_2 , and 2A_2 states to be 12.91, 13.03, and 13.59 eV, respectively. The latter results are in fair agreement with the early (1974) experimental ordering²⁵ of 12.75, 13.57, and 13.03 eV for 2A_1 , 2B_2 , and 2A_2 , respectively. Dunning, Hay, and Goddard suggested an experimental misinterpretation due to ozone deviating from Koopmans theorem, from which the experimentalists qualitatively assigned 2A_2 and 2B_2 . There have been a few other theoretical studies that mislabeled the ozone doublet ground state.^{35,36} In 1981, Kosugi, Kuroda, and Iwata³⁷ confirmed Dunning's analysis,³⁴ showing that Koopman's theorem incorrectly predicts the third state of O_3^+ to be the first state (2A_2) and thus explaining earlier problems.

In 1983³⁸ and 1991,³⁹ complete active space self consistent field (CASSCF) potential energy surfaces (PES) for doublet states of O_3^+ were reported, showing a low-lying conical intersection. The study of Schmelz, Chambaud, Rosmus, Köppel, Cederbaum, and Werner³⁹ used a multireference configuration interaction (MRCI) method employing CASSCF natural orbitals to order the doublet and quartet states of the ozone cation with respect to $O_3 \tilde{X}^1A_1$. They predicted 2A_1 (12.44 eV), 2B_2 (12.49 eV), 2A_2 (13.17 eV), 4A_2 (13.43 eV), 4B_2 (13.93 eV), 2B_1 (14.12 eV), 4A_1 (14.35 eV), and 4B_1 (17.42 eV). Starting from these computations, Muller, Koppel, and Cederbaum investigated vibronic coupling effects and nuclear dynamics arising from the conical intersection PES of the doublet state of O_3^+ .⁴⁰⁻⁴²

Recently, high level *ab initio* methods have been applied to the vertical ionization of ozone,^{43,44} with recent papers by Willitsch, Innocenti, Dyke, and Merkt³² and Ohtsuka, Hasegawa, and Nakatsuji.⁴⁵ Willitsch *et al.* computed excitation energies with MRCI including single and doubles excitations following CASSCF calculations with the aug-cc-pVTZ basis set.

They also used multireference second-order perturbation theory (CASPT2) with the cc-pVQZ basis set, a CASSCF potential surface, and evaluated harmonic vibrational frequencies at the CASSCF level of theory with the aug-cc-pVTZ basis set. Their theoretical predictions agree with their PFI-ZEKE experimental values and unambiguously determine the ordering of O_3^+ states to be \tilde{X}^2A_1 , \tilde{A}^2B_2 , and \tilde{B}^2A_2 , in agreement with Hay, Dunning, and Goddard.³⁴ Ohtsuka, Hasegawa, and Nakatsuji used a multi-exponentially generated fourth-order method (MEG4/EX-MEG4), a multi-reference implementation of the symmetry-adapted cluster-configuration interaction (SAC-CI), to consider the valence and ionized states of ozone. They reported theoretical results for several excited electronic states of ozone and the ozone cation.

The dissociation of the ozone radical cation is of crucial interest if the quartet states are to be observed. Vestal and Mauclaire⁴⁶ reported the first photodissociation reactions on O_3^+ in 1977 using a tandem quadrupole photodissociation mass spectrometer. Their work explored two dissociation pathways for the ozone radical cation: collisional dissociation leads to the production of O_2^+ while the dominant product in photodissociation is O^+ . They deduced dissociation energies for the ground state of O_3^+ to be 1.85 and 0.60 eV for $O^+ + O_2$ and $O_2^+ + O$, respectively. Later in that same year, Weiss, Berkowitz, and Appelman⁴⁷ detected $O^+ + O_2$ and $O + O_2^+$ formation from O_3 at 15.21 and 13.13 eV, respectively, from photoionization experiments. In 1980, Moseley, Ozenne, and Cosby⁴⁸ reported a photodissociation energy of $O_3^+ \rightarrow O_2 + O^+$ at 2.16 eV while their collision induced dissociation experiment yielded 0.59 eV for $O_3^+ \rightarrow O_2^+ + O$. A year later, Hiller and Vestal⁴⁹ reinterpreted Moseley, Ozenne, and Cosby's photodissociation data to yield a photodissociation energy of 1.776 eV, while assigning their own 1.860 eV value. Although these papers suggest possible photodissociation pathways, Goss and Morrison⁵⁰ were the first experimentalists to label the fourth ionized state of ozone, $\tilde{C}^2B_1 O_3^+$,

responsible for $O_3 \rightarrow O_2 + O^+$ with an observed energy of 15.03 eV. In 2001, Mocellin, *et. al.*⁵¹ recorded the total and partial ion yields of ozone using time-of-flight techniques to confirm that two states, $\tilde{X}^2A_1 O_3^+$ and $\tilde{A}^2B_2 O_3^+$, are bound after ionization. The first direct experimental evidence for the predissociation state of the ozone cation, $\tilde{C}^2B_1 O_3^+$, was presented on the basis of resonant auger electron spectra of core excited ozone in 2003.⁴⁴

Over the past forty years, the doublet states of the ozone radical cation have received much attention; however, only one paper mentions the quartet states of O_3^+ . The present research extends the theoretical characterization of ozone to include the quartet states of O_3^+ . This research provides experimentalists with vertical excitation energies from several ozone triplet states, which are also examined at high levels of theory.

5.3 COMPUTATIONAL DETAILS

Geometries for all states of ozone and the ozone cation were optimized using the CASSCF,⁵²⁻⁵⁵ unrestricted coupled cluster theory from a restricted open-shell Hartree-Fock reference including all single and double excitations (UCCSD),⁵⁶⁻⁵⁹ and UCCSD methods with the effects of connected triple excitations included perturbatively [UCCSD(T)].⁶⁰⁻⁶² Dunning's correlation-consistent polarized-core-valence basis sets, cc-pCVXZ (X = T, Q, and 5),^{63,64} were used without frozen core approximations. The largest basis set, cc-pCV5Z, included 435 contracted Gaussian functions. The CASSCF procedure for the ozone radical cation places all 23 electrons in 15 molecular orbitals with 59588 (4A_1), 60436 (4B_1), 59740 (4B_2), 60476 (4A_2), 77598 (2A_1), 75366 (2B_1), 77514 (2B_2), and 75282 (2A_2) configuration state functions (CSFs) for O_3^+ . Similarly, the CASSCF procedure for neutral ozone places 24 electrons in 15 molecular orbitals, with total configuration numbers 24189 (3B_1), 25035 (3B_2), 24159 (3A_2), and 16683 (1A_1).

Potential energy curves were computed using the full-valence CASSCF method with the cc-pVTZ basis set. Bond angles were incremented by 5° between 70°-155°, constrained, and bond lengths were allowed to relax. Geometry optimizations and potential surfaces were computed using the MOLPRO 2002.6 package.⁶⁴⁻⁷²

Harmonic vibrational frequencies were determined at the optimized cc-pCVTZ UCCSD and cc-pCVTZ UCCSD(T) geometries using ACESII^{73,74} analytic second derivatives.⁷⁵⁻⁷⁷ The UCCSD adiabatic zero-point vibration corrected energies, T_0 , are seen in Tables 5.6 and 7 and used cc-pCVTZ UCCSD's ZPVE values. The remaining coupled cluster methods used cc-pCVTZ UCCSD(T) ZPVEs for their zero-point vibrational corrections. It became evident that higher order coupled cluster methods are needed to obtain reliable results with single determinant based methods. Accordingly, the cc-pCVDZ^{63,64} UCCSDT(Q)^{78,79} energy correction was evaluated using Kállay's MRCC^{77,80-84} interface with the ACESII package. The full triples plus perturbative quadruple excitations correction was evaluated as the difference between two single point energies, cc-pCVDZ UCCSDT(Q) and cc-pCVDZ UCCSD(T), at the optimized cc-pCV5Z UCCSD(T) geometry.

5.4 RESULTS AND DISCUSSION

5.4.1 GEOMETRIES

In Table 5.1 the theoretical geometries are reported for the quartet states of the ozone radical cation, with the appropriate electron configurations given in Table 5.4. The electron configurations for the four states differ by which one of the four orbitals is doubly occupied: $6a_1$, $1a_2$, $4b_2$, or $2b_1$. The theoretical bond angles qualitatively agree with the Walsh diagram, seen in Figure 5.1. Walsh's diagram predicts the $6a_1^2 1a_2 4b_2 2b_1$ (4A_1) state to be the most bent because the $6a_1$ orbital is doubly occupied. This is followed structurally by $6a_1 1a_2 4b_2 2b_1^2$ (4B_1), in

which the doubly occupied $2b_1$ orbital is seen in Figure 5.1 to have no real preference to a bent or linear structure. The last two quartet states contain doubly occupied orbitals that prefer linear structures, with the $4b_2$ orbital having a steeper curve than $1a_2$. Thus, $6a_1 1a_2 4b_2^2 2b_1$ (4B_2) state should have a larger bond angle than $6a_1 1a_2^2 4b_2 2b_1$ (4A_2). The Walsh diagram therefore predicts the bond angles to fall in the order ${}^4A_1 < {}^4B_1 < {}^4A_2 < {}^4B_2$, which order matches the theoretical cc-pCV5Z UCCSD(T) geometries: 89.8° , 97.6° , 113.8° , and 124.6° , respectively.

Optimized triplet state structures for neutral ozone are reported in Table 5.2, with their configurations shown in Table 5.4. The treatment of the 3A_1 state is unreliable with single determinant methods because of its extreme multireference nature, demonstrated in Table 5.4. For the remaining three states, the electron configurations place six electrons in four orbitals: $6a_1$, $1a_2$, $4b_2$, and $2b_1$. Walsh's diagram predicts the $6a_1$ orbital to favor strongly bent structures while the $4b_2$ and $1a_2$ orbitals are predisposed to linear geometries. Thus, the Walsh diagram predicts the configuration $6a_1 1a_2^2 4b_2^2 2b_1$ (3B_1) to have the largest bond angle. The two remaining states, $6a_1^2 1a_2^2 4b_2 2b_1$ (3A_2) and $6a_1^2 1a_2 4b_2^2 2b_1$ (3B_2), differ in their occupations of $4b_2$ and $1a_2$. Since the $1a_2$ orbital does not favor linearity as much as $4b_2$, the 3A_2 state should (in Walsh's picture) have a smaller bond angle. Our theoretical bond angles agree with this simple Walsh diagram ordering: 97.9° , 108.5° , and 128.5° for 3A_2 , 3B_2 , and 3B_1 , respectively. The theoretical 3A_2 ozone structure r_e differs from the experimental r_o by 0.013 \AA and 1.0 degrees.

The theoretical results for the doublet states of the ozone radical cation (see Table 5.1) also follow the Walsh diagram predictions for the bond angle order. Only one of the lowest-lying doublet states has a singly occupied $6a_1$, giving rise to the largest bond angle, $6a_1 1a_2^2 4b_2^2$ (2A_1); while the configuration with $4b_2$ unoccupied should have the smallest angle, $6a_1^2 1a_2^2 2b_1$ (2B_1). The remaining two doublet states have three electrons in $1a_2$ and $4b_2$. A state with a

doubly occupied $4b_2$, namely $6a_1^2 1a_2 4b_2^2$ (2A_2), should (Walsh argument) have a larger bond angle than the state with a doubly occupied $1a_2$, namely $6a_1^2 1a_2^2 4b_2$ (2B_2). The present *ab initio* predictions follow the Walsh pattern with 71.0° , 104.2° , 112.8° , and 132.7° for 2B_1 , 2B_2 , 2A_2 , and 2A_1 , respectively. The 2A_1 geometry agrees roughly with the recent experimental results of Merkt,³² but with a shorter bond length by 0.023 \AA and a bond angle different by 1.2° . However, the 2B_2 structure at the UCCSD(T) level of theory differs from experiment³² by 0.100 \AA and 7.1° . This discrepancy could conceivably be rationalized by examining the second significant configuration for the 2B_2 state, $6a_1 1a_2 4b_2^2 2b_1$, compared to the dominant configuration, $6a_1^2 1a_2^2 4b_2$. With the absence of the doubly occupied $6a_1$ and the presence of a doubly occupied $4b_2$, this second configuration might have a substantially larger bond angle. Incorporation of this configuration into a geometry optimization might yield a bond angle closer to the Willitsch value.³² Willitsch attributes this discrepancy to the anharmonicity of the potential in the vicinity of the equilibrium geometry. A more complete discussion of the structural predictions will be given in the conclusions.

Optimized stationary points for the ground state structures for ozone, molecular oxygen, and the molecular oxygen cation are reported in Tables 5.2 and 5.3, respectively. There is excellent agreement for O_2 and O_2^+ , the bond distances differing by 0.0027 \AA and 0.0022 \AA .⁸⁵ Despite the $\tilde{X}^1A_1 O_3$ multireference nature, cc-pCV5Z UCCSD(T) gives good agreement with the experimental r_e structure^{12,13} of 0.007 \AA and 0.4° .

5.4.2 Vibrational Frequencies

Predicted harmonic vibrational frequencies are reported in Tables 5.3 and 5.5. The UCCSD(T) results agree satisfactorily with the experimentally derived harmonic frequencies,^{14,15} differing by 25 , 5 , and -25 cm^{-1} for ω_1 , ω_2 , and ω_3 , respectively. This comparison is consistent

with Bartlett and coworkers' comments about the necessity of triple excitations for accurate harmonic frequencies.^{9,10,21} For example, for neutral O₃ coupled cluster theory with the singles and doubles ansatz (CCSD) predicts ω_1 and ω_3 to be nearly equal, 1283 and 1273 cm⁻¹, respectively. Including the effects of perturbative triples, coupled cluster theory shows a dramatic improvement, lowering these two harmonic frequencies by 125 and 211 cm⁻¹, to within 25 cm⁻¹ of experiment. The remarkable effect of triples is not restricted to the ground state of ozone: ⁴A₁ O₃⁺ (ω_3), ²A₁ O₃⁺ (ω_1 and ω_3), and ²B₂ O₃⁺ (ω_3) all exhibit significant differences of 233, 137, 168, and 133 cm⁻¹, respectively, between CCSD and CCSD(T).

For the triplet states, there is reasonable agreement with experiment for most harmonic vibrational frequencies. For the ³B₁ and ³B₂ states, the UCCSD(T) frequencies fall inside the experimental error ranges. However, the ³A₂ frequencies are not so close to Anderson and Mauersberger's¹⁷ experiment, differing by 34 and 59 cm⁻¹ for ω_1 and ω_2 , respectively.

For the ground state of the ozone radical cation, the present theoretical results fall within Weiss, Berkowitz, and Appleman's⁴⁷ suggested experimental errors. The other available experiment to compare with theory is for the ²B₂ state. Our coupled cluster prediction for ω_1 (1278 cm⁻¹) differs from experiment (1380 ± 40 cm⁻¹) by over at least 60 cm⁻¹. As mentioned earlier, this state is severely multi-reference and also affected by anharmonicity.³² Further theoretical investigations including quartic force fields and multi reference coupled cluster methods are needed to understand this apparent disagreement between theory and experiment. It is of course possible that the rather large stated experimental error bars (± 40 cm⁻¹) were overly optimistic. The ²B₁ state of O₃⁺ has a nearly equilateral structure, and its imaginary vibrational frequency indicates a transition state leading to a C_s structure. The remaining two states, ⁴B₂ and ²A₂, have one imaginary vibrational frequency and are also transition states to C_s minima.

5.4.3 Energetics

The bending potential energy curves for the ozone radical cation and ozone are sketched in Figures 5.2 and 5.3, respectively. For the doublet ozone radical cation species, Figure 5.2 is in excellent agreement with Schmelz's³⁹ earlier research. Both theoretical models show 2A_1 , 2B_2 , 2A_2 , and 2B_1 with minima at about 130, 105, 115, and 70°, respectively. The state responsible for predissociation, 2B_1 , is nearly 2 eV higher in energy than 2A_1 and 2B_2 in the range of 90 to 130 degrees before falling to its minimum near 70°. For the triplet states, the CASSCF PES predicts the 3A_2 state to be higher in energy than 3B_2 . Three of the four quartet states, 4A_1 , 4A_2 , and 4B_2 , are similar in energy to the 2B_1 state, which is responsible for the premature dissociation of $O_3^+ \rightarrow O^+ + O_2$. However, with the error in the triplet excited states mentioned above, higher levels of theory than CASSCF must be utilized to illuminate the quartet states of the ozone radical cation. The first subsection in this energetics discussion justifies UCCSD(T) and UCCSDT(Q), while the second part describes the ionizations and excitations to the quartet states of the ozone radical cation.

5.4.3.1 Method Justification

The energetic ordering of the triplet states of ozone has been a very challenging problem²¹ for single determinant coupled cluster methods. Table 5.6 shows how the inclusion of higher excitations reverses the energetic order of the 3B_2 and 3A_2 states. The CASSCF and UCCSD methods predict 3B_2 to be the lowest excited electronic state by 0.11 and 0.37 eV, respectively, while UCCSD(T) predicts the two states to be nearly degenerate. The inclusion of perturbative quadruple excitations confirms the experimental ordering of the 3A_2 , 3B_2 , and 3B_1 states, with energies relative to 3A_2 of 0.13, and 0.28 eV for 3B_2 and 3B_1 , respectively. These energy differences are in remarkable agreement with Anderson and Mauersberger's

experiments,¹⁷ differing by 0.02 eV (${}^3B_2 \leftarrow {}^3A_2$) and 0.01 eV (${}^3B_1 \leftarrow {}^3A_2$). Although UCCSDT(Q) provides an excellent energy separation $\Delta E({}^3A_2 - {}^3B_2)$ between the two triplet states, UCCSD(T) is sufficient to describe the triplet excitations from the ozone ground state. Our UCCSD(T) predictions are in fine agreement with experiment¹⁷ with differences of 0.02 (${}^3A_2 T_e$), 0.02 (${}^3A_2 T_0$), 0.03 (${}^3B_2 T_e$), 0.07 (${}^3B_2 T_0$), 0.04 (${}^3B_1 T_e$), and 0.02 eV (${}^3B_1 T_0$).

The ionization energies of neutral ozone to the doublet cation states are also reported in Table 5.6. The same energetic ordering is obtained from UCCSD(T) for the doublet states of the ozone cation, differing from Merkt's results³² by 0.06 eV. UCCSD(T) performs satisfactorily in describing ${}^2A_1 T_0$ (differs from experiment by 0.03 eV),³² ${}^2B_2 T_0$ (0.09),³² ${}^2B_2 T_v$ (0.05),^{23,26} and ${}^2A_2 T_v$ (0.04).^{23,26} However, UCCSD(T) differs by 0.20 electron volts for ${}^2A_1 T_v$ and ${}^2B_1 T_v$ (vertical excitation energy). The inclusion of quadruple excitations improves the theoretical predictions for ${}^2A_1 T_v$ and ${}^2B_1 T_v$ to 13.22 and 15.11 eV, respectively, which are in good agreement with experiment.^{47,50}

Table 5.7 reports the two dissociation energies (to $O_2 + O^+$ and $O_2^+ + O$) for ozone radical cation electronic states for $\tilde{X} {}^2A_1 O_3^+$. This work confirms that the two lowest doublet cation states, $\tilde{X} {}^2A_1 O_3^+$ and $\tilde{A} {}^2B_2 O_3^+$, are bound with respect to ${}^2\Pi_g O_2^+ + {}^3P O$ by 0.63 and 0.53 eV, respectively. Experimentalists⁴⁶⁻⁴⁸ report 0.60 eV for $\tilde{X} {}^2A_1 O_3^+$ which result is in excellent agreement with our UCCSDT(Q) prediction of 0.63 eV. The other available experimental result with which to compare involves the photodissociation pathway for ${}^2A_1 O_3^+$. Vestal and coworkers derived a dissociation barrier of 1.85 eV from two experiments^{46,49} and a reinterpretation of Moseley's results⁴⁸. The UCCSDT(Q) prediction is nearly a one eV higher than experiment. However, Table 5.7 shows our theoretical thermochemical bond energy ($O_3^+ \rightarrow O_2^+ + O$) for the ozone cation to be 2.14 eV which is in essentially perfect agreement with

accepted bond energy of 2.165 ± 0.02 eV.⁴⁸ For the ozone cation dissociation value, two experiments deduced the 2B_1 vertical ionization energy from the ground state of ozone for 15.21⁴⁶ and 15.03 eV,⁵⁰ which bracket the UCCSDT(Q) predicted value of 15.11 eV. Vestal started from the ground state of ozone and deduced a dissociation energy of 1.85 eV for \tilde{X}^2A_1 O_3^+ from the appearance of O_3^+ and O_2^+ in his spectrum. Since Goss and Morrison report that the \tilde{C}^2B_1 O_3^+ state is responsible for the ozone radical dissociation, we compare the vertical ionization potentials of \tilde{C}^2B_1 O_3^+ and \tilde{X}^2A_1 O_3^+ from \tilde{X}^1A_1 O_3 to pursue Vestal's experiment. Our perturbative quadruples method predicts the dissociation energy of the ozone radical cation to be 1.89 eV, 0.04 eV off from experiment. As a byproduct of the theoretical dissociation energies, Table 5.3 reports ionization energies for oxygen and molecular oxygen. Since UCCSD(T) has already essentially converged to the experimentally observed energies of 13.61⁸⁶ and 12.07⁸⁷ eV for 4S $O^+ \leftarrow {}^3P$ O and ${}^2\Pi_g$ $O_2^+ \leftarrow {}^3\Sigma_g^-$ O_2 , respectively, the perturbative quadruples corrections are not included.

5.4.3.2 Ionization and Electronic Excitation

The UCCSDT(Q) correction seems necessary to obtain accurate relative energies for the triplet states of ozone, the ionization to the doublet states of the ozone cation, and the predissociation limit for the ozone cation. However, UCCSD(T) performs very satisfactorily with only a few properties differing from experiment by more than 0.10 eV. Thus, the UCCSDT(Q) method is not reported for the ozone and the ozone radical cation in Table 5.8. The remaining discussion of energetics revolves around theoretical predictions of the positions of the quartet states of the ozone cation relative to several different points along the ozone surfaces (1A_1 , 3A_2 , 3B_2 , and 3B_1) and the ozone cation surfaces (2A_1 and 2B_2).

Although there could exist other dissociation pathways for the ozone cation, this work assumes the 2B_1 O_3^+ state is responsible for the dissociation of the ozone radical cation over the entire PES. Thus, a state is bound/unbound if its vertical excitation energy is less/more than the 2B_1 vertical excitation energy at a particular geometry.

5.4.3.2.1 $O_3^+ \leftarrow {}^3A_2$ O_3

Table 5.8 reports the theoretically obtained IPs for the 3A_2 state of ozone. Two likely ionization pathways to the quartet states involve (qualitatively) removing an electron from one of the nearly degenerate, doubly occupied $6a_1$ (${}^4A_2 \leftarrow {}^3A_2$) or $1a_2$ (${}^4A_1 \leftarrow {}^3A_2$) orbitals. The latter ionization potential (${}^4A_1 \leftarrow {}^3A_2$) pertains to the relationship between the lowest triplet neutral ozone state (3A_2) and the lowest quartet ozone cation state, with an adiabatic IP of 12.34 eV. From the potential curves (Figures 5.2 and 5.3) and structures (Tables 5.1 and 5.2), the 4A_1 and 3A_2 states have very similar geometries, resulting in similar adiabatic and vertical ionization energies. The ${}^4A_2 \leftarrow {}^3A_2$ transition is also possible, leading to the second lowest quartet state of the ozone cation with a IP_e predicted of 12.51 eV. The 4A_2 state has a bond angle 16° wider than 3A_2 , leading to an increased vertical ionization energy 12.85 eV. However, the vertical IP is still within the predissociation limit of 2B_1 by 0.06 eV. The last two ionization pathways from the 3A_2 to the quartet states of the ozone radical cation involve the second electronic configuration ($\bullet\bullet\bullet 6a_1 1a_2 4b_2^2 2b_1^2$) with $4b_2$ and $2b_1$ doubly occupied. Removal of a single electron from these orbitals results in the ${}^4B_1 \leftarrow {}^3A_2$ or ${}^4B_2 \leftarrow {}^3A_2$ excitations. However, 4B_1 is not a bound excited electronic state (by nearly 3 eV) and any ionization to this state should dissociate to ${}^3\Sigma_g^- O_2$ and ${}^4S O^+$. The last ionization, ${}^4B_2 \leftarrow {}^3A_2$, has a reasonable adiabatic excitation energy, 12.85 eV; but these two structures differ by nearly 30° and its T_v increases by 1 eV to 13.96 eV, which causes the 4B_2 state to be dissociative by 1.05 eV.

The two most practical pathways from ozone to the doublet states of O_3^+ are the removal of a singly occupied electron from the $2b_1$ orbital (yielding ${}^2B_2 \leftarrow {}^3A_2$) or from the $4b_2$ orbital (yielding ${}^2B_1 \leftarrow {}^3A_2$). The former ionization, ${}^2B_2 \leftarrow {}^3A_2$, has the lowest vertical IP, 11.73 eV, for 3A_2 while the process ${}^2B_1 \leftarrow {}^3A_2$ lies a full electron volt higher in energy due to the significant geometry differences between the two states and is responsible for predissociation. The other ionization processes are ${}^2A_1 \leftarrow {}^3A_2$ (ionize $2b_1$; $4b_2 \leftarrow 6a_1$) and ${}^2A_2 \leftarrow {}^3A_2$ (ionize $2b_1$; $4b_2 \leftarrow 1a_2$) with vertical ionization energies of 13.23 and 12.79 eV, respectively. Although ${}^2A_1 \leftarrow {}^3A_2$ has the lowest adiabatic IP for 3A_2 , its vertical IP is 0.32 eV above the T_v of 2B_1 while the ${}^2A_2 \leftarrow {}^3A_2$ process is viable by 0.12 eV. Thus, the four most likely ionizations from the 3A_2 state are ${}^2B_2 \leftarrow {}^3A_2$, ${}^4A_1 \leftarrow {}^3A_2$, ${}^4A_2 \leftarrow {}^3A_2$, and ${}^2A_2 \leftarrow {}^3A_2$, with vertical IPs of 11.73, 12.46, 12.85, and 12.79 eV and adiabatic IPs of 11.55, 12.34, 12.51, and 12.29 eV, respectively. Experimentally, it will be demanding to distinguish ${}^4A_2 \leftarrow {}^3A_2$ from ${}^2A_2 \leftarrow {}^3A_2$, due to the two final states being nearly degenerate.

5.4.3.2.2 $O_3^+ \leftarrow {}^3B_2 O_3$

Although the 3B_2 state is not the lowest triplet state, it may to be the state which experimentalists should use to obtain the quartet states, since it has the smallest vertical excitation energy from $\tilde{X}^1A_1 O_3$. Table 5.8 reports T_e , T_0 , and T_v predictions for the ionization of the 3B_2 state. If one takes the 3B_2 ozone electronic configuration, $6a_1^2 1a_2 4b_2^2 2b_1$, and removes an electron from the different orbitals (in a simple MO picture), the following ionization processes result: ${}^2A_2 \leftarrow {}^3B_2$, ${}^4A_1 \leftarrow {}^3B_2$, ${}^2B_1 \leftarrow {}^3B_2$, and ${}^4B_2 \leftarrow {}^3B_2$. However, this qualitative ${}^2B_1 \leftarrow {}^3B_2$ ionization does not correspond to the *ab initio* 2B_1 electron configuration. Instead, the ${}^2B_1 \leftarrow {}^3B_2$ ionization may be viewed as a two step process: ionization of a $4b_2$ electron followed

by the excitation $1a_2 \leftarrow 4b_2$. The resulting vertical IP, 13.07 eV, leads to dissociation into $^3\Sigma_g^-$ O_2 and 4S O^+ . The $^4B_2 \leftarrow ^3B_2$ pathway lies just above the 2B_2 vertical limit by 0.12 eV. The remaining three computed ionizations are two step routes: $^4A_2 \leftarrow ^3B_2$, $^2B_2 \leftarrow ^3B_2$, and $^2A_1 \leftarrow ^3B_2$. The first of these pathways removes a $4b_2$ electron and includes a symmetry forbidden $1a_2 \leftarrow 6a_1$ transition for a T_v of 12.58 eV. The $^2B_2 \leftarrow ^3B_2$ ionization involves a $2b_1$ electron ejection and subsequent $1a_2 \leftarrow 4b_2$ excitation, with an energy of 11.85 eV. The last two step process is a combination of the two mechanisms just mentioned: removal of a $2b_1$ electron and inclusion of a symmetry forbidden transition, $1a_2 \leftarrow 6a_1$ (T_v of 12.36 eV). Excluding symmetry forbidden transitions, only three schemes are realistic from the 3B_2 excited state: $^2B_2 \leftarrow ^3B_2$ (11.85 eV), $^2A_2 \leftarrow ^3B_2$ (12.49 eV) and $^4A_1 \leftarrow ^3B_2$ (12.82 eV).

5.4.3.2.3 $O_3^+ \leftarrow ^3B_1$ O_3

The third lowest triplet state, 3B_1 , is another possible ionization source for quartet states of O_3^+ . Table 5.8 reports theoretical ionization potentials from the 3B_1 state. The dissociation limit for 3B_1 warrants a short discussion. There exists extreme multireference character of the 2B_1 O_3^+ wavefunction at the 3B_1 O_3 equilibrium geometry resulting in cc-pCV5Z CASSCF CI coefficients of 0.77 and -0.51 from the most significant configurations. Thus, it may be challenging to reliably predict a vertical ionization energy of 2B_1 . Three processes from the 3B_1 electronic state of ozone are $^2A_1 \leftarrow ^3B_1$ (corresponding in qualitative terms to removal of an electron from a singly occupied $2b_1$ orbital), $^4A_2 \leftarrow ^3B_1$ (ejection of an electron from the doubly occupied $4b_2$ orbital), and $^4B_2 \leftarrow ^3B_1$ (ionization of an electron from the doubly occupied $1a_2$ orbital) with vertical IPs of 11.26, 12.46, and 12.65 eV, respectively. The only other single photon process occurs from the second most important electron configuration for the 3B_1 ($6a_1^2 1a_2 4b_2 2b_1^2$) state with the removal of an electron from the doubly occupied $2b_1$ orbital, 4A_1

$\leftarrow {}^3B_1$. However, this process has a large vertical excitation energy of 13.93 eV and the 4A_1 state is expected to dissociate into ${}^4S\ O^+$ and ${}^3\Sigma_g^- O_2$. The remaining ionization pathways considered here are two step processes which occur from 3B_1 . The ${}^2B_2 \leftarrow {}^3B_1$ process arises from removal of a $2b_1$ electron followed conceptually by $6a_1 \leftarrow 4b_2$ or $1a_2 \leftarrow 2b_1$ to yield the 2B_2 state, with a total predicted vertical IP of 12.15 eV. The second path, ${}^2A_2 \leftarrow {}^3B_1$, also removes a $2b_1$ electron plus a second single excitation, $6a_1 \leftarrow 1a_2$ or $4b_2 \leftarrow 2b_1$, also requiring 12.15 eV for the overall vertical ionization energy. However, the ${}^2B_2 \leftarrow {}^3B_1$ process is an unlikely transition, since $6a_1 \leftarrow 1a_2$ and $4b_2 \leftarrow 2b_1$ are both symmetry forbidden electronic transitions. Beyond reasonable doubt, ${}^2A_1 \leftarrow {}^3B_1$ is a bound pathway with vertical and adiabatic IPs of 11.26 and 11.07 eV, respectively. Tentatively, ${}^4A_2 \leftarrow {}^3B_1$, ${}^2A_2 \leftarrow {}^3B_1$, and ${}^4B_2 \leftarrow {}^3B_1$ are bound mechanisms, since sufficient energy for 2B_1 predissociation is not available.

5.4.3.2.4 ${}^4O_3^+ \leftarrow {}^2O_3^+$

As an alternative to initially exciting an electron from $\tilde{X}^1A_1 O_3$ to the triplet state and then ionizing, there exists the pathway of ionization (to a doublet state of O_3^+), followed by the spin-forbidden excitation to a quartet state. Table 5.8 reports the theoretical predictions for these spin forbidden transitions. With a ${}^4A_1 \leftarrow {}^2A_1$ vertical electronic excitation of 4.10 eV, the 4A_1 state will dissociate upon electronic transition. A second transition, ${}^4B_2 \leftarrow {}^2A_1$, is a tentative transition with a vertical IP_v of 2.03 eV. The third transition, ${}^4A_2 \leftarrow {}^2A_1$, is an energetically viable excitation, but it is also symmetry forbidden. Thus, there are no robust mechanisms for the formation of quartet O_3^+ via the ground electronic state of the ozone radical cation. For the first excited state of the ozone cation, there are two symmetry-allowed, spin-forbidden bound excitations to the quartet states: ${}^4A_1 \leftarrow {}^2B_2$ and ${}^4A_2 \leftarrow {}^2B_2$, with vertical excitation energies of 1.36 and 1.26 eV, respectively.

5.4.3.2.5 ${}^4\text{O}_3^+ \leftarrow {}^1\text{O}_3$

In Table 5.8, possible excitation energies from the ground state of ozone are shown. In conjunction with ${}^2\text{B}_1$ vertical ionization of 15.11 eV, ${}^4\text{A}_1 \text{O}_3^+ \leftarrow {}^1\text{A}_1 \text{O}_3$, ${}^4\text{B}_2 \text{O}_3^+ \leftarrow {}^1\text{A}_1 \text{O}_3$, and ${}^4\text{A}_2 \text{O}_3^+ \leftarrow {}^1\text{A}_1 \text{O}_3$ are bound processes with T_v of 14.90, 14.39, and 13.91 eV, respectively. Schmelz and coworkers³⁹ CASSCF and MRCI computations order the vertical IPs as ${}^2\text{A}_1$, ${}^2\text{B}_2$, ${}^2\text{A}_2$, ${}^4\text{A}_2$, ${}^4\text{B}_2$, ${}^2\text{B}_1$, ${}^4\text{A}_1$, and ${}^4\text{B}_1$ while our UCCSD(T) predictions switch the ${}^4\text{A}_1$ and ${}^2\text{B}_1$ states. The present CASSCF energies are within 0.15 eV of Schmelz's work while our coupled cluster relative energies are more than 0.5 eV larger than the MRCI results.

4.5 CONCLUSIONS

The potential energy surfaces for many different electronic states of ozone and the ozone radical cation have been thoroughly examined with CASSCF and coupled cluster theory. Inclusion of perturbative triples excitations yields excellent agreement with many experimental results, while perturbative quadruples excitations seem necessary for the ozone radical cation triplet energy spacing and dissociation limits.

Stanton and coworkers⁹⁻¹¹ state that triple excitations are needed for accurate geometry and vibrational frequency results for the $\tilde{X}^1\text{A}_1$ ground state of O_3 ; the present research extends this statement to triplet states of ozone and doublet states of the ozone radical cation. In most cases, the cc-pCV5Z UCCSD(T) method agrees with experimentally deduced bond distances and bond angles, except for the ${}^2\text{B}_2$ state. There our structure differs from that of Willitsch by 0.100 Å and 7.1°. ³² Merkt and coworkers suggests anharmonicity as the key reason for the theoretical inconsistency since they are observing an r_0 structure and a fundamental vibration. This could conceivably be a factor in the ${}^2\text{B}_2$ harmonic frequency differing by 100 ± 40 wavenumbers from experiment, and a more elaborate perturbation treatment is necessary for an accurate theoretical

prediction. An interesting by-product of the geometry discussion is that ozone and the ozone cation qualitatively follow the Walsh diagram for bond angle deductions.

While triple excitations are needed for accurate geometry and vibrational frequency predictions for $\tilde{X}^1A_1 O_3$, quadruple excitations appear necessary for coupled cluster methods to energetically order the triplet states of ozone, 3A_2 , 3B_2 , and 3B_1 , which have relative energies of 0.00, 0.13, and 0.28 eV. In addition to the triplet state energy spacings, the UCCSDT(Q) correlation is also essential for accurate thermochemical dissociation limits of the ozone radical cation. For the $\tilde{X}^2A_1 O_3^+ \rightarrow ^2\Pi_g O_2^+ + ^3P O$ dissociation, the quadruple excitations improve the UCCSD(T) energy of 0.44 eV to 0.63 eV which is in agreement with experiments⁴⁶⁻⁴⁸ to within 0.03 eV. For the second dissociation pathway, $\tilde{X}^2A_1 O_3^+ \rightarrow ^3\Sigma_g^- O_2 + ^4S O^+$, the perturbative quadruples corrected the UCCSD(T) value of 1.93 to 2.14 eV which agrees with the experimentally expected bond energy of 2.165 eV.⁴⁸ Although there is a dramatic effect on the thermochemical bond energies, the UCCSDT(Q) correction is not as important in the $^2B_1 O_3^+$ predissociation pathway. The UCCSDT(Q) method adds -0.05 eV to the UCCSD(T) energy of 1.94 eV to obtain a value of 1.89 eV, 0.03 eV from experiment.^{46,49} While UCCSD(T) was unable to quantitatively characterize a few ozone properties, it is successful in determining equilibrium geometries, harmonic vibrations, adiabatic and vertical singlet-triplet excitations, and adiabatic and vertical singlet-doublet ionization potentials.

From the energetic discussion above, three quartet minima lie below the 2B_1 dissociation limit and may be possible bound states with respect to photodissociation. From the ground state of ozone, vertical ionizations to 4A_2 , 4B_2 , and 4A_1 are possible at 13.91, 14.39, and 14.90 eV, compared to 15.11 eV for the 2B_1 state responsible for predissociation. Other possible pathways

to the quartet states are ${}^4A_1 \leftarrow {}^3A_2$, ${}^4A_2 \leftarrow {}^3A_2$, ${}^4A_1 \leftarrow {}^3B_2$, ${}^4A_2 \leftarrow {}^3B_1$, ${}^4B_2 \leftarrow {}^3B_1$, ${}^4A_1 \leftarrow {}^2B_2$, and ${}^4A_2 \leftarrow {}^2B_2$ with vertical IPs of 12.46, 12.85, 12.82, 12.46, 12.65, 1.36, and 1.26 eV, respectively.

This research has investigated ozone and the ozone radical cation with the most sophisticated coupled cluster methods yet applied to these systems. This research suggests several different avenues for experimentalists to detect and characterize the excited states of the ozone radical cation.

5.6 ACKNOWLEDGEMENTS

This research was supported by the Department of Energy, Office of Basic Energy Sciences, Chemical Sciences, Fundamental Interactions Team. We thank Professor Michael Duncan for helpful discussions.

5.7 REFERENCES

- ¹ N. J. Mason and S. K. Pathak, *Contemporary Phys.* **38**, 289 (1997).
- ² R. P. Wayne, *Chemistry of Atmospheres*, 3rd Ed. (Oxford University Press, Oxford, 2000).
- ³ V. Vaida and J. D. Simons, *Science* **268**, 1443 (1995).
- ⁴ J. Chappuis, *C. R. Acad. Sci.* **91**, 985 (1880).
- ⁵ R. Bacis, A. J. Bouvier, and J. M. Flaud, *Spectrochim. Acta A* **54**, 17 (1998).
- ⁶ J. I. Steinfeld, S. M. Adlergolden, and J. W. Gallagher, *J. Phys. Chem. Ref. Data* **16**, 911 (1987).
- ⁷ J. M. Flaud and R. Bacis, *Spectrochim. Acta A* **54**, 3 (1998).
- ⁸ V. G. Tyuterev, S. Tashkun, P. Jensen, A. Barbe, and T. Cours, *J. Mol. Spec.* **198**, 57 (1999).

- 9 D. H. Magers, W. N. Lipscomb, R. J. Bartlett, and J. F. Stanton, *J. Chem. Phys.* **91**, 1945
(1989).
- 10 J. D. Watts, J. F. Stanton, and R. J. Bartlett, *Chem. Phys. Lett.* **178**, 471 (1991).
- 11 J. D. Watts and R. J. Bartlett, *J. Chem. Phys.* **108**, 2511 (1998).
- 12 T. Tanaka and Y. Morino, *J. Mol. Spec.* **33**, 538 (1970).
- 13 J. C. Depannemaecker and J. Bellet, *J. Mol. Spec.* **66**, 106 (1977).
- 14 A. Barbe, A. Chichery, T. Cours, V. G. Tyuterev, and J. J. Plateaux, *J. Mol. Struct.* **616**,
55 (2002).
- 15 A. Barbe, C. Secroun, and P. Jouve, *J. Mol. Spec.* **49**, 171 (1974).
- 16 P. Borowski, M. Fulcher, P. A. Malmqvist, and B. O. Roos, *Chem. Phys. Lett.* **237**, 195
(1995).
- 17 S. M. Anderson and K. Mauersberger, *J. Geophys. Res. Atm.* **100**, 3033 (1995).
- 18 U. Wachsmuth and B. Abel, *J. Geophys. Res. Atm.* **108**, 4473 (2003).
- 19 S. F. Deppe, U. Wachsmuth, B. Abel, M. Bittererova, S. Y. Grebenshchikov, R. Siebert,
and R. Schinke, *J. Chem. Phys.* **121**, 5191 (2004).
- 20 D. W. Arnold, C. S. Xu, E. H. Kim, and D. M. Neumark, *J. Chem. Phys.* **101**, 912 (1994).
- 21 J. D. Watts and R. J. Bartlett, *Spectrochim. Acta A* **55**, 495 (1999).
- 22 C. R. Brundle, *Chem. Phys. Lett.* **26**, 25 (1974).
- 23 T. Cvitas, L. Klasinc, and B. Kovac, *Int. J. Quant. Chem.* **29**, 657 (1986).
- 24 J. M. Dyke, L. Golob, N. Jonathan, A. Morris, and M. Okuda, *J. Chem. Soc. Far. Trans.*
70, 1828 (1974).
- 25 D. C. Frost, S. T. Lee, and C. A. McDowell, *Chem. Phys. Lett.* **24**, 149 (1974).
- 26 S. Katsumata, H. Shiromaru, and T. Kimura, *Bull. Chem. Soc. Jpn.* **57**, 1784 (1984).

- 27 T. N. Radwan and D. W. Turner, *J. Chem. Soc. A*, 85 (1966).
- 28 M. J. Weiss, J. Berkowitz, and E. H. Appelman, *J. Chem. Phys.* **66**, 2049 (1977).
- 29 A. Mocellin, K. Wiesner, F. Burmeister, O. Bjorneholm, and A. N. de Brito, *J. Chem. Phys.* **115**, 5041 (2001).
- 30 J. T. Moseley, J. B. Ozenne, and P. C. Cosby, *J. Chem. Phys.* **74**, 337 (1981).
- 31 M. Probst, K. Hermansson, J. Urban, P. Mach, D. Muigg, G. Denifl, T. Fiegele, N. J. Mason, A. Stamatovic, and T. D. Mark, *J. Chem. Phys.* **116**, 984 (2002).
- 32 S. Willitsch, F. Innocenti, J. M. Dyke, and F. Merkt, *J. Chem. Phys.* **122**, 24311 (2005).
- 33 H. Couto, A. Mocellin, C. D. Moreira, M. P. Gomes, A. N. de Brito, and M. C. A. Lopes, *J. Chem. Phys.* **124**, 204311 (2006).
- 34 P. J. Hay, T. H. Dunning, and W. A. Goddard, *J. Chem. Phys.* **62**, 3912 (1975).
- 35 H. Basch, *J. Am. Chem. Soc.* **97**, 6047 (1975).
- 36 L. S. Cederbaum, W. Domcke, W. von Niessen, and W. P. Kraemer, *Mol. Phys.* **34**, 381 (1977).
- 37 N. Kosugi, H. Kuroda, and S. Iwata, *Chem. Phys.* **58**, 267 (1981).
- 38 P. Malquist, H. Agren, and B. O. Roos, *Chem. Phys. Lett.* **98**, 444 (1983).
- 39 T. Schmelz, G. Chambaud, P. Rosmus, H. Koppel, L. S. Cederbaum, and H. J. Werner, *Chem. Phys. Lett.* **183**, 209 (1991).
- 40 H. Muller, H. Koppel, and L. S. Cederbaum, *New J. Chem.* **17**, 7 (1993).
- 41 H. Muller, H. Koppel, and L. S. Cederbaum, *J. Chem. Phys.* **101**, 10263 (1994).
- 42 H. Muller, H. Koppel, L. S. Cederbaum, T. Schmelz, G. Chambaud, and P. Rosmus, *Chem. Phys. Lett.* **197**, 599 (1992).
- 43 M. H. Palmer and A. D. Nelson, *Mol. Phys.* **100**, 3601 (2002).

- 44 K. Wiesner, R. F. Fink, S. L. Sorensen, M. Andersson, R. Feifel, I. Hjelte, C. Miron, A.
N. de Brito, L. Rosenqvist, H. Wang, S. Svensson, and O. Bjorneholm, *Chem. Phys. Lett.*
375, 76 (2003).
- 45 Y. Ohtsuka, J. Hasegawa, and H. Nakatsuji, *Chem. Phys.* **332**, 262 (2007).
- 46 M. L. Vestal and G. H. Mauclaire, *J. Chem. Phys.* **67**, 3767 (1977).
- 47 M. J. Weiss, J. Berkowitz, and E. H. Appelman, *J. Chem. Phys.* **66**, 2049 (1977).
- 48 J. T. Moseley, J. B. Ozenne, and P. C. Cosby, *J. Chem. Phys.* **74**, 337 (1981).
- 49 J. F. Hiller and M. L. Vestal, *J. Chem. Phys.* **77**, 1248 (1982).
- 50 S. P. Goss and J. D. Morrison, *J. Chem. Phys.* **76**, 5175 (1982).
- 51 A. Mocellin, K. Wiesner, F. Burmeister, O. Bjorneholm, and A. N. de Brito, *J. Chem.*
Phys. **115**, 5041 (2001).
- 52 C. E. Dykstra, H. F. Schaefer, and W. Meyer, *J. Chem. Phys.* **65**, 2740 (1976).
- 53 W. Meyer, *J. Chem. Phys.* **64**, 2901 (1976).
- 54 C. E. Dykstra, R. A. Chiles, and M. D. Garrett, *J. Comp. Chem.* **2**, 266 (1981).
- 55 H. J. Werner and E. A. Reinsch, *J. Chem. Phys.* **76**, 3144 (1982).
- 56 A. C. Scheiner, G. E. Scuseria, T. J. Lee, J. E. Rice, and H. F. Schaefer, *J. Chem. Phys.*
87, 5391 (1987).
- 57 G. D. Purvis and R. J. Bartlett, *J. Chem. Phys.* **76**, 1910 (1982).
- 58 G. E. Scuseria, C. L. Janssen, and H. F. Schaefer, *J. Chem. Phys.* **89**, 7382 (1988).
- 59 G. E. Scuseria, A. C. Scheiner, T. J. Lee, J. E. Rice, and H. F. Schaefer, *J. Chem. Phys.*
86, 2881 (1987).
- 60 G. E. Scuseria, *Chem. Phys. Lett.* **176**, 27 (1991).

- 61 K. Raghavachari, G. W. Trucks, J. A. Pople, and M. Head-Gordon, *Chem. Phys. Lett.*
157, 479 (1989).
- 62 G. E. Scuseria and T. J. Lee, *J. Chem. Phys.* **93**, 5851 (1990).
- 63 D. E. Woon and T. H. Dunning, *J. Chem. Phys.* **103**, 4572 (1995).
- 64 T. H. Dunning, *J. Chem. Phys.* **90**, 1007 (1989).
- 65 R. D. Amos, A. Bernhardsson, A. Berning, P. Celani, D. L. Cooper, M. J. O. Deegan, A.
J. Dobbyn, F. Eckert, C. Hampel, G. Hetzer, P. J. Knowles, T. Korona, R. Lindh, A. W.
Lloyd, S. J. McNicholas, F. R. Manby, W. Meyer, M. E. Mura, A. Nicklass, P. Palmieri,
R. M. Pitzer, G. Rauhut, M. Schutz, U. Schumann, H. Stoll, A. J. Stone, R. Tarroni, T.
Thorsteinsson, and H. J. Werner, *MOLPRO* (2002).
- 66 R. Lindh, U. Ryu, and B. Liu, *J. Chem. Phys.* **95**, 5889 (1991).
- 67 R. Lindh, *Theor. Chim. Acta.* **85**, 423 (1993).
- 68 G. Rauhut, A. E. Azhary, F. Eckert, U. Schumann, and H. J. Werner, *Spectrochim. Acta*
A **55**, 651 (1999).
- 69 M. J. O. Deegan and P. J. Knowles, *Chem. Phys. Lett.* **227**, 321 (1994).
- 70 C. Hampel and H. J. Werner, *J. Chem. Phys.* **104**, 6286 (1996).
- 71 M. Schutz and H. J. Werner, *Chem. Phys. Lett.* **318**, 370 (2000).
- 72 M. Schutz, *J. Chem. Phys.* **113**, 9986 (2000).
- 73 J.F. Stanton, J. Gauss, J.D. Watts, P.G. Szalay, R.J. Bartlett with contributions from A.A.
Auer, D.B. Bernholdt, O. Christiansen, M.E. Harding, M. Heckert, O. Heun, C. Huber, D.
Jonsson, J. Jusélius, W.J. Lauderdale, T. Metzroth, C. Michauk, D.R. Price, K. Ruud, F.
Schiffmann, A. Tajti, M.E. Varner, J. Vázquez and the integral packages: MOLECULE

- (J. Almlöf and P.R. Taylor), PROPS (P.R. Taylor), and ABACUS (T. Helgaker, H.J. Aa. Jensen, P. Jørgensen, and J. Olsen).
- 74 J. F. Stanton, J. Gauss, J. D. Watts, W. J. Lauderdale, and R. J. Bartlett, *Int. J. Quant. Chem. Symp.* **26**, 879 (1992).
- 75 P.G. Szalay, J. Gauss, and J. F. Stanton, *Theor. Chim. Acta.* **100**, 5 (1998).
- 76 J. Gauss and J. F. Stanton, *J. Chem. Phys.* **104**, 2574 (1996).
- 77 M. Kállay and J. Gauss, *J. Chem. Phys.* **120**, 6841 (2004).
- 78 S. A. Kucharski, *J. Chem. Phys.* **97**, 4282 (1992).
- 79 N. Oliphant, *J. Chem. Phys.* **95**, 6645 (1991).
- 80 M. Kállay and P. R. Surjan, *J. Chem. Phys.* **115**, 2945 (2001).
- 81 M. Kállay, P. G. Szalay, and P. R. Surjan, *J. Chem. Phys.* **117**, 980 (2002).
- 82 M. Kállay, J. Gauss, and P. G. Szalay, *J. Chem. Phys.* **119**, 2991 (2003).
- 83 M. Kállay and J. Gauss, *J. Chem. Phys.* **121**, 9257 (2004).
- 84 M. Kállay and J. Gauss, *J. Chem. Phys.* **123**, 214105 (2005).
- 85 K. P. Huber and G. Herzberg, *Molecular Spectra and Molecular Structure IV. Constants of Diatomic Molecules.* (Van Nostrand Reinhold Company Inc., New York, 1979).
- 86 C. E. Moore, *Atomic Energy Levels As Derived from the Analysis of Optical Spectra.* (1949).
- 87 R. G. Tonkyn, J. W. Winniczek, and M. G. White, *Chem. Phys. Lett.* **164**, 137 (1989).
- 88 A. J. Bouvier, D. Inard, V. Veyret, B. Bussery, R. Bacis, S. Churassy, J. Brion, J. Malicet, and R. H. Judge, *J. Mol. Spec.* **190**, 189 (1998).
- 89 M. Allan, N. J. Mason, and J. A. Davies, *J. Chem. Phys.* **105**, 5665 (1996).

Table 5.1. Optimized geometries for O_3^+ states (bond distances in Angstroms; angles in degrees).

Basis Set	Theory	4A_1		4A_2		4B_2		4B_1	
		r_e	θ_e	r_e	θ_e	r_e	θ_e	r_e	θ_e
cc-pCVTZ	CASSCF	1.3754	90.43	1.3398	113.28	1.3475	123.60	1.4897	99.73
cc-pCVQZ	CASSCF	1.3734	90.58	1.3373	113.19	1.3449	123.57	1.4879	99.36
cc-pCV5Z	CASSCF	1.3732	90.60	1.3372	113.18	1.3447	123.55	1.4877	99.34
cc-pCVTZ	UCCSD	1.3444	89.60	1.3113	113.64	1.3098	125.07	1.4449	96.01
cc-pCVQZ	UCCSD	1.3384	89.81	1.3046	113.63	1.3029	125.13	1.4373	95.82
cc-pCV5Z	UCCSD	1.3371	89.82	1.3033	113.61	1.3015	125.09	1.4354	95.82
cc-pCVTZ	UCCSD(T)	1.3618	89.58	1.3251	113.83	1.3303	124.60	1.4720	97.56
cc-pCVQZ	UCCSD(T)	1.3561	89.77	1.3185	113.79	1.3233	124.64	1.4647	97.25
cc-pCV5Z	UCCSD(T)	1.3549	89.78	1.3173	113.76	1.3219	124.59	1.4626	97.25
Basis Set	Theory	2A_1		2B_2		2B_1		2A_2	
		r_e	θ_e	r_e	θ_e	r_e	θ_e	r_e	θ_e
cc-pCVTZ	CASSCF	1.2476	130.62	1.2896	104.51	1.3661	71.34	1.3012	112.68
cc-pCVQZ	CASSCF	1.2450	130.65	1.2872	104.59	1.3640	71.49	1.2985	112.72
cc-pCV5Z	CASSCF	1.2449	130.63	1.2870	104.61	1.3638	71.47	1.2983	112.74
cc-pCVTZ	UCCSD	1.2034	134.09	1.2477	103.79	1.3389	69.18	1.2717	112.85
cc-pCVQZ	UCCSD	1.1981	134.19	1.2423	103.93	1.3328	69.28	1.2654	112.91
cc-pCV5Z	UCCSD	1.1970	134.18	1.2412	103.96	1.3316	69.22	1.2642	112.91
cc-pCVTZ	UCCSD(T)	1.2345	132.57	1.2784	104.01	1.3535	70.92	1.2920	112.79
cc-pCVQZ	UCCSD(T)	1.2283	132.71	1.2722	104.12	1.3477	71.10	1.2854	112.84
cc-pCV5Z	UCCSD(T)	1.2272	132.70	1.2711	104.15	1.3465	71.02	1.2841	112.83
Experiment ^a		1.25	131.5	1.371	111.3				

^a Reference 32.

Table 5.2. Optimized geometries for O₃ states (bond distances in Angstroms; angles in degrees).

Basis Set	Theory	³ A ₂		³ B ₂		³ B ₁		³ A ₁ (³ Σ _g ⁻)		¹ A ₁ O ₃	
		r _e	θ _e	r _e	θ _e	r _e	θ _e	r _e	θ _e	r _e	θ _e
cc-pCVTZ	CASSCF	1.3622	99.13	1.3726	108.36	1.3388	124.42	1.6923	180.00	1.2840	116.70
cc-pCVQZ	CASSCF	1.3593	99.25	1.3693	108.41	1.3354	124.48	1.6921	180.00	1.2806	116.79
cc-pCV5Z	CASSCF	1.3588	99.30	1.3688	108.44	1.3350	124.47	1.6911	180.00	1.2801	116.82
cc-pCVTZ	UCCSD	1.3193	97.17	1.3448	108.46	1.2837	129.45	^a	^a	1.2471	117.67
cc-pCVQZ	UCCSD	1.3133	97.36	1.3380	108.52	1.2773	129.52	^a	^a	1.2412	117.79
cc-pCV5Z	UCCSD	1.3120	97.42	1.3365	108.53	1.2760	129.47	^a	^a	1.2399	117.81
cc-pCVTZ	UCCSD(T)	1.3389	97.73	1.3574	108.48	1.3063	128.41	^a	^a	1.2728	117.03
cc-pCVQZ	UCCSD(T)	1.3331	97.84	1.3509	108.52	1.3000	128.51	^a	^a	1.2663	117.17
cc-pCV5Z	UCCSD(T)	1.3321	97.90	1.3496	108.53	1.2987	128.45	^a	^a	1.2649	117.19
	Experiment ^b	1.345	98.9								
	Experiment ^c									1.2717	116.47
	Experiment ^d									1.2715	117.47

^a With a linear structure, the ³A₁ (³Σ_g⁻) state is too multireference in character for single determinant methods.

^b Reference 88.

^c Reference 12

^d Reference 13

Table 5.3. Optimized geometries (in Angstroms), harmonic vibrational frequencies (in cm^{-1}), and ionization potentials (in eV) for O_2 and O_2^+ .

Basis Set	Theory	$^3\Sigma_g^- \text{O}_2$		$^2\Pi_g \text{O}_2^+$		$^4\text{S O}^+ \leftarrow ^3\text{P O}$	$^2\Pi_g \text{O}_2^+ \leftarrow ^3\Sigma_g^- \text{O}_2$	
		r_e	ω	r_e	ω	IP_e	IP_e	IP_0
cc-pCVTZ	CASSCF	1.2176	1539	1.1212	1901	11.96	10.09	10.12
cc-pCVQZ	CASSCF	1.2154	1547	1.1200	1909	11.97	10.07	10.09
cc-pCV5Z	CASSCF	1.2152	1548	1.1199	1909	11.97	10.07	10.09
cc-pCVTZ	UCCSD	1.1973	1682	1.1058	2044	13.30	11.97	11.99
cc-pCVQZ	UCCSD	1.1929	1700	1.1024	2068	13.45	12.06	12.08
cc-pCV5Z	UCCSD	1.1919	1703	1.1015	2071	13.51	12.10	12.12
cc-pCVTZ	UCCSD(T)	1.2099	1591	1.1184	1919	13.34	11.90	11.92
cc-pCVQZ	UCCSD(T)	1.2057	1606	1.1150	1941	13.50	12.01	12.03
cc-pCV5Z	UCCSD(T)	1.2048	1608	1.1142	1944	13.56	12.05	12.07
Experiment ^a		1.2075	1580	1.1164	1905	13.61 ^b		12.07 ^c

^a Reference 85.
^b Reference 86.
^c Reference 87.

Table 5.4. cc-pCV5Z CASSCF CI coefficients ($> \pm 0.23$) and corresponding electron configurations.

State	CI	Electron Configuration
$^4A_1 O_3^+$	0.922	... ^a $1b_1^2 5a_1^2 6a_1^2 1a_2 4b_2 2b_1$
$^4B_1 O_3^+$	0.887	... $1b_1^2 5a_1^2 6a_1 1a_2 4b_2 2b_1^2$
$^4B_2 O_3^+$	0.919	... $1b_1^2 5a_1^2 6a_1 1a_2 4b_2^2 2b_1$
$^4A_2 O_3^+$	0.941	... $1b_1^2 5a_1^2 6a_1 1a_2^2 4b_2 2b_1$
$^3A_1 O_3$	0.759	+++ ^b $1\pi_u^4 1\pi_g^4 2\pi_u^2$
$(^3\Sigma_g^- O_3)$	0.832	+++ $1\pi_u^4 1\pi_g^2 2\pi_u^4$
$^3B_1 O_3$	0.895	... $1b_1^2 5a_1^2 6a_1 1a_2^2 4b_2^2 2b_1$
	-0.305	... $1b_1^2 5a_1^2 6a_1^2 1a_2 4b_2 2b_1^2$
$^3B_2 O_3$	0.956	... $1b_1^2 5a_1^2 6a_1^2 1a_2 4b_2^2 2b_1$
$^3A_2 O_3$	0.888	... $1b_1^2 5a_1^2 6a_1^2 1a_2^2 4b_2 2b_1$
	-0.336	... $1b_1^2 5a_1^2 6a_1 1a_2 4b_2^2 2b_1^2$
$^2A_1 O_3^+$	0.886	... $1b_1^2 5a_1^2 6a_1 1a_2^2 4b_2^2$
	-0.239	... $1b_1^2 5a_1^2 6a_1^2 1a_2 4b_2 2b_1$
$^2B_1 O_3^+$	0.905	... $1b_1^2 5a_1^2 6a_1^2 1a_2^2 2b_1$
$^2B_2 O_3^+$	0.870	... $1b_1^2 5a_1^2 6a_1^2 1a_2^2 4b_2$
	-0.291	... $1b_1^2 5a_1^2 6a_1 1a_2 4b_2^2 2b_1$
$^2A_2 O_3^+$	0.910	... $1b_1^2 5a_1^2 6a_1^2 1a_2 4b_2^2$
	0.241	... $1b_1 5a_1^2 6a_1^2 1a_2 4b_2^2 2b_1$
$^1A_1 O_3$	0.908	... $1b_1^2 5a_1^2 6a_1^2 1a_2^2 4b_2^2$
	-0.289	... $1b_1^2 5a_1^2 6a_1^2 4b_2^2 2b_1^2$
$^3\Sigma_g^- O_2$	0.958	$1\sigma_g^2 1\sigma_u^2 2\sigma_g^2 2\sigma_u^2 3\sigma_g^2 1\pi_u^4 1\pi_g^2$
$^2\Pi_g O_2^+$	0.969	$1\sigma_g^2 1\sigma_u^2 2\sigma_g^2 2\sigma_u^2 3\sigma_g^2 1\pi_u^4 1\pi_g^a$
		^a ■■■ = $1a_1^2 2a_1^2 1b_2^2 3a_1^2 2b_2^2 4a_1^2 3b_2^2$
		^b ††† = $1\sigma_g^2 2\sigma_g^2 1\sigma_u^2 3\sigma_g^2 2\sigma_u^2 4\sigma_g^2 3\sigma_u^2$

Table 5.5. cc-pCVTZ harmonic vibrational frequencies (in cm^{-1}), infrared intensities (in km mol^{-1}) in parentheses, and zero-point vibrational energies (ZPVE) (in eV) for O_3 and O_3^+ .

State	$\omega_1 (a_1)$			$\omega_2 (a_1)$			$\omega_3 (b_2)$			ZPVE	
	UCCSD	UCCSD(T)	Exp (Harm)	UCCSD	UCCSD(T)	Exp (Harm)	UCCSD	UCCSD(T)	Exp (Harm)	UCCSD	UCCSD(T)
$^4A_1 \text{ O}_3^+$	1185 (52.5)	1136 (50.7)		614 (4.6)	584 (4.5)		382 (142.1)	148 (50.9)		0.14	0.12
$^4B_1 \text{ O}_3^+$	906 (37.2)	857 (40.0)		419 (4.9)	382 (5.7)		422 (808.3)	452 (1178.0)		0.11	0.10
$^4B_2 \text{ O}_3^+$	1004 (46.9)	941 (44.4)		555 (16.6)	529 (15.0)		513 <i>i</i> (168.5)	753 <i>i</i> (0.2)		0.10	0.09
$^4A_2 \text{ O}_3^+$	1051 (41.0)	999 (43.0)		524 (5.1)	502 (5.7)		125 (3.2)	233 (0.4)		0.11	0.11
$^3B_1 \text{ O}_3$	1056 (1.4)	988 (2.1)		584 (2.3)	559 (1.8)	555 ± 15 ^a	640 (107.8)	603 (10.9)		0.14	0.13
$^3B_2 \text{ O}_3$	1110 (0.3)	1069 (0.1)	1090 ± 80 ^c	620 (2.9)	596 (2.6)	580 ± 50 ^b	711 (9.7)	578 (6.3)		0.15	0.14
$^3A_2 \text{ O}_3$	1232 (0.7)	1156 (1.6)	1190 ± 15 ^a	620 (2.4)	587 (2.7)	528 ± 5 ^a	216 (71.0)	250 (4.9)		0.13	0.12
$^2A_1 \text{ O}_3^+$	1207 (33.7)	1069 (35.7)	1050 ± 50 ^e	689 (13.7)	648 (13.6)	617 ± 0.1 ^g	1205 (1.3)	1037 (4.7)		0.19	0.17
$^2B_1 \text{ O}_3^+$	1301 (33.1)	1228 (38.1)		750 (8.1)	656 (6.0)		492 <i>i</i> (7.2)	294 <i>i</i> (8.4)		0.13	0.12
$^2B_2 \text{ O}_3^+$	1356 (45.2)	1278 (55.9)	1380 ± 40 ^f	707 (1.9)	659 (1.8)		276 (43.6)	143 (67.1)		0.15	0.13
$^2A_2 \text{ O}_3^+$	1179 (25.5)	1151 (27.1)		696 (1.4)	673 (1.5)		662 <i>i</i> (17.3)	704 <i>i</i> (14.5)		0.12	0.11
$^1A_1 \text{ O}_3$	1283 (0.0)	1158 (0.3)	1133 ± 0.4 ^d	767 (7.5)	720 (6.1)	715 ± 0.4 ^d	1273 (203.5)	1062 (113.3)	1087 ± 0.3 ^d	0.21	0.18

^a Reference 17.
^b Reference 20.
^c Reference 89.
^d Reference 14.
^e Reference 47.
^f Fundamental Frequency from Reference 22 and 26.
^g Fundamental Frequency from Reference 32.

Table 5.6. Comparison of theoretical and experimental excitation energies and ionization potentials (in eV) with respect to the \tilde{X}^1A_1 state of O_3 .

		${}^3X O_3 \leftarrow {}^1A_1 O_3$															
Basis	Method	3A_2				3B_2				3B_1				3A_1			
		T_e	T_0	T_v	ΔT_0	T_e	T_0	T_v	ΔT_0	T_e	T_0	T_v	ΔT_0	T_e	T_0	T_v	ΔT_0
cc-pCVTZ	CASSCF	1.43		2.07		1.33		1.73		1.73		1.98		4.61		8.07	
cc-pCVQZ	CASSCF	1.46		2.10		1.35		1.76		1.76		2.01		4.66		8.12	
cc-pCV5Z	CASSCF	1.46		2.11		1.35		1.76		1.77		2.02		4.68		8.12	
cc-pCVTZ	UCCSD	1.08	1.00	1.96	0.39	0.67	0.62	1.27	0.00	1.37	1.30	1.69	0.68			8.12	
cc-pCVQZ	UCCSD	1.13	1.05	2.01	0.37	0.73	0.68	1.33	0.00	1.40	1.34	1.72	0.66			8.21	
cc-pCV5Z	UCCSD	1.14	1.06	2.02	0.37	0.74	0.69	1.35	0.00	1.41	1.35	1.73	0.66			8.22	
cc-pCVTZ	UCCSD(T)	1.22	1.16	1.92	0.01	1.19	1.15	1.61	0.00	1.48	1.43	1.75	0.29			7.96	
cc-pCVQZ	UCCSD(T)	1.25	1.19	1.97	0.00	1.25	1.20	1.67	0.01	1.51	1.46	1.78	0.27			8.04	
cc-pCV5Z	UCCSD(T)	1.26	1.20	1.98	0.00	1.26	1.22	1.69	0.02	1.52	1.47	1.79	0.27			8.04	
Experiment ^a		1.24	1.18		0.00	1.29	1.29		0.11	1.48	1.45		0.27				
		${}^2X O_3^+ \leftarrow {}^1A_1 O_3$															
Basis	Method	2A_1				2B_2				2B_1				2A_2			
		T_e	T_0	T_v	ΔT_0	T_e	T_0	T_v	ΔT_0	T_e	T_0	T_v	ΔT_0	T_e	T_0	T_v	ΔT_0
cc-pCVTZ	CASSCF	10.86		11.12		11.01		11.23		11.87		12.93		11.77		11.81	
cc-pCVQZ	CASSCF	10.87		11.12		11.01		11.24		11.88		12.95		11.77		11.81	
cc-pCV5Z	CASSCF	10.87		11.12		11.01		11.24		11.89		12.95		11.77		11.81	
cc-pCVTZ	UCCSD	12.62	12.61	13.05	0.00	12.90	12.84	13.24	0.23	13.13	13.05	15.32	0.45	13.09	13.00	13.16	0.40
cc-pCVQZ	UCCSD	12.76	12.74	13.19	0.00	13.05	12.99	13.40	0.25	13.31	13.23	15.51	0.49	13.24	13.15	13.31	0.41
cc-pCV5Z	UCCSD	12.82	12.80	13.25	0.00	13.11	13.05	13.46	0.25	13.36	13.28	15.58	0.48	13.30	13.21	13.37	0.41
cc-pCVTZ	UCCSD(T)	12.34	12.32	12.67	0.00	12.57	12.52	12.84	0.19	13.22	13.16	14.53	0.83	13.33	13.26	13.38	0.94
cc-pCVQZ	UCCSD(T)	12.49	12.48	12.84	0.00	12.74	12.68	13.01	0.20	13.41	13.34	14.76	0.86	13.50	13.43	13.55	0.95
cc-pCV5Z	UCCSD(T)	12.56	12.55	12.90	0.00	12.80	12.75	13.08	0.20	13.47	13.40	14.84	0.85	13.56	13.50	13.61	0.95
Experiment			12.52 ^b	13.13 ^d	0.00		12.66 ^b	13.03 ^c	0.14			15.21 ^d				13.57 ^c	
												15.03 ^e					

^a Reference 17.
^b Reference 32.
^c References 23 and 26.
^d Reference 47.
^e Reference 50.

Table 5.7. Comparison of experimental and theoretical dissociation energies (in eV) for ${}^2A_1 O_3^+$ and ${}^2B_2 O_3^+$. (See Appendix A for theoretical dissociation energies for remaining O_3^+ states.)

Basis	Method	${}^2A_1 O_3^+ \rightarrow$					${}^2B_2 O_3^+ \rightarrow$	
		${}^2\Pi_g O_2^+ + {}^3P O$		${}^3\Sigma_g^- O_2 + {}^4S O^+$			${}^2\Pi_g O_2^+ + {}^3P O$	
		D_e	D_0	D_e	D_0	2B_1	D_e	D_0
cc-pCVTZ	UCCSD	-0.50	-0.43	0.83	0.74	2.28	-0.78	-0.76
cc-pCVQZ	UCCSD	-0.42	-0.36	0.97	0.88	2.32	-0.71	-0.70
cc-pCV5Z	UCCSD	-0.39	-0.33	1.01	0.93	2.33	-0.69	-0.67
cc-pCVTZ	UCCSD(T)	0.38	0.33	1.82	1.75	1.85	0.15	0.14
cc-pCVQZ	UCCSD(T)	0.46	0.41	1.96	1.88	1.92	0.21	0.21
cc-pCV5Z	UCCSD(T)	0.49	0.44	2.01	1.93	1.94	0.25	0.24
	UCCSDT(Q)	0.68	0.63	2.21	2.14	1.89	0.54	0.53
Bond Energy			0.60		2.17			
Experiment								
	Reference 49					1.86		
	Reference 46		0.60			1.85		
	Reference 48		0.59			1.77		
	Reference 47		0.61					

Table 5.8. Theoretical cc-pCV5Z UCCSD(T) adiabatic (T_e), ZPVE-corrected adiabatic (T_0), and vertical ionization potentials (T_v) in eV. (See Appendix A for additional CASSCF, UCCSD, and UCCSD(T) energy predictions.)

$O_3^+ \leftarrow {}^3A_2 O_3$				$O_3^+ \leftarrow {}^3B_2 O_3$				$O_3^+ \leftarrow {}^3B_1 O_3$			
State	T_e	T_0	T_v	State	T_e	T_0	T_v	State	T_e	T_0	T_v
4A_1	12.35	12.34	12.46	4A_2	12.53	12.49	12.58	4A_2	12.26	12.24	12.46
4A_2	12.53	12.51	12.85	4A_1	12.35	12.33	12.82	4B_2	12.61	12.57	12.65
4B_2	12.88	12.85	13.96	4B_2	12.88	12.83	13.19	4A_1	12.09	12.07	13.93
4B_1	15.34	15.32	15.83	4B_1	15.34	15.31	15.73	4B_1	15.08	15.05	16.38
2B_2	11.54	11.55	11.73	2B_2	11.54	11.53	11.85	2A_1	11.04	11.07	11.26
Exp ^a		11.48		Exp ^b		11.37		Exp ^c		11.07	
2A_2	12.30	12.29	12.79	2A_1	11.30	11.33	12.36	2B_2	11.28	11.28	12.15
2B_1	12.21	12.20	12.91	Exp ^b		11.23		Exp ^c		11.21	
2A_1	11.30	11.35	13.23	2A_2	12.30	12.28	12.49	2A_2	12.04	12.02	12.45
Exp ^a		11.34		2B_1	12.21	12.18	13.07	2B_1	11.94	11.81	12.95
${}^4X O_3^+ \leftarrow {}^1A_1 O_3$ (eV)				${}^4O_3^+ \leftarrow {}^2A_1 O_3^+$				${}^4O_3^+ \leftarrow {}^2B_2 O_3^+$			
State	T_e	T_0	T_v	State	T_e	T_0	T_v	State	T_e	T_0	T_v
4A_2	13.79	13.71	13.91	4A_1	1.05	1.00	4.10	4A_1	0.80	0.79	1.36
4B_2	14.14	14.05	14.39	4A_2	1.23	1.16	1.85	4B_2	1.33	1.30	2.23
4A_1	13.61	13.54	14.90	4B_2	1.58	1.50	2.03	4B_1	3.80	3.77	4.95
4B_1	16.60	16.53	18.00	4B_1	4.04	3.98	6.61	4A_2	0.98	0.96	1.26

^a $T_0 [{}^2(B_2, A_1) O_3^+ \leftarrow {}^1A_1 O_3] - T_0 [{}^3A_2 O_3 \leftarrow {}^1A_1 O_3]$, See Table 6
^b $T_0 [{}^2(B_2, A_1) O_3^+ \leftarrow {}^1A_1 O_3] - T_0 [{}^3B_2 O_3 \leftarrow {}^1A_1 O_3]$, See Table 6
^c $T_0 [{}^2(B_2, A_1) O_3^+ \leftarrow {}^1A_1 O_3] - T_0 [{}^3B_1 O_3 \leftarrow {}^1A_1 O_3]$, See Table 6

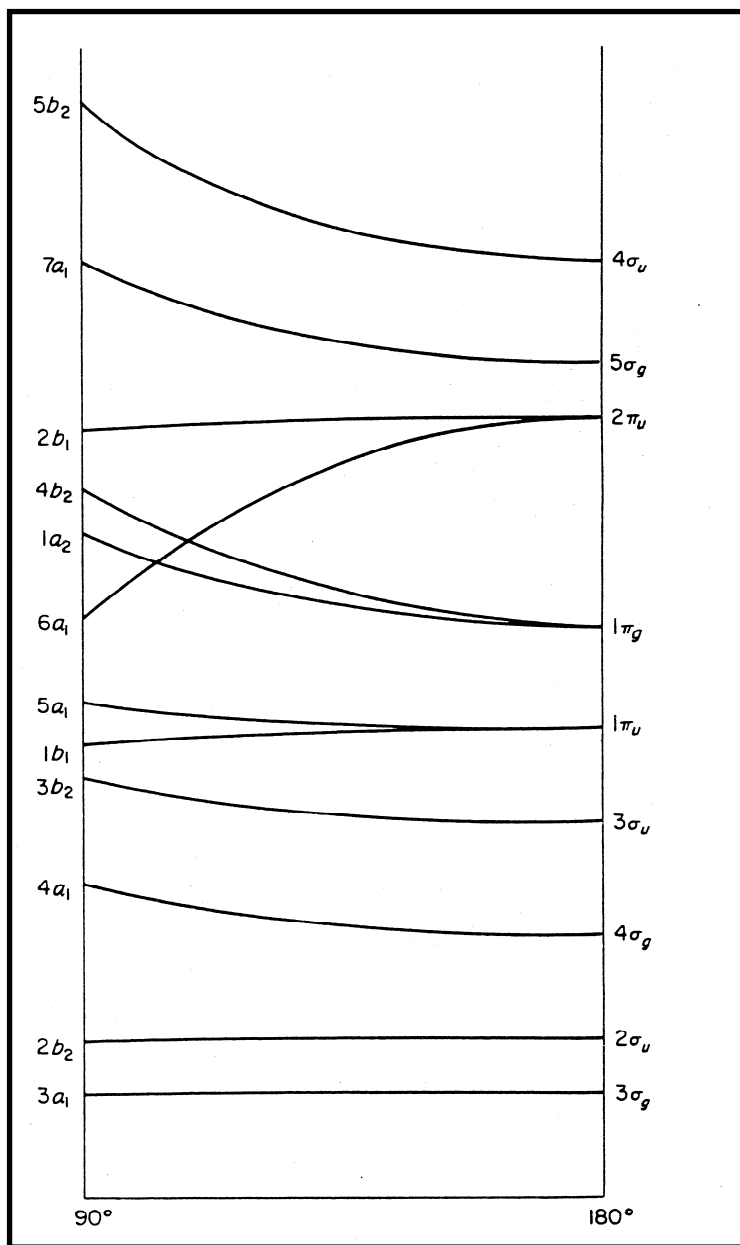


Figure 5.1. Walsh Diagram for XY₂.

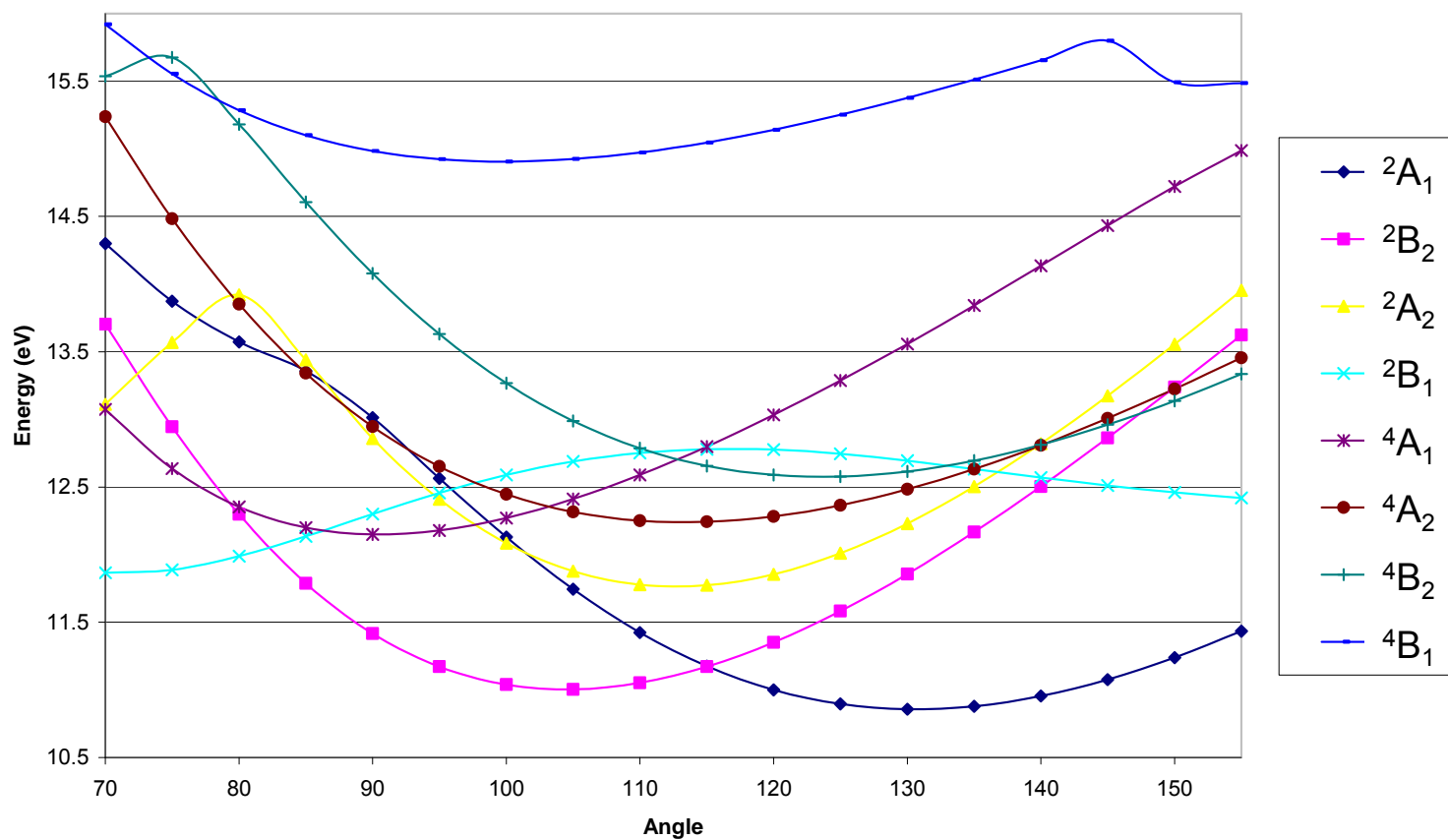


Figure 5.2. cc-pVTZ CASSCF potential energy curves for O_3^+ (reference energy is the \tilde{X}^1A_1 state of O_3). Each point represents a constrained geometrical optimization for a fixed bond angle.

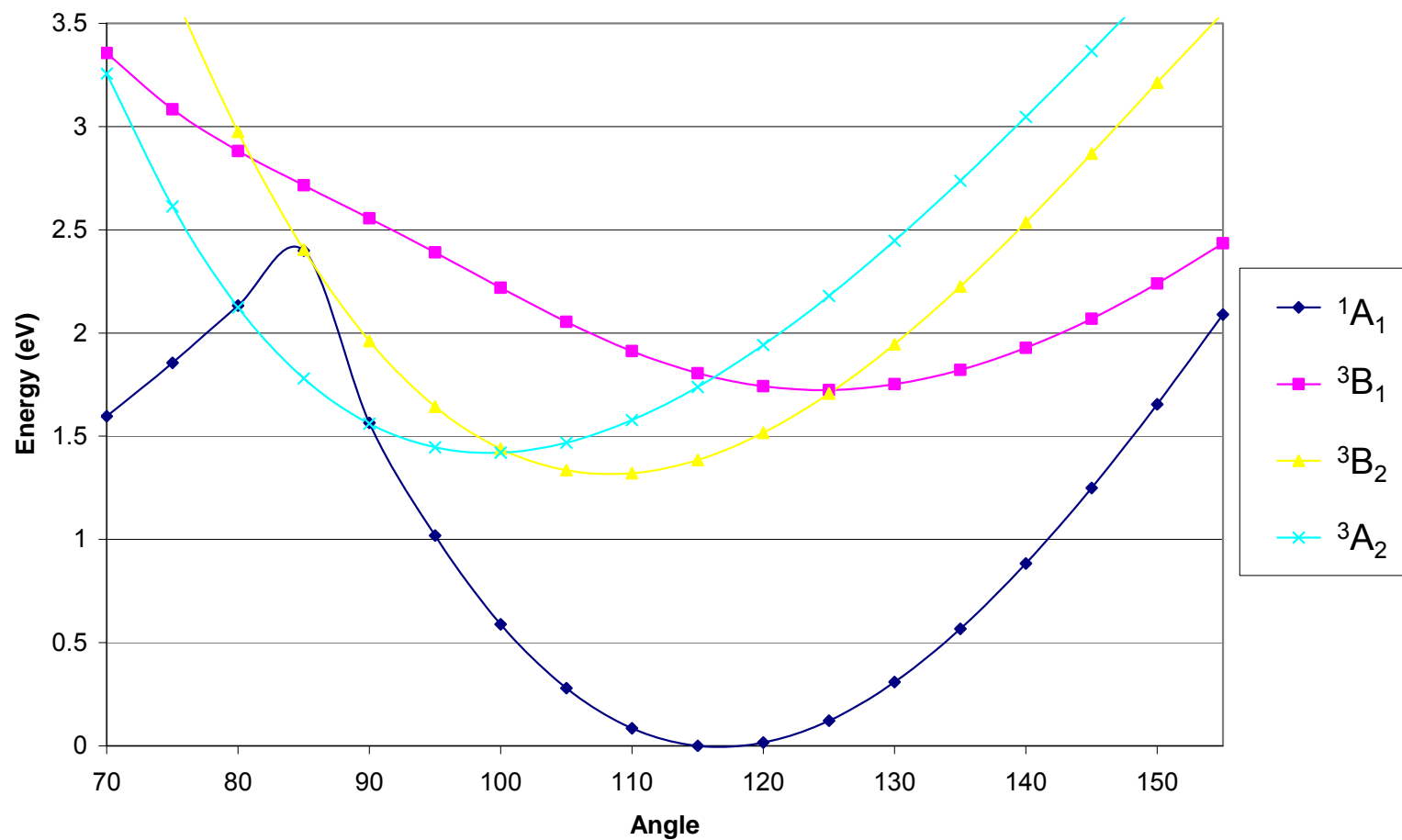


Figure 5.3. cc-pVTZ CASSCF potential energy curves for O_3 . Each point represents a constrained geometrical optimization for a fixed bond angle.

CHAPTER 6

THE SIC₂ SAGA CONTINUES: REVISED BARRIER TO LINEARITY, EQUILIBRIUM STRUCTURES, FUNDAMENTAL FREQUENCIES, AND ENTHALPY OF FORMATION[†]

[†]Lucas D. Speakman, Etienne Lanthier, Justin M. Turney, Tucker Carington, Jr., Henry F. Schaefer III, and Wesley D. Allen, and. To be submitted to the *Journal of Chemical Physics*.

6.1 ABSTRACT

Silicon dicarbide, SiC_2 , remains one of the most demanding challenges for computational methods to achieve converged predictions for the topography, energetics, and vibrational dynamics of the ground state potential energy surface. The silicon dicarbide system exhibits a mercurial surface for the circumnavigation of Si^+ about C_2^- in that almost all conceivable variations are observed, depending on level of theory and basis set. While the minimum is a “T-shaped” C_{2v} structure at the highest levels of theory, the barrier to linearity ranges from -5.09 to $6.59 \text{ kcal mol}^{-1}$ depending on the choice of basis set and correlation treatment. To address basis set incompleteness and to provide a high-order correlation treatment necessary for accurate predictions, we have developed a composite approach. It consists of a complete basis set coupled-cluster with singles and doubles method augmented by a perturbative triples term [CBS CCSD(T)], plus a coupled-cluster scheme with a full triples correction (aug-cc-pVTZ CCSDT), a mass-velocity and Darwin relativistic term [aug-cc-pVTZ CCSD(T)], and a core-valence electron correlation adjustment [aug-cc-pCVQZ CCSD(T)]. Although higher-order coupled-cluster treatments affect the barrier to linearity, -1.73 (SCF), 2.17 (MP2), 2.04 (CCSD), 0.37 [CCSD(T)], 0.26 (CCSDT), 0.11 [CCSDT(Q)], 0.06 (CCSDTQ), and 0.23 [CCSDTQ(P)] kcal mol^{-1} , we limit the composite approach to full triples because of its excellent approximation to CCSDTQ(P). Our composite method (*c*-CBS CCSDT) is systematically applied to the ground state structures, the quartic force field, and the global potential energy surface of SiC_2 . The *c*-CBS CCSDT method yields a barrier to linearity of $5.45 \pm 0.1 \text{ kcal mol}^{-1}$, bond distances of 1.8305 (1.6875) \AA and 1.2686 (1.2822) \AA for $r_{\text{Si-C}}$ and $r_{\text{C-C}}$ of the “T-shaped” (linear) structures, fundamental vibrational frequencies for the “T-shaped” ground state of 1752 , 846 , and 15 cm^{-1} , and $\Delta_f H_0^\circ(\text{SiC}_2)$ of $152.45 \pm 0.20 \text{ kcal mol}^{-1}$.

6.2 INTRODUCTION

One of the primary focuses of recent work in our laboratory has been the pursuit of chemical accuracy in spectroscopic and thermochemical properties. While most chemical systems require only the *ab initio* “Gold Standard” of cc-pCVQZ CCSD(T) to achieve this level of accuracy, some molecules require a more rigorous and computational demanding analysis. Silicon dicarbide has been a daunting task for *ab initio* methods to confirm definitive experimental spectroscopy on this system. We endeavor for a sub-chemical accuracy potential energy surface for calculation of the ro-vibrational levels of SiC₂.

The scientific history of silicon dicarbide began in 1926, when Merrill¹ and Sanford² discovered uncataloged bands near 5000 Å from several carbon rich stars. The source of these electronic transitions was not identified for nearly thirty years. In 1955, Kleman³ reproduced the emission bands in a graphite furnace charged with silicon. Based on experimental conditions, Kleman concluded that the emitting species was SiC₂, and proposed a linear geometry analogous to that of C₃.

This linear assumption was the basis for spectroscopic interpretation for over thirty years. An early matrix isolation study by Weltner and McLeod⁴ and gas-phase experiments by Verma and Nagaraj⁵ furthered the assignment as $\tilde{X}^1\Sigma^+ / ^1\Pi$ transitions of linear SiC₂, with ground-state fundamental frequencies for C-C and Si-C stretching near 1742 and 852 cm⁻¹, respectively. The vibronic analyses resulted in unexpected anharmonicities and peculiar intensities. Weltner and McLeod justified their analysis by involving vibronic interactions with the bending frequency of the excited state, while Verma and Nagaraj invoked Fermi resonances to explain the irregularity. In 1982, Bondybey⁶ examined the matrix isolation and gas-phase laser-induced fluorescence spectra of SiC₂ by vaporizing solid silicon carbide with a pulsed YAG laser. While Bondybey

noted that the linear geometry was not clear given the exceedingly flat bending potential in C_3 , and the reluctance of silicon to form π bonds, earlier assumptions of linearity were preserved in accordance with Walsh's rules. His reinterpretation of Merrill-Sanford successfully explained a previously problematic feature by assigning it to a hot band. The first *ab initio* study on SiC_2 came a year later at the DZP RHF level of theory.⁷ In agreement with previous experiments, the ground electronic state was predicted to have a highly ionic, linear structure with a dipole of 4.8 D. The more covalent excited linear state was ~ 2.5 eV higher in energy.

The first non-linear ground state was proposed less than a year later, both by experimentalists at Rice and *ab initio* theorists from Berkeley. Michalopoulos, Geusic, Langridge-Smith, and Smalley⁸ obtained full rotational resolution by performing resonant-two-photon ionization of cold molecular beams containing SiC_2 . Analysis of their spectrum in terms of linear geometries resulted in extremely short C-C and Si-C bond lengths and an abnormally large lambda doubling parameter for the excited state. They turned to theoretical methods to help explain their results. Grev and Schaefer⁹ found a cyclic, "T-shaped" C_{2v} saddle point connected to the linear $\tilde{X}^1\Sigma^+$ minimum lying 5.1 kcal mol⁻¹ higher in energy at the DZP SCF level of theory. Ensuing CISD single point computations placed the cyclic structure below the linear structure. With additional *d*-type polarization functions, a final energy prediction of ΔE (ring – linear) = -4.7 kcal mol⁻¹ was given to the Rice group. The Rice experimental group fitted asymmetric-top rotational constants to their data. They obtained bond lengths for the ground state which were in remarkable agreement with the structure of the predicted "T-shaped" stationary point. Additional evidence for a C_{2v} structure came from the Rice spectrum: the electronic transition is polarized along the inertial *b* axis, and the odd/even K levels in the lower/upper (000) vibronic manifolds are absent. This is expected for \tilde{X}^1A_1 and \tilde{A}^1B_2

electronic states with equivalent carbon nuclei of zero spin. Thus, the Merrill-Sanford 4977 Å line arises from the $\tilde{X}^1A_1 / \tilde{A}^1B_2$ transitions of a SiC₂ ring. The low-lying upper state is formed by an in-plane $\pi \rightarrow \pi^*$ excitation within the weak, highly strained carbon-carbon triple bond.

With a new basis for interpreting SiC₂, several detailed spectroscopic works emerged. In 1985, matrix isolation Fourier transform experiments observed only four new symmetric stretching bands resulting from ¹³C substitution, further supporting equivalent carbon nuclei in SiC₂.¹⁰ Shepherd and Graham reviewed the current matrix isolation studies on SiC₂.¹¹ Under the new C_{2v} selection rules, Bondybey's⁶ interval of 354 cm⁻¹ suggests the bending mode, ν_3 , to be approximately 180 cm⁻¹. The molecule is best described as a T-shaped Si⁺C₂⁻ species, due to the similar C-C bond distance and stretching fundamental in C₂: 1.268 Å and 1758 cm⁻¹ for SiC₂ and 1.268 Å and 1742 cm⁻¹ for C₂⁻. The gaseous emission spectrum of Kleman³ needed to be reinterpreted to give a symmetric Si-C stretch mode, ν_2 , at 837 cm⁻¹. In 1990, the highly anharmonic bending mode was first observed in an argon matrix to be ν_3 at 160.4 cm⁻¹.¹² A Jacobi-type force field best fits the isotopic frequency data.

High-resolution rotational spectroscopy of SiC₂ appeared in the late 1980s through the early 1990s.¹³⁻²³ The culmination of these studies resulted in 1.26855(36) and 1.83232(58) Å for $r_s(\text{C-C})$ and $r_s(\text{Si-C})$, respectively.^{13,16,23} A gas-phase ν_3 frequency of 186 ± 11 cm⁻¹ was deduced from the inertial defect in the rotational constants.^{14,15} While a simple anharmonic model satisfactorily fit the large-amplitude ν_3 mode, it required decatic centrifugal distortion parameters to fit the observed frequencies within experimental errors.¹⁸⁻²²

The vibrational analyses of SiC₂ concluded in 1994 with a combined experimental and theoretical study performed by Ross, Butenhoff, Rohlfiing, and Rohlfiing.²⁴ Stimulated emission

pumping was implemented to determine rovibrational energies levels with up to 14 quanta of excitation in the large-amplitude bending mode. These results were combined with existing vibrational term values²⁵ and microwave lines,^{14,18} and globally fit to a semirigid bender Hamiltonian.²⁶⁻²⁸ The potential energy function derived from the fit extrapolated to a linear SiC₂ transition state. However, the experiment could not completely rule out a shallow minimum, since the experiment only sampled angles within 30° of linearity. The extrapolated barrier to linearity was 5.4 ± 0.6 kcal mol⁻¹.

Theoretical work since the discovery of the T-shaped ground state has revealed a significant challenge for *ab initio* methods to identify the linear or T-shaped stationary points as minima or transition states. Early theoretical studies demonstrated large oscillations in the Møller-Plesset series and significant basis set dependence; the barrier to linearity ranged from 1.4 to -5.5 kcal mol⁻¹.²⁹ At the MP4 level, Oddershede, Sabin, Diercksen, and Grüner³⁰ found a shallow linear well lying 0.84 kcal mol⁻¹ above the T-shaped minimum; a possible L-shaped structure, analogous to KCN in the gas phase. Sadlej, Diercksen, Oddershede, and Sabin³¹ extended the study of methodological dependence through CCSDT, with three important results: 1) carefully constructed basis sets can cause RHF to predict the T-shaped structure as the lowest in energy; 2) including higher angular momentum functions stabilizes the T-shaped isomer; and 3) the linear isomer is stabilized by triple excitations. They concluded that highly correlated methods, i.e. CCSDT or higher, in conjunction with a large basis set will be necessary to definitively confirm the barrier to linearity.

Nielsen, Allen, Császár, and Schaefer³² studied the topography of SiC₂. Each of the linear, L-shaped, and T-shaped structures is the global minimum at some level of theory; a bent stationary point exists whenever the linear form is a minimum. Only at aug-cc-pVTZ CCSD(T)

are the L-shaped and bent structures shown to be spurious. With quadruple excitations and basis set incompleteness, relativistic, core-correlation, and non-Born-Oppenheimer corrections, the barrier to linearity ranged between 5.3 and 6.0 kcal mol⁻¹. This is due to uncertainty in higher-order correlation effects.^{32,33} This group revisited the problem in 2003 using the Focal Point approximation to yield a CBS CCSDT barrier to linearity of 5.45 kcal mol⁻¹.³⁴ Recognizing the importance of post-CCSDT corrections for sub-chemical accuracy, the BD(TQ)/cc-pVTZ computations moved the final prediction to 6.3 kcal mol⁻¹, which lies outside the experimental range²⁴ of 5.4 ± 0.6 kcal mol⁻¹.

A year later, Largo, Redondo, and Barrientos produced a theoretical work examining the competition between linear and cyclic isomers in second-row dicarbides.³⁵ This article gave an insightful view on the trend of dicarbides: XC₂ (X = Na, Mg, and Al) prefers a C_{2v} minimum while XC₂ (X = P, S, and Cl) favors a linear minimum. Since silicon dicarbide is known to be a “T-shaped” molecule, it is interesting to note that silicon is the point at which the lowest energetic isomer of XC₂ switches from C_{2v} to a linear form.

Recent advancements in materials science have focused some attention on Silicon carbide clusters, Si_nC_m (*n, m* ≤ 4).³⁶⁻³⁹ In general these results have longer Si-C experimental bond lengths than by 0.017, 0.023, 0.025, and 0.029 Å for LDA/6-311++G**,^{37,38} BL3LYP/aug-cc-pVQZ,³⁶ B3PW91/6-31G(d),³⁹ and MP2/aug-cc-pVQZ,³⁶ respectively.

6.3 COMPUTATIONAL DETAILS

Silicon dicarbide, SiC₂, remains one of the most demanding challenges for computational methods to achieve converged predictions for the topography, energetics, and vibrational dynamics of the ground state potential energy surface. The silicon dicarbide system exhibits a mercurial surface for the circumnavigation of Si⁺ about C₂⁻ in that almost all conceivable

variations are observed, depending on level of theory and basis set. To address basis set incompleteness and to provide a high-order correlation treatment necessary for accurate predictions, we have developed a composite approach for computing equilibrium structures, the quartic force field, and the global potential energy surface.

With conventional methods, it is possible to approach the complete basis set (CBS) limit systematically, using carefully constructed families of basis sets, such as the aug-cc-pVXZ basis sets.⁴⁰⁻⁴² While near exponential convergence is observed for Hartree-Fock energies, utilizing a three point $a + be^{-cX}$ fit,^{43,44} correlation energies employ a two point $a + bX^{-3}$ functional form. In these equations, X is the cardinal number of the basis set.⁴⁵ The determination of the energy at the CBS limit is vital in the focal-point analysis of Allen and co-workers.⁴⁶ The focal-point scheme systematically approaches both the CBS and full configuration interaction (Full CI) limits. Extrapolations for correlation energies are usually limited to coupled-cluster with singles and doubles method, augmented by a perturbative triples term [CCSD(T)]. Higher order correlation treatments and other small corrections are included in an additive fashion. This approach has been used numerous times, yielding chemical accuracy.^{33,47-54} To account for higher levels of electron correlation, absolute barriers to linearity were computed through CCSDTQ(P)/cc-pVDZ//CCSD(T)/aug-cc-pVTZ³² resulting in -1.29 (SCF), 2.30 (MP2), 2.38 (CCSD), 0.64 [CCSD(T)], 0.54 (CCSDT), 0.37 [CCSDT(Q)], 0.32 (CCSDTQ), and 0.51 [CCSDTQ(P)] kcal mol⁻¹. Due to the excellent agreement of CCSDT with CCSDTQ(P), the composite method was limited to full triples. Additional corrections consisted of a mass-velocity and Darwin relativistic term and a core-valence electron correlation adjustment. Thus, our composite method includes the following terms [with necessary computations enclosed in brackets]:

$$\begin{aligned}
c - \text{CBS CCSDT} &= E_{\text{CBS CCSD(T)}}^{\text{aug-cc-pVXZ (X=T,Q,5) RHF}} \\
&\quad \left[E_{\text{aug-cc-pVXZ (X=Q,5) CCSD(T)}} \right] \\
&\quad + \Delta E_{\text{core}} \left[E_{\text{CCSD(T)(AE)}}^{\text{aug-cc-pCVQZ}} - E_{\text{CCSD(T)(fc)}}^{\text{aug-cc-pCVQZ}} \right] \\
&\quad + \Delta E_{\text{CCSDT}} \left[E_{\text{CCSDT}}^{\text{aug-cc-pVTZ}} - E_{\text{CCSD(T)}}^{\text{aug-cc-pVTZ}} \right] \\
&\quad + E_{\text{MVD}} \left[E_{\text{MVD-CCSD(T)}}^{\text{aug-cc-pVTZ}} \right]
\end{aligned}$$

Hartree-Fock and CCSD(T) single points were computed with MOLPRO 2006.1,⁵⁵ while relativistic and full triples additive correction were computed with ACESII.^{56,57} Higher-order coupled cluster excitations were made possible by the string-based MRCC code of Kállay and coworkers.⁵⁸⁻⁶³ The T-shaped and linear isomers of SiC₂ were optimized through the PSI3.4 package.⁶⁴

In order to quantify the anharmonicity contributions to the fundamental frequencies, the third and fourth derivatives of the molecular energy were computed by numerical differentiation of tightly converged, 10⁻¹¹ E_h, energies at 35 displaced geometries for the C_{2v} structure. The internal coordinates were chosen as S₁ = r(C-C), S₂ = 2^{-1/2}[r₁(Si-C) + r₂(Si-C)], and S₃ = 2^{-1/2}[r₁(Si-C) - r₂(Si-C)] where *r* represents a bond distance. Vibrational anharmonicities were computed by application of second-order perturbation theory (VPT2)^{52,65-71} to the quartic force field in reduced normal coordinates. The MATHEMATICA⁷² program INTDIF2005^{73,74} was used to compute the force constants in internal coordinates; INTDER2005^{75,76} was used to execute the nonlinear transformation to the Cartesian space,^{77,78} whereupon the ANHARM^{76,79} program was run for the VPT2 analysis.

While a standard set of internal coordinates was used for the quartic force field analysis, Jacobi coordinates provide a more natural description of T-shaped molecules executing large-amplitude pinwheel motion. These coordinates were defined as S₁ = r(C-C), S₂ = R(Si-C₂), and

$S_3 = \rho(\text{Si-C}_2)$. R involves the distance between the silicon atom and the midpoint of the C-C bond, and ρ is the angle between a carbon atom, midpoint of the C-C bond, and the silicon atom. The potential energy surface (PES) was built by finding the minimum energy path (MEP): First, $S_3(\rho)$ was varied from 0° to 90° in 10° increments and $S_1(r)$ and $S_2(R)$ coordinates were optimized at each point. At each MEP point, coordinates $S_1(r)$ and $S_3(\rho)$ were held constant, while single points were computed as $S_2(R)$ shifted from -0.4 \AA to 1.0 \AA by 0.1 \AA and $\pm 0.02 \text{ \AA}$ from the MEP. Next, $S_2(R)$ and $S_3(\rho)$ were held constant at each MEP point, and $S_1(r)$ adjusted by $\pm 0.010 \text{ \AA}$ and $\pm 0.005 \text{ \AA}$ to determine the force constant. To have a more accurate description of $S_1(r)$ as $S_2(R)$ moves, $S_3(\rho)$ was held firm and $S_2(R)$ fixed at $\pm 0.2 \text{ \AA}$ from its MEP; $S_1(r)$ was then optimized and its force constant determined at the two geometries. Thus for each $S_3(\rho)$ coordinate, 27 single points were computed resulting in 270 points for a quadrant. By symmetry, our PES included 972 total sampled geometries. Using MATHEMATICA,⁷² the points along $S_3(\rho)$ were fitted to a Morse potential. The exponential pre-factor took a Gaussian curve form, which depicts the large-amplitude motion, $S_2(R)$. The force constants of $S_1(r)$ were extrapolated to define the stiff C-C bond.

6.4 RESULTS AND DISCUSSION

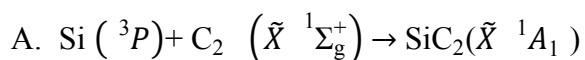
Experimental r_e geometries were determined by Nielsen *et. al.*³² by interfacing high-resolution rotational spectroscopy from Bogey *et. al.*¹⁹ and theoretical vibration-rotation interaction constants (α_i) to yield 1.8222 \AA and 1.2694 \AA for $r(\text{Si-C})$ and $r(\text{C-C})$, respectively. Until now, *ab initio* methods had not been able to converge to within 0.010 \AA of the experimentally derived silicon carbon bond distance for the T-shaped isomer. Table 6.1 clearly shows the basis set sensitivity and ineffectiveness as aug-cc-pVTZ, aug-cc-pVQZ, and aug-cc-pV5Z miscalculate $r_e(\text{Si-C})$ by -0.0313 , -0.0207 , and -0.0166 \AA , respectively. Even explicitly

including all core electrons through the aug-cc-pCVQZ CCSD(T) – (AE) level of theory only reduces the error to -0.0111 Å. However, theory and experiment do agree within 0.010 Å when the *c*-CBS CCSDT method is implemented. Although it is not as pronounced as in the $r_e(\text{Si-C})$ case, $r_e(\text{C-C})$ holds the same pattern of errors of -0.0105, -0.0056, -0.0044, and -0.0017 for aug-cc-pVTZ, aug-cc-pVQZ, aug-cc-pV5Z, and aug-cc-pCVQZ, respectively. The *c*-CBS CCSDT method is in fantastic agreement with experiment, to within 0.0008 Å. To test the validity of the *c*-CBS CCSDT treatment of electron correlation, cc-pVDZ CCSDTQ(P) single point energies at *c*-CBS CCSDT geometries resulted in -1.73 (SCF), 2.17 (MP2), 2.04 (CCSD), 0.37 [CCSD(T)], 0.26 (CCSDT), 0.11 [CCSDT(Q)], 0.06 (CCSDTQ), and 0.23 [CCSDTQ(P)] kcal mol⁻¹. Again, CCSDT is an excellent approximation to CCSDTQ(P). In general, the *c*-CBS CCSDT geometries shift the barrier to linearity by -0.30 kcal mol⁻¹. For C₂ electronic states structures, there is a balance of theoretical errors, with aug-cc-pV5Z being ~0.002 Å longer than experiment, while *c*-CBS CCSDT is ~0.002 Å shorter.

Key thermochemical quantities for SiC₂, such as the barrier to linearity and heat of formation, can be determined with increased accuracy as a result of more precise equilibrium structures and our composite method. Table 6.2 shows the incremented valence focal point analysis for the barrier to linearity. The focal point treatment at *c*-CBS CCSDT geometries is in almost perfect agreement with the Ross *et. al.*²⁴ value of 5.4 ± 0.6 kcal mol⁻¹. It is interesting to note that the triple excitation contributions decrease as the basis set increases while the remaining correlation treatments increase the barrier to linearity. Also, this table supports the earlier observations³¹ that triple excitations stabilize the linear form by 1.45 kcal mol⁻¹. To assess the accuracy of this quantity, an examination of the incremented focal point table is necessary. First, the full triple excitation corrects the perturbative triples by ~0.10 kcal mol⁻¹.

Second, the $\delta[\text{CCSDT}(\text{Q})]$ adjustment is an order of magnitude smaller than the $\delta[\text{CCSD}(\text{T})]$ correction. From the preceding paragraph, we can see that CCSDTQ corrects the CCSDT(Q) by 0.05 kcal mol⁻¹. The higher-order post correlation treatment [CCSDTQ(P) – CCSDT(Q)] accounts for 0.12 kcal mol⁻¹. Following these patterns for higher order excitations, electron correlation has converged to within 0.10 kcal mol⁻¹. Thus, we state with confidence that sub-chemical accuracy has been reached for the silicon dicarbide barrier to linearity.

The second important thermochemical quantity reported is SiC₂'s heat of formation. The heat of formation can be effectively investigated by means of the following reactions:



The focal point analysis, along with the established thermochemical⁸⁰ data, are shown in Tables 6.3 and 6.4 for paths A and B, respectively. Earlier computational values of $\Delta H_{f,0}^\circ$ were 153.9 and 155.4 kcal mol⁻¹ for methods A and B, respectively, with a final $\Delta H_{f,0}^\circ = 155 \pm 3$ kcal mol⁻¹.³² This quantity is significantly larger than the experimentally accepted value of 145.6 ± 6.9 kcal mol⁻¹.⁸⁰ In pursuit of sub-chemical accuracy, our computed values of $\Delta H_{f,0}^\circ$ for the two pathways differ by a tenth of a kcal mol⁻¹! Although it is superfluous to say that our correlation treatment is converged within 0.1 kcal mol⁻¹, it illustrates the balance of CCSDTQ(P) with experiment. This balance is also shown in the next section describing the singlet-triplet energy difference of C₂. The recovery of valence electron correlation in method A is expected to be more problematic than in method B due to the multi-determinant ground state wavefunction arising from the $(3\sigma_g)^2 \rightarrow (2\sigma_u)^2$ excitation. This nondynamical correlation effect manifested itself in the substantial contribution of higher order electron correlation treatment. The increment

between CCSDTQ(P) and CCSDT(Q) was $0.52 \text{ kcal mol}^{-1}$. In comparison, method B has for only $0.17 \text{ kcal mol}^{-1}$ for the same increment of theory. For a true $0.1 \text{ kcal mol}^{-1}$ convergence of the correlation energy, a multi-reference coupled cluster method, such as MK-MRCCSDT,⁸¹⁻⁸⁶ is required. Due to the precise $\Delta H_{f,0}^\circ$ agreement of the two channels, it was not performed in this work. We advance a value of $\Delta H_{f,0}^\circ = 152.45 \pm 0.20 \text{ kcal mol}^{-1}$.

While examining the two channels for the heat of formation, it was necessary to compute both the $\tilde{X}^1 \Sigma_g^+$ and $\tilde{a}^3 \Pi_u$ states of C_2 . Since it only has 12 electrons, higher orders of electron correlation were possible. These are presented in Table 6.5. This table illustrates why single determinant methods fail to describe multi-reference situations with traditional coupled cluster methods; at CCSDT, it corrected the perturbative triple excitations by $-1.94 \text{ kcal mol}^{-1}$. This is the same magnitude as the energy splitting itself! Even the CCSDTQP correction on CCSDTQ(P) was $-0.16 \text{ kcal mol}^{-1}$. This correction brings our value within $0.12 \text{ kcal mol}^{-1}$ of Huber and Herzberg's experimental value of $2.05 \text{ kcal mol}^{-1}$.⁸⁷ Although the correlation treatment is slowly converging, its oscillations are not within the range of sub-chemical accuracy. However, if we limited the table to CCSDTQ(P), like the previous focal point tables, the singlet-triplet energy difference becomes $2.09 \text{ kcal mol}^{-1}$, which is only $0.04 \text{ kcal mol}^{-1}$ from the experiment value. Again, this illustrates the agreement of CCSDTQ(P) with experiment and indicates the precise agreement of the heat of formation values.

Definitive studies of the unusual rovibrational dynamics of SiC_2 required analytic representations of the PES. Force constants determined by *c*-CBS CCSDT level of theory are listed in Table 6.6 in two sets of internal coordinates: 1) a standard valence set of symmetrized bond distances; and 2) the Si- C_2 Jacobi variables as discussed in the Methods section. These two surfaces yield nearly indistinguishable values for the stretching fundamental vibration modes, as

seen in Table 6.7; 1757 vs. 1752 cm^{-1} and 843 vs. 846 cm^{-1} for the VPT2 and surface potentials, respectively. While the aug-cc-pVTZ CCSD(T) level of theory was insufficient to obtain quantitative information about the ν_3 vibrational levels, both *c*-CBS CCSDT surfaces significantly improve the accuracy of the bending mode. However, the large-amplitude bending motion is in better agreement with experiment on the Jacobi surface than the quartic force field by 9 cm^{-1} . The Jacobi surface, Figure 6.1, has a dramatic appeal because the silicon atom can be displaced over 1.0 Å away and not dissociate! As the aug-cc-pVTZ CCSD(T) surface indicated,³² there are no depressions in the contours to indicate from an L-shaped minimum. With an accurate Jacobi surface in hand, accurate rovibrational levels were computed through a collaboration with Professor Tucker Carington, Jr.. His advanced results are in excellent agreement with the stimulated emission pumping experiments of Ross *et. al.*²⁴

6.5 CONCLUSIONS

An extensive methodological composite level of theory, including extrapolation to the complete basis set limit and additive full triple excitations, electron core-valence, and relativistic corrections, has been developed to investigate one of the most demanding systems known to *ab initio* methods. For the first time, theory agrees with experiment regarding the $r_e(\text{Si-C})$ and $r_e(\text{C-C})$ bond distances to within 0.01 and 0.001 Å, respectively. Sub-chemical accuracy has been achieved for the barrier to linearity of $5.45 \pm 0.10 \text{ kcal mol}^{-1}$. Although sub-chemical accuracy was not reached for the SiC_2 heat of formation or the singlet-triplet energy difference of C_2 , CBS CCSDTQ(P) values agree with experiment to within 0.1 kcal mol^{-1} . The Jacobi potential energy surface of SiC_2 provides one of the most accurate theoretical surfaces in the literature to date. This surface allowed us to obtain the first quantitative theoretical rovibrational levels and finally confirm the spectroscopic analyses of this system. More than a quarter of century after the first

confirmation of the T-shaped isomer of SiC₂, the definitive theoretical chapter of the SiC₂ saga has finally been written.

6.6 ACKNOWLEDGEMENTS

This work was supported by the Department of Energy and the Natural Sciences and Engineering Research Council of Canada.

6.7 REFERENCES

- ¹ P. W. Merrill, *Publ. Astron. Soc. Pac.* **38**, 175 (1926).
- ² R. F. Sanford, *Publ. Astron. Soc. Pac.* **38**, 177 (1926).
- ³ B. Kleman, *Astrophys. J.* **123** (1), 162 (1956).
- ⁴ W. Weltner and D. McLeod, *J. Chem. Phys.* **41** (1), 235 (1964).
- ⁵ R. D. Verma and S. Nagaraj, *Can. J. Phys.* **52** (19), 1938 (1974).
- ⁶ V. E. Bondybey, *J. Phys. Chem.* **86** (17), 3396 (1982).
- ⁷ S. Green, *Astrophys. J.* **266** (2), 895 (1983).
- ⁸ D. L. Michalopoulos, M. E. Geusic, P. R. R. Langridgesmith, and R. E. Smalley, *J. Chem. Phys.* **80** (8), 3556 (1984).
- ⁹ R. S. Grev and H. F. Schaefer, *J. Chem. Phys.* **80** (8), 3552 (1984).
- ¹⁰ R. A. Shepherd and W. R. M. Graham, *J. Chem. Phys.* **82** (11), 4788 (1985).
- ¹¹ R. A. Shepherd and W. R. M. Graham, *J. Chem. Phys.* **88** (5), 3399 (1988).
- ¹² J. D. Presillamarquez, W. R. M. Graham, and R. A. Shepherd, *J. Chem. Phys.* **93** (8), 5424 (1990).
- ¹³ H. Bredohl, I. Dubois, H. Leclercq, and F. Melen, *J. Mol. Spec.* **128** (2), 399 (1988).
- ¹⁴ C. A. Gottlieb, J. M. Vrtilek, and P. Thaddeus, *Astrophys. J.* **343** (1), L29 (1989).

- 15 J. Cernicharo, C. A. Gottlieb, M. Guelin, P. Thaddeus, and J. M. Vrtilik, *Astrophys. J.* **341** (1), L25 (1989).
- 16 R. D. Suenram, F. J. Lovas, and K. Matsumura, *Astrophys. J.* **342** (2), L103 (1989).
- 17 J. Cernicharo, M. Guelin, C. Kahane, M. Bogey, C. Demuynck, and J. L. Destombes, *Astron. Astrophys.* **246** (1), 213 (1991).
- 18 M. Bogey, C. Demuynck, D. L. Destombes, and A. D. Walters, *Astron. Astrophys.* **247**, L13 (1991).
- 19 M. Bogey, M. Cordonnier, C. Demuynck, and J. L. Destombes, *Structures and Conformations on Non-Rigid Molecules*. (Kluwer, Dordrecht, 1993).
- 20 L. H. Coudert, *J. Mol. Spec.* **160** (1), 225 (1993).
- 21 S. Chandra and A. Sahu, *Astron. Astrophys.* **272** (2), 700 (1993).
- 22 M. Izuha, S. Yamamoto, and S. Saito, *Spectrochim. Acta A* **50** (8-9), 1371 (1994).
- 23 P. Thaddeus, S. E. Cummins, and R. A. Linke, *Astrophys. J.* **283** (2), L45 (1984).
- 24 S. C. Ross, T. J. Butenhoff, E. A. Rohlfing, and C. M. Rohlfing, *J. Chem. Phys.* **100** (6), 4110 (1994).
- 25 T. J. Butenhoff and E. A. Rohlfing, *J. Chem. Phys.* **95** (1), 1 (1991).
- 26 P. R. Bunker, *Ann. Rev. Phys. Chem.* **34**, 59 (1983).
- 27 P. R. Bunker and B. M. Landsberg, *J. Mol. Spec.* **67** (1-3), 374 (1977).
- 28 P. Jensen, *Comp. Phys. Rep.* **1** (1), 1 (1983).
- 29 G. Fitzgerald, S. J. Cole, and R. J. Bartlett, *J. Chem. Phys.* **85** (3), 1701 (1986).
- 30 J. Oddershede, J. R. Sabin, G. H. F. Diercksen, and N. E. Gruner, *J. Chem. Phys.* **83** (4), 1702 (1985).

- 31 A. J. Sadlej, G. H. F. Diercksen, J. Oddershede, and J. R. Sabin, *Chem. Phys.* **122** (2),
297 (1988).
- 32 I. M. B. Nielsen, W. D. Allen, A. G. Csaszar, and H. F. Schaefer, *J. Chem. Phys.* **107** (4),
1195 (1997).
- 33 A. G. Csaszar, W. D. Allen, and H. F. Schaefer, *J. Chem. Phys.* **108** (23), 9751 (1998).
- 34 J. P. Kenny, W. D. Allen, and H. F. Schaefer, *J. Chem. Phys.* **118** (16), 7353 (2003).
- 35 A. Largo, P. Redondo, and C. Barrientos, *J. Am. Chem. Soc.* **126** (44), 14611 (2004).
- 36 X. F. Duan, J. Wei, L. Burggraf, and D. Weeks, *Comput. Mater. Sci.* **47** (3), 630 (2010).
- 37 P. Pradhan and A. K. Ray, *Theochem-J. Mol. Struct.* **716** (1-3), 109 (2005).
- 38 P. Pradhan and A. K. Ray, *Eur. Phys. J. D* **37** (3), 393 (2006).
- 39 J. L. Deng, K. H. Su, X. Wang, Q. F. Zeng, L. F. Cheng, Y. D. Xu, and L. T. Zhang, *Eur.*
Phys. J. D **49** (1), 21 (2008).
- 40 T. H. Dunning, *J. Chem. Phys.* **90** (2), 1007 (1989).
- 41 R. A. Kendall, T. H. Dunning, and R. J. Harrison, *J. Chem. Phys.* **96** (9), 6796 (1992).
- 42 D. E. Woon and T. H. Dunning, *J. Chem. Phys.* **98** (2), 1358 (1993).
- 43 D. Feller, *J. Chem. Phys.* **98** (9), 7059 (1993).
- 44 E. F. Valeev, W. D. Allen, R. Hernandez, C. D. Sherrill, and H. F. Schaefer, *J. Chem.*
Phys. **118** (19), 8594 (2003).
- 45 T. Helgaker, W. Klopper, H. Koch, and J. Noga, *J. Chem. Phys.* **106** (23), 9639 (1997).
- 46 A. L. L. East and W. D. Allen, *J. Chem. Phys.* **99** (6), 4638 (1993).
- 47 E. F. Valeev, W. D. Allen, H. F. Schaefer, and A. G. Csaszar, *J. Chem. Phys.* **114** (7),
2875 (2001).

- 48 G. Tarczay, A. G. Csaszar, W. Klopper, V. Szalay, W. D. Allen, and H. F. Schaefer, *J. Chem. Phys.* **110** (24), 11971 (1999).
- 49 G. S. Tschumper, M. L. Leininger, B. C. Hoffman, E. F. Valeev, H. F. Schaefer, and M. Quack, *J. Chem. Phys.* **116** (2), 690 (2002).
- 50 E. F. Valeev, W. D. Allen, A. L. L. East, and A. G. Csaszar, *J. Phys. Chem. A* **105** (12), 2716 (2001).
- 51 N. D. K. Petraco, W. D. Allen, and H. F. Schaefer, *J. Chem. Phys.* **116** (23), 10229 (2002).
- 52 K. Aarset, A. G. Csaszar, E. L. Sibert, W. D. Allen, H. F. Schaefer, W. Klopper, and J. Noga, *J. Chem. Phys.* **112** (9), 4053 (2000).
- 53 M. S. Schuurman, S. R. Muir, W. D. Allen, and H. F. Schaefer Iii, *J. Chem. Phys.* **120** (24), 11586 (2004).
- 54 J. M. Gonzales, C. Pak, R. S. Cox, W. D. Allen, H. F. Schaefer, A. G. Csaszar, and G. Tarczay, *Chem.-Eur. J.* **9** (10), 2173 (2003).
- 55 MOLPRO, version 2006.1, a package of *ab initio* programs, H.-J. Werner, P. J. Knowles, R. Lindh, F. R. Manby, M. Schütz, P. Celani, T. Korona, G. Rauhut, R. D. Amos, A. Bernhardsson, A. Berning, D. L. Cooper, M. J. O. Deegan, A. J. Dobbyn, F. Eckert, C. Hampel and G. Hetzer, A. W. Lloyd, S. J. McNicholas, W. Meyer and M. E. Mura, A. Nicklass, P. Palmieri, R. Pitzer, U. Schumann, H. Stoll, A. J. Stone, R. Tarroni and T. Thorsteinsson, see <http://www.molpro.net>.
- 56 J. F. Stanton, J. Gauss, J. D. Watts, W. J. Lauderdale, and R. J. Bartlett, *Int. J. Quant. Chem. Sym.* **26**, 879 (1992).

- 57 J. F. Stanton, J. Gauss, J. D. Watts, P. G. Szalay, R. J. Bartlett, D. E. B. with contributions from A.A. Auer, O. Christiansen, M.E. Harding, M. Heckert, O. Heun, D. J. C. Huber, J. Jusélius, W.J. Lauderdale, T. Metzroth, C. Michauk, D.R. Price, K. Ruud, F. Schiffmann, A. Tajti, M.E. Varner, J. Vázquez and the integral packages: MOLECULE (J. Almlöf and P.R. Taylor), PROPS (P.R. Taylor), and, and H. J. A. J. ABACUS (T. Helgaker, P. Jørgensen, and J. Olsen). See, also J.F. Stanton, J. Gauss, J.D. Watts, W.J. Lauderdale, R.J. Bartlett *Int. J. Quantum Chem. Symp.* **26** (1992), 879. Current version see <http://www.aces2.de>.
- 58 M. Kallay and J. Gauss, *J. Chem. Phys.* **123** (21), 13 (2005).
- 59 M. Kallay and J. Gauss, *J. Chem. Phys.* **121** (19), 9257 (2004).
- 60 M. Kallay and J. Gauss, *J. Chem. Phys.* **120** (15), 6841 (2004).
- 61 M. Kallay, J. Gauss, and P. G. Szalay, *J. Chem. Phys.* **119** (6), 2991 (2003).
- 62 M. Kallay, P. G. Szalay, and P. R. Surjan, *J. Chem. Phys.* **117** (3), 980 (2002).
- 63 M. Kallay and P. R. Surjan, *J. Chem. Phys.* **115** (7), 2945 (2001).
- 64 T. D. Crawford, C. D. Sherrill, F. V. Edward, T. F. Justin, A. K. Rollin, L. L. Matthew, T. B. Shawn, L. J. Curtis, T. S. Edward, P. K. Joseph, and D. A. Wesley, *J. Comp. Chem.* **28** (9), 1610 (2007).
- 65 A. L. L. East, C. S. Johnson, and W. D. Allen, *J. Chem. Phys.* **98** (2), 1299 (1993).
- 66 J. K. G. Watson, *Vibrational Spectra and Structure*. (Elsevier, Amsterdam, 1977).
- 67 D. A. Clabo, W. D. Allen, R. B. Remington, Y. Yamaguchi, and H. F. Schaefer, *Chem. Phys.* **123** (2), 187 (1988).
- 68 W. D. Allen, Y. Yamaguchi, A. G. Csaszar, D. A. Clabo, R. B. Remington, and H. F. Schaefer, *Chem. Phys.* **145** (3), 427 (1990).

69 I. M. Mills, *Molecular Spectroscopy: Modern Research*. (Academic, New York, 1972).

70 D. Papousek and M. R. Aliev, *Molecular Vibrational-Rotational Spectra*. (Elsevier,
Amsterdam, 1982).

71 H. H. Nielsen, *Rev. Mod. Phys.* **23** (2), 90 (1951).

72 MATHEMATICA (Wolfram Research, Inc., Champaign, IL, 2003).

73 (INTDIF2005 is an abstract program written by Wesley D. Allen for MATHEMATICA
to perform general numerical differentiations to high orders of electronic structure data.).

74 R. L. DeKock, M. J. McGuire, P. Piecuch, W. D. Allen, H. F. Schaefer, K. Kowalski, S.
A. Kucharski, M. Musial, A. R. Bonner, S. A. Spronk, D. B. Lawson, and S. L. Laursen,
J. Phys. Chem. A **108** (15), 2893 (2004).

75 (INTDER2005 is a general program written by W. D. Allen, which performs sundry
vibrational analyses and higher order nonlinear transformations among force field
representations.).

76 K. Sarka and J. Demaison, *Computational Molecular Spectroscopy*. (Wiley, Chichester,
2000).

77 W. D. Allen and A. G. Csaszar, *J. Chem. Phys.* **98** (4), 2983 (1993).

78 W. D. Allen, A. G. Császár, V. Szalay, and I. M. Mills, *Mol. Phys.* **89** (5), 1213
(1996).

79 (ANHARM is a FORTRAN program for VPT2 analysis written by Y. Yamaguchi and
H. F. Schaefer III).

80 *JANAF Thermochemical Tables, 3rd Ed.* (Journal of Physical Chemistry Reference Data,
1985).

- 81 F. A. Evangelista, A. C. Simmonett, W. D. Allen, H. F. Schaefer, Iii, and J. Gauss, *J. Chem. Phys.* **128** (12), 124104 (2008).
- 82 F. A. Evangelista, E. Prochnow, J. Gauss, H. F. Schaefer, and Iii, *J. Chem. Phys.* **132** (7), 074107 (2010).
- 83 U. S. Mahapatra, B. Datta, and D. Mukherjee, *Mol. Phys.* **94** (1), 157 (1998).
- 84 F. A. Evangelista, W. D. Allen, H. F. Schaefer, and Iii, *J. Chem. Phys.* **125** (15), 154113 (2006).
- 85 F. A. Evangelista, W. D. Allen, H. F. Schaefer, and Iii, *J. Chem. Phys.* **127** (2), 024102 (2007).
- 86 E. Prochnow, F. A. Evangelista, H. F. Schaefer, Iii, W. D. Allen, and J. Gauss, *J. Chem. Phys.* **131** (6), 064109 (2009).
- 87 K. P. Huber and G. Herzberg, *Constants of Diatomic Molecules*. (Van Nostrand Reinhold Company, New York, 1979).

Table 6.1. Bond lengths of SiC₂ and C₂ molecules (in Å).

		SiC ₂				C ₂	
		T-Shape		Linear		¹ Σ _g ⁺	³ Π _u
Basis Set	Theory	<i>r_e</i> (C-C)	<i>r_e</i> (Si-C)	<i>r_e</i> (C-C)	<i>r_e</i> (Si-C)	<i>r_e</i> (C-C)	<i>r_e</i> (C-C)
aug-cc-pVTZ	CCSD(T)	1.2799	1.8535	1.2921	1.7057	1.2508	1.3198
aug-cc-pVQZ	CCSD(T)	1.2751	1.8429	1.2880	1.6986	1.2460	1.3152
aug-cc-pV5Z	CCSD(T)	1.2738	1.8388	1.2738	1.8388	1.2448	1.3141
aug-cc-pCVQZ	CCSD(T)	1.2711	1.8333	1.2844	1.6905	1.2428	1.3118
<i>c</i> -CBS	CCSDT ^a	1.2686	1.8305	1.2822	1.6875	1.2408	1.3099
	Experiment ^b	1.2694	1.8222			1.2425	1.3119

^a *c*-CBS CCSDT = Δ*E_e* [CBS CCSDT] + Δ_{core} [CCSD(T)/aug-cc-pCVQZ] + Δ_{rel} [CCSD(T) MVD/aug-cc-pVTZ]

^b High-resolution rotational constants by M. Bogey, M. Cordonnier, C. Demuyneck, and J. L. Destombes, in *Structures and Conformations of Non-Rigid Molecules*, edited by J. Laane, M. Dakkouri, B. van der Veken, and H. Oberhammer (Kluwer, Dordrecht, 1993), p. 303 were reinterpreted by I. M. B. Nielsen, W. D. Allen, A. g. Császár, and H. F. Schaefer, *J. Chem. Phys.* **107**, 1195 (1997) to yield *r_e* parameters.

Table 6.2. Valence focal point analysis of the barrier to linearity (in kcal mol⁻¹). The symbol δ denotes the increment in the relative energy (ΔE_e) with respect to the preceding level of theory in the hierarchy RHF \rightarrow MP2 \rightarrow CCSD \rightarrow CCSD(T) \rightarrow CCSDT \rightarrow CCSDT(Q) \rightarrow CCSDTQ \rightarrow CCSDTQ(P). Square brackets signify results obtained from basis set extrapolations or additive assumptions. Final predictions are boldfaced.

Basis Set	ΔE_e [RHF]	δ [MP2]	δ [CCSD]	δ [CCSD(T)]	δ [CCSDT]	δ [CCSDT(Q)]	ΔE_e [CCSDT(Q)]
aug-cc-pVDZ	-1.11	2.63	0.18	-1.74	-0.06	-0.18	[-0.19]
aug-cc-pVTZ	0.52	5.01	-0.21	-1.59	-0.09	-0.21	[+3.42]
aug-cc-pVQZ	0.81	5.60	-0.28	-1.44	[-0.09]	[-0.21]	[+4.40]
aug-cc-pV5Z	0.89	5.88	-0.28	-1.40	[-0.09]	[-0.21]	[+4.79]
CBS LIMIT	[+0.92]	[+6.17]	[-0.28]	[-1.36]	[-0.09]	[-0.21]	[+5.15]
Fit	$a+be^{-cX}$	$a + bX^3$	$a + bX^3$	$a + bX^3$	Additive	Additive	
Points (X)	3,4,5	4,5	4,5	4,5			
$\Delta E_e \text{ (final)} = \Delta E_e \text{ [CBS CCSDT(Q)]} + \Delta_{\text{core}} \text{ [CCSD(T)/aug-cc-pCVQZ]} + \Delta_{\text{rel}} \text{ [CCSD(T) MVD/aug-cc-pVTZ]} + \Delta_{\text{post}} \text{ [CCSDTQ(P)/cc-pVDZ]} = 5.15 + 0.26 - 0.08 + 0.12 = \mathbf{5.45 \text{ kcal mol}^{-1}}$							

Table 6.3. Valence focal point analyses of the heat of formation for path A (in kcal mol⁻¹). The symbol δ denotes the increment in the relative energy (ΔE_e) with respect to the preceding level of theory in the hierarchy RHF \rightarrow MP2 \rightarrow CCSD \rightarrow CCSD(T) \rightarrow CCSDT \rightarrow CCSDT(Q). Square brackets signify results obtained from basis set extrapolations or additive assumptions. Final predictions are boldfaced.

A. Si (³ P) + C ₂ (¹ Σ _g ⁺) \rightarrow SiC ₂ (T)							
Basis Set	ΔE_e [RHF]	δ [MP2]	δ [CCSD]	δ [CCSD(T)]	δ [CCSDT]	δ [CCSDT(Q)]	ΔE_e [CCSDT(Q)]
aug-cc-pVDZ	-170.22	30.06	0.07	5.96	-1.08	1.58	[-133.63]
aug-cc-pVTZ	-176.14	25.55	-2.53	6.45	-0.98	1.81	[-145.84]
aug-cc-pVQZ	-177.25	23.54	-3.10	6.51	[-0.98]	[1.81]	[-159.46]
aug-cc-pV5Z	-177.94	21.80	-2.20	6.54	[-0.98]	[1.81]	[-150.96]
CBS LIMIT	[-178.33]	[+19.96]	[-1.25]	[+6.58]	[-0.98]	[1.81]	[-152.21]
Fit	$a+be^{-cX}$	$a + bX^3$	$a + bX^3$	$a + bX^3$	Additive	Additive	
Points (X)	3,4,5	4,5	4,5	4,5			

$$\Delta E_0(\text{final}) = \Delta E_e[\text{CBS CCSDT(Q)}] + \Delta_{\text{core}}[\text{CCSD(T)/aug-cc-pCVQZ}] + \Delta_{\text{rel}}[\text{CCSD(T) MVD/aug-cc-pVTZ}]$$

$$+ \Delta_{\text{ZPVE}}[\text{VPT2/c-CBS CCSDT}] + \Delta_{\text{post}}[\text{CCSDTQ(P)/cc-pVDZ}] = -152.21 - 1.15 + 0.20 + 1.34 - 0.52 = \mathbf{-152.34 \text{ kcal mol}^{-1}}$$

$$\Delta H_{f,0}^\circ(\text{SiC}_2) = \Delta E_0 + \Delta H_{f,0}^\circ(^3P \text{ Si}) + \Delta H_{f,0}^\circ(^1\Sigma_g^+ \text{ C}_2) = -152.42 + 106.66 + 198.2 = \mathbf{152.5 \text{ kcal mol}^{-1}}$$

^a JANAF Thermochemical Tables, 3rd ed., J. Phys. Chem. Ref. Data **14**, Supp. No. 1 (1985).

Table 6.4. Valence focal point analyses of the heat of formation for path B (in kcal mol⁻¹). The symbol δ denotes the increment in the relative energy (ΔE_e) with respect to the preceding level of theory in the hierarchy RHF \rightarrow MP2 \rightarrow CCSD \rightarrow CCSD(T) \rightarrow CCSDT \rightarrow CCSDT(Q). Square brackets signify results obtained from basis set extrapolations or additive assumptions. Final predictions are boldfaced.

B. Si (³ P) + C ₂ (³ Π _u) \rightarrow SiC ₂ (T)							
Basis Set	ΔE_e [RHF]	δ [MP2]	δ [CCSD]	δ [CCSD(T)]	δ [CCSDT]	δ [CCSDT(Q)]	ΔE_e [CCSDT(Q)]
aug-cc-pVDZ	-114.59	-25.87	8.67	-2.88	0.66	-0.18	[-134.19]
aug-cc-pVTZ	-121.32	-32.18	7.93	-3.11	0.95	-0.27	[-148.00]
aug-cc-pVQZ	-122.52	-34.95	7.87	-3.25	[0.95]	[-0.27]	[-152.17]
aug-cc-pV5Z	-123.21	-37.02	8.99	-3.29	[0.95]	[-0.27]	[-153.84]
CBS LIMIT	[-123.59]	[-39.19]	[+10.17]	[-3.33]	[0.95]	[-0.27]	[-155.25]
Fit	$a+be^{-cX}$	$a + bX^3$	$a + bX^3$	$a + bX^3$	Additive	Additive	
Points (X)	3,4,5	4,5	4,5	4,5			

$$\Delta E_0(\text{final}) = \Delta E_e[\text{CBS CCSDT(Q)}] + \Delta_{\text{core}}[\text{CCSD(T)/aug-cc-pCVQZ}] + \Delta_{\text{rel}}[\text{CCSD(T) MVD/aug-cc-pVTZ}] + \Delta_{\text{ZPVE}}[\text{VPT2/c-CBS CCSDT}] + \Delta_{\text{post}}[\text{CCSDTQ(P)/cc-pVDZ}] = -155.25 - 1.24 + 0.22 + 1.66 + 0.17 = \mathbf{-154.44 \text{ kcal mol}^{-1}}$$

$$\Delta H_{f,0}^\circ(\text{SiC}_2) = \Delta E_0 + \Delta H_{f,0}^\circ(^3P \text{ Si}) + \Delta H_{f,0}^\circ(^3\Pi_u \text{ C}_2) = -154.44 + 106.66 + 200.2 = \mathbf{152.4 \text{ kcal mol}^{-1}}$$

$$\Delta H_{f,0}^\circ(^3P \text{ Si}) = 106.66 \text{ kcal mol}^{-1} \text{ }^a$$

$$\Delta H_{f,0}^\circ(^1\Sigma_g^+ \text{ C}_2) = 198.2 \text{ kcal mol}^{-1} \text{ }^a$$

$$\Delta H_{f,0}^\circ(^3\Pi_u \text{ C}_2) = 200.2 \text{ kcal mol}^{-1} \text{ }^a$$

^a JANAF Thermochemical Tables, 3rd ed., J. Phys. Chem. Ref. Data **14**, Supp. No. 1 (1985).

Table 6.5. Valence focal point analysis of the C₂ energy split (in kcal mol⁻¹). The symbol δ denotes the increment in the relative energy (ΔE_e) with respect to the preceding level of theory in the hierarchy RHF \rightarrow MP2 \rightarrow CCSD \rightarrow CCSD(T) \rightarrow CCSDT \rightarrow CCSDT(Q) \rightarrow CCSDTQ \rightarrow CCSDTQ(P) \rightarrow CCSDTQP. Square brackets signify results obtained from basis set extrapolations or additivity assumptions. Final predictions are boldfaced.

Basis Set	ΔE_e [RHF]	δ [MP2]	δ [CCSD]	δ [CCSD(T)]	δ [CCSDT]	δ [CCSDT(Q)]	δ [CCSDTQ]	δ [CCSDTQ(P)]	δ [CCSDTQP]	ΔE_e [CCSDTQP]
aug-cc-pVDZ	-55.63	55.92	-8.60	8.85	-1.74	1.77	-1.03	0.36	-0.16	[-0.26]
aug-cc-pVTZ	-54.83	57.73	-10.46	9.56	-1.94	2.07	-1.05	[+0.36]	[-0.16]	[+1.28]
aug-cc-pVQZ	-54.73	58.49	-10.96	9.76	[-1.94]	[2.07]	[-1.05]	[+0.36]	[-0.16]	[+1.84]
aug-cc-pV5Z	-54.73	58.81	-11.19	9.83	[-1.94]	[2.07]	[-1.05]	[+0.36]	[-0.16]	[+2.00]
CBS LIMIT	[-54.74]	[+59.15]	[-11.43]	[+9.90]	[-1.94]	[2.07]	[-1.05]	[+0.36]	[-0.16]	[+2.17]
Fit	$a+be^{-cX}$	$a + bX^{-3}$	$a + bX^{-3}$	$a + bX^{-3}$	Additive	Additive	Additive	Additive	Additive	
Points (X)	3,4,5	4,5	4,5	4,5						
ΔE_e (final) = ΔE_e [CBS CCSDTQP] + Δ_{core} [CCSD(T)/aug-cc-pCVQZ] + Δ_{rel} [CCSD(T) MVD/aug-cc-pVTZ] + Δ_{ZPVE} [VPT2/c-CBS CCSDT] = 2.17 + 0.09 - 0.02 - 0.31 = 1.93 kcal mol⁻¹ Experiment ¹ = 2.05 kcal mol ⁻¹										

¹ K.P. Huber and G. Herzberg, *Constants of Diatomic Molecules* (data prepared by J.W. Gallagher and R.D. Johnson, III) in NIST Chemistry WebBook, NIST Standard Reference Database Number 69, Eds. P.J. Linstrom and W.G. Mallard, National Institute of Standards and Technology, Gaithersburg MD, 20899.

Table 6.6. Complete quartic force fields of SiC₂. The units of force constants are consistent with energies in aJ, distances in Å, and angles in rad.

				Valence Internal Coordinates			Jacobi Internal Coordinates		
				$S_1 = r(\text{C-C})$ $S_2 = 2^{-1/2}[r_1(\text{Si-C}) + r_2(\text{Si-C})]$ $S_3 = 2^{-1/2}[r_1(\text{Si-C}) - r_2(\text{Si-C})]$			$S_1 = r(\text{C-C})$ $S_2 = R(\text{Si-C}_2)$ $S_3 = \rho(\text{Si-C}_2)$		
<i>i</i>	<i>j</i>	<i>k</i>	<i>l</i>	aug-cc-pVTZ CCSD(T) VPT2 ^a	<i>c</i> -CBS CCSDT VPT2 ^b	<i>c</i> -CBS CCSDT Surface ^b	aug-cc-pVTZ CCSD(T) VPT2 ^a	<i>c</i> -CBS CCSDT VPT2 ^b	<i>c</i> -CBS CCSDT Surface ^b
1	1			10.995	11.461	11.358	10.840	11.298	11.235
2	1			-0.6526	-0.6851	-0.6038	0.0258	0.0225	0.1380
2	2			2.7527	2.8672	2.8858	4.8492	5.0465	5.0771
3	3			0.1208	0.2675	0.2835	0.08711	0.18800	0.20080
1	1	1		-67.44	-70.07	-69.50	-66.86	-69.49	-69.30
2	1	1		0.715	0.697	0.231	1.465	1.506	0.583
2	2	1		0.991	1.105	0.666	-3.152	-3.223	-4.005
2	2	2		-9.293	-9.775	-9.788	-20.73	-21.76	-21.77
3	3	1		-1.491	-1.604	-1.962	-2.539	-2.512	-2.799
3	3	2		-8.963	-9.410	-9.550	-9.575	-9.852	-9.992
1	1	1	1	336.7	348.4	358.1	338.3	350.0	355.2
2	1	1	1	1.62	1.56	-3.57	-1.52	-1.64	-5.53
2	2	1	1	-2.22	-2.12	2.29	-5.39	-5.59	-2.36
2	2	2	1	-2.53	-3.03	-8.58	16.44	16.99	3.94
2	2	2	2	27.28	29.34	29.41	73.76	79.19	79.30
3	3	1	1	1.01	1.24	4.89	-6.56	-6.52	-5.11
3	3	2	1	0.47	1.01	-0.52	-5.04	-4.64	-6.01
3	3	2	2	28.15	30.11	30.50	37.99	39.79	40.25
3	3	3	3	76.13	71.12	74.09	50.67	46.72	48.39

Table 6.7. Harmonic and anharmonic frequencies of T-shaped SiC₂ (in cm⁻¹).

	$\omega_1 (a_1)$	$\omega_2 (a_1)$	$\omega_3 (b_2)$
aug-cc-pVTZ CCSD(T) VPT2 ^a	1751	798	137
<i>c</i> -CBS CCSDT VPT2	1788	814	204
<i>c</i> -CBS CCSDT PES	1783	817	210
Experiment ^b	1756.8(44)	844.0(16)	
	$\nu_1 (a_1)$	$\nu_2 (a_1)$	$\nu_3 (b_2)$
<i>c</i> -CBS CCSDT VPT2	1757	843	176
<i>c</i> -CBS CCSDT PES	1752	846	185
Experiment ^b	1746.0(28)	840.6(12)	196.37(4)

^a I. M. B. Nielsen, W. D. Allen, A. g. Császár, and H. F. Schaefer, J. Chem. Phys. **107**, 1195 (1997).

^b T. J. Butenhoff and E. A. Rohlfing, J. Chem. Phys. **95**, 1 (1991).

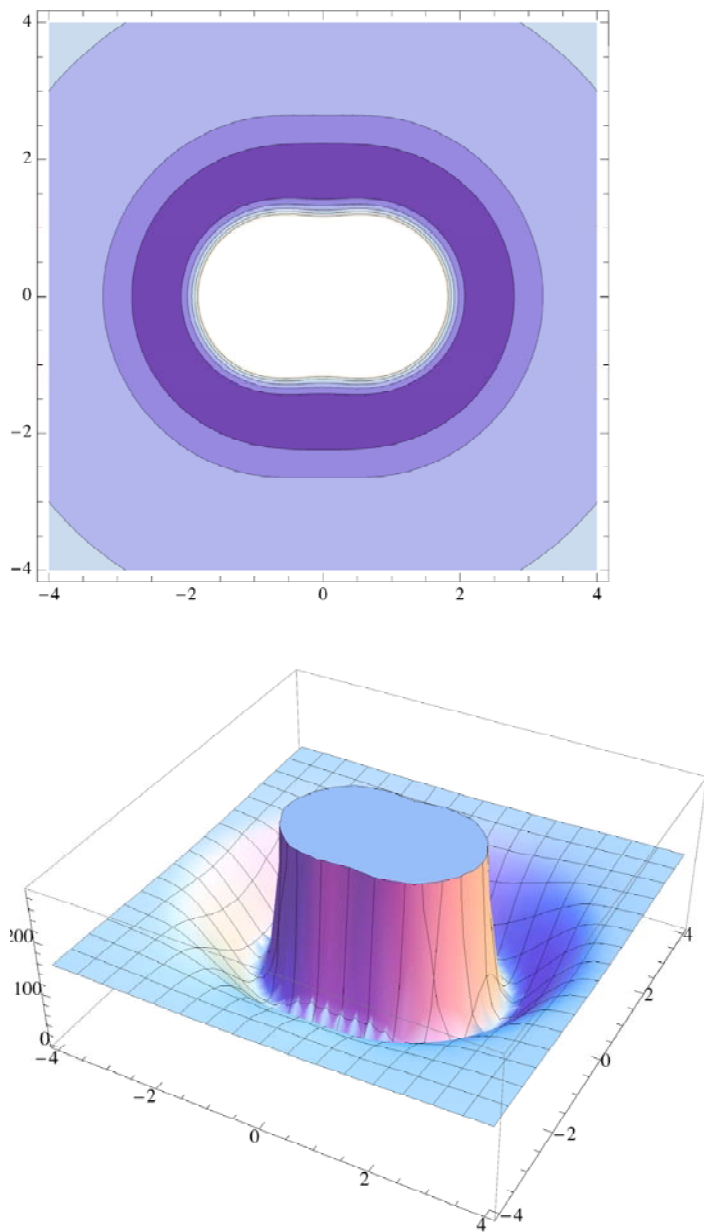


Figure 6.1. Two-dimensional and three-dimensional potential energy surfaces of SiC_2 (x,y coordinates in \AA , z axis in kcal mol^{-1}).

CHAPTER 7

CONCLUSIONS

Coupled Cluster (CC) theory stands as the most robust and widely applicable single-reference method for the treatment of electron correlation. Explicitly including dynamical electron correlation is the only means to reach chemical and sub-chemical accuracy. The question is usually asked, why use such an expensive calculation when DFT and other methods can approximate the answer? In most situations, energy barriers are larger than 50 kcal mol⁻¹, and errors of 3-5 kcal mol⁻¹ are acceptable. However, it is apparent that such large errors are unacceptable when working with barriers which are less than 5 kcal mol⁻¹. The focal point analysis of Allen provides a systematic tool to examine basis set and electron correlation convergence. While there is no way to systematically improve DFT, CC will eventually converge to the full configuration interaction limit.

By pushing *ab initio* limits, we have demonstrated the feasibility of computing accurate thermochemical parameters for several important molecules which have been problematic for less robust theoretical techniques. The discrepancy between experiment and theory for the barrier to rotation of benzaldehyde was successfully removed by examining the experimental interpretation of their spectra. Coupled Cluster theory was able to account for electron correlation in ways which an experimental model could not.

With adiabatic and zero-point vibration energy dissociation energies of 2.05 and 0.11 kcal mol⁻¹, respectively, gallium pentahydride may exist as a weak complex between gallane and molecular hydrogen at low temperatures. It is unequivocal that hydrogen scrambling does not

occur through a C_{2v} structure, since it lies 30 kcal mol⁻¹ higher in energy. Continued theoretical characterization of the deprotonation of BH₅ and AlH₅ illuminated a peculiarity; GaH₅ has a larger deprotonation value than AlH₅. Normally, the gap in observed properties falls between boron and aluminum, with gallium properties often very similar to those of aluminum.

The most powerful feature of CC is the ability to determine the quality of your investigation and design procedures to systematically improve your accuracy. Although expensive, the CCSDT(Q) level of the theory was necessary to reach quantitative agreement with experiment regarding the ozone radical cation triplet energy spacing and dissociation limits. Several possible excitations/ionization pathways were suggested to Prof. Merkt to facilitate the experimental synthesis of the quartet states of the ozone cation.

While quadruple excitations were necessary for ozone, the more sophisticated CCSDTQ(P) level of theory was essential for determining SiC₂'s barrier to linearity with sub-chemical accuracy. For over thirty years, computational chemists had not been able to agree with experiment on several key thermochemical properties of silicon dicarbide. The *c*-CBS CCSDT potential energy surface for SiC₂ exposed no shallow minimum. Ours is the first theoretical paper to agree with experimental bond lengths to within 0.01 Å, and to have a near perfect agreement with experiment for SiC₂'s barrier to linearity.

These four examples demonstrate the excellent performance of Coupled Cluster theory in computational chemistry, as an effective means to make definitive predictions of energetics, structures, and electronic properties of molecules, when chemical or sub-chemical accuracy is required.

APPENDIX A

SUPPLEMENTARY MATERIAL FOR CHAPTER 5

Table A.1. Dissociation energies (in eV) for the quartet and doublet states of the ozone radical cation.

		$X O_3^+ \rightarrow {}^3\Sigma_g^- O_2 + {}^4S O^+$								$X O_3^+ \rightarrow {}^2\Pi_g O_2 + {}^3P O$								
Basis	Method	4A_1		4A_2		4B_2		4B_1		4A_1		4A_2		4B_2		4B_1		
		D_e	D_0	D_e	D_0	D_e	D_0	D_e	D_0	D_e	D_0	D_e	D_0	D_e	D_0	D_e	D_0	
cc-pCVTZ	UCCSD	0.44	0.41	0.39	0.39	-0.06	-0.06	-2.66	-2.67	-0.89	-0.88	-0.93	-0.95	-1.39	-1.42	-3.99	-4.01	
cc-pCVQZ	UCCSD	0.51	0.48	0.48	0.48	0.01	0.02	-2.63	-2.63	-0.88	-0.87	-0.91	-0.93	-1.38	-1.41	-4.02	-4.04	
cc-pCV5Z	UCCSD	0.54	0.51	0.52	0.52	0.04	0.05	-2.60	-2.60	-0.86	-0.86	-0.89	-0.91	-1.37	-1.40	-4.01	-4.03	
cc-pCVTZ	UCCSD(T)	0.84	0.82	0.65	0.64	0.32	0.33	-2.11	-2.12	-0.60	-0.60	-0.79	-0.80	-1.12	-1.14	-3.55	-3.56	
cc-pCVQZ	UCCSD(T)	0.92	0.90	0.74	0.73	0.39	0.40	-2.07	-2.07	-0.58	-0.58	-0.76	-0.77	-1.10	-1.13	-3.56	-3.58	
cc-pCV5Z	UCCSD(T)	0.96	0.94	0.78	0.77	0.43	0.44	-2.04	-2.04	-0.56	-0.56	-0.73	-0.75	-1.09	-1.12	-3.55	-3.57	
Basis	Method	2A_1		2B_2		2B_1		2A_2		2A_1		2B_2		2B_1		2A_2		
		D_e	D_0	D_e	D_0	D_e	D_0	D_e	D_0	D_e	D_0	D_e	D_0	D_e	D_0	D_e	D_0	
cc-pCVTZ	UCCSD	0.83	0.74	0.55	0.51	0.32	0.30	0.36	0.35	-0.50	-0.43	-0.78	-0.76	-1.01	-1.01	-0.97	-0.98	
cc-pCVQZ	UCCSD	0.97	0.88	0.67	0.63	0.41	0.39	0.48	0.47	-0.42	-0.36	-0.71	-0.70	-0.97	-0.97	-0.91	-0.92	
cc-pCV5Z	UCCSD	1.01	0.93	0.72	0.68	0.47	0.45	0.53	0.52	-0.39	-0.33	-0.69	-0.67	-0.94	-0.94	-0.87	-0.89	
cc-pCVTZ	UCCSD(T)	1.82	1.75	1.58	1.55	0.93	0.91	0.82	0.81	0.38	0.33	0.15	0.14	-0.50	-0.50	-0.61	-0.62	
cc-pCVQZ	UCCSD(T)	1.96	1.88	1.71	1.68	1.04	1.02	0.95	0.93	0.46	0.41	0.21	0.21	-0.45	-0.46	-0.55	-0.56	
cc-pCV5Z	UCCSD(T)	2.01	1.93	1.76	1.73	1.10	1.08	1.00	0.99	0.49	0.44	0.25	0.24	-0.41	-0.42	-0.51	-0.52	
Experiment	2A_1		2A_1		2A_1		2A_1		2A_1		2A_1		2A_1		2A_1		2A_1	
	D_e	D_0	D_e	D_0	D_e	D_0	D_e	D_0	D_e	D_0	D_e	D_0	D_e	D_0	D_e	D_0	D_e	D_0
Reference 49			1.86															
Reference 46				1.85								0.60						
Reference 48				1.77 ^a									0.59					
Reference 47													0.61					

^a Reinterpreted by Reference 49.

Table A.2. Theoretical ionization potentials with respect to the 3A_2 state of O_3 (in eV).

		$^4X O_3^+ \leftarrow ^3A_2 O_3$											
Basis	Method	4A_1			4A_2			4B_2			4B_1		
		T_e	T_0	T_v	T_e	T_0	T_v	T_e	T_0	T_v	T_e	T_0	T_v
cc-pCVTZ	CASSCF	10.73		10.83	10.82		11.06	11.16		11.99	13.49		13.92
cc-pCVQZ	CASSCF	10.71		10.82	10.80		11.04	11.15		11.98	13.49		13.92
cc-pCV5Z	CASSCF	10.71		10.82	10.80		11.03	11.15		11.97	13.48		13.92
cc-pCVTZ	UCCSD	11.93	11.94	12.04	11.97	11.95	12.35	12.43	12.40	13.68	15.03	15.01	15.55
cc-pCVQZ	UCCSD	12.09	12.10	12.20	12.12	12.09	12.49	12.59	12.56	13.84	15.23	15.21	15.74
cc-pCV5Z	UCCSD	12.15	12.16	12.26	12.18	12.15	12.55	12.65	12.62	13.90	15.30	15.28	15.81
cc-pCVTZ	UCCSD(T)	12.10	12.09	12.21	12.29	12.27	12.61	12.62	12.59	13.70	15.05	15.03	15.55
cc-pCVQZ	UCCSD(T)	12.28	12.27	12.39	12.46	12.44	12.78	12.80	12.77	13.89	15.27	15.25	15.75
cc-pCV5Z	UCCSD(T)	12.35	12.34	12.46	12.53	12.51	12.85	12.88	12.85	13.96	15.34	15.32	15.83
		$^2X O_3^+ \leftarrow ^3A_2 O_3$											
Basis	Method	2A_1			2B_2			2B_1			2A_2		
		T_e	T_0	T_v	T_e	T_0	T_v	T_e	T_0	T_v	T_e	T_0	T_v
cc-pCVTZ	CASSCF	9.44		10.79	9.58		9.79	10.44		11.15	10.34		10.74
cc-pCVQZ	CASSCF	9.41		10.77	9.55		9.76	10.43		11.13	10.31		10.71
cc-pCV5Z	CASSCF	9.41		10.76	9.55		9.75	10.42		11.13	10.31		10.71
cc-pCVTZ	UCCSD	11.54	11.60	13.99	11.82	11.84	12.11	12.05	12.05	13.23	12.01	12.00	12.58
cc-pCVQZ	UCCSD	11.63	11.70	14.11	11.92	11.94	12.22	12.18	12.18	13.38	12.12	12.10	12.68
cc-pCV5Z	UCCSD	11.68	11.74	14.16	11.97	11.99	12.27	12.23	12.22	13.44	12.16	12.15	12.73
cc-pCVTZ	UCCSD(T)	11.12	11.17	13.00	11.35	11.36	11.54	12.01	12.00	12.67	12.12	12.10	12.60
cc-pCVQZ	UCCSD(T)	11.24	11.29	13.17	11.49	11.49	11.67	12.15	12.15	12.84	12.25	12.24	12.74
cc-pCV5Z	UCCSD(T)	11.30	11.35	13.23	11.54	11.55	11.73	12.21	12.20	12.91	12.30	12.29	12.79
Experiment ^a		11.34			11.48								

^a $T_0 [^2X (X = A_1, B_2) O_3^+ \leftarrow ^1A_1 O_3] - T_0 [^3A_2 O_3 \leftarrow ^1A_1 O_3]$ See Table 8

Table A.3. Theoretical ionization potentials with respect to 3B_2 state of O_3 (in eV).

		${}^4X O_3^+ \leftarrow {}^3B_2 O_3$											
Basis	Method	4A_1			4A_2			4B_2			4B_1		
		T_e	T_0	T_v	T_e	T_0	T_v	T_e	T_0	T_v	T_e	T_0	T_v
cc-pCVTZ	CASSCF	10.83		11.21	10.92		10.97	11.26		11.53	13.59		13.95
cc-pCVQZ	CASSCF	10.82		11.20	10.91		10.96	11.26		11.53	13.59		13.96
cc-pCV5Z	CASSCF	10.82		11.20	10.91		10.96	11.26		11.53	13.59		13.97
cc-pCVTZ	UCCSD	12.34	12.32	12.85	12.38	12.34	12.44	12.84	12.78	13.19	15.44	15.40	15.82
cc-pCVQZ	UCCSD	12.48	12.47	13.00	12.51	12.47	12.57	12.98	12.93	13.34	15.62	15.58	16.01
cc-pCV5Z	UCCSD	12.54	12.53	13.06	12.57	12.52	12.63	13.05	12.99	13.40	15.69	15.65	16.08
cc-pCVTZ	UCCSD(T)	12.13	12.10	12.59	12.32	12.28	12.37	12.65	12.60	12.96	15.08	15.04	15.46
cc-pCVQZ	UCCSD(T)	12.28	12.26	12.75	12.46	12.43	12.52	12.81	12.76	13.12	15.27	15.24	15.65
cc-pCV5Z	UCCSD(T)	12.35	12.33	12.82	12.53	12.49	12.58	12.88	12.83	13.19	15.34	15.31	15.73
		${}^2X O_3^+ \leftarrow {}^3B_2 O_3$											
Basis	Method	2A_1			2B_2			2B_1			2A_2		
		T_e	T_0	T_v	T_e	T_0	T_v	T_e	T_0	T_v	T_e	T_0	T_v
cc-pCVTZ	CASSCF	9.54		10.37	9.68		9.97	10.54		11.42	10.44		10.63
cc-pCVQZ	CASSCF	9.52		10.35	9.66		9.95	10.53		11.41	10.42		10.60
cc-pCV5Z	CASSCF	9.52		10.35	9.66		9.95	10.53		11.41	10.42		10.60
cc-pCVTZ	UCCSD	11.95	11.99	13.42	12.23	12.22	12.78	12.46	12.43	14.28	12.42	12.38	12.66
cc-pCVQZ	UCCSD	12.03	12.07	13.52	12.32	12.31	12.87	12.58	12.55	14.44	12.51	12.48	12.76
cc-pCV5Z	UCCSD	12.07	12.11	13.57	12.37	12.36	12.92	12.62	12.59	14.50	12.55	12.52	12.80
cc-pCVTZ	UCCSD(T)	11.15	11.18	12.17	11.38	11.37	11.68	12.03	12.01	12.81	12.14	12.12	12.32
cc-pCVQZ	UCCSD(T)	11.25	11.28	12.30	11.49	11.48	11.80	12.16	12.14	13.00	12.25	12.23	12.43
cc-pCV5Z	UCCSD(T)	11.30	11.33	12.36	11.54	11.53	11.85	12.21	12.18	13.07	12.30	12.28	12.49
Experiment ^a		11.23			11.37								

^a $T_0 [{}^2X (X = A_1, B_2) O_3^+ \leftarrow {}^1A_1 O_3] - T_0 [{}^3B_2 O_3 \leftarrow {}^1A_1 O_3]$ See Table 8

Table A.4. Theoretical ionization potentials with respect to the 3B_1 state of O_3 (in eV).

		$^4X O_3^+ \leftarrow ^3B_1 O_3$											
Basis	Method	4A_1			4A_2			4B_2			4B_1		
		T_e	T_0	T_v	T_e	T_0	T_v	T_e	T_0	T_v	T_e	T_0	T_v
cc-pCVTZ	CASSCF	10.42		11.67	10.51		10.63	10.85		10.85	13.18		14.08
cc-pCVQZ	CASSCF	10.41		11.67	10.50		10.62	10.84		10.85	13.18		14.10
cc-pCV5Z	CASSCF	10.41		11.66	10.49		10.61	10.84		10.84	13.17		14.10
cc-pCVTZ	UCCSD	11.65	11.64	13.73	11.69	11.65	11.94	12.15	12.10	12.19	14.75	14.71	16.30
cc-pCVQZ	UCCSD	11.81	11.81	13.93	11.84	11.81	12.09	12.31	12.27	12.36	14.95	14.92	16.53
cc-pCV5Z	UCCSD	11.87	11.87	14.00	11.90	11.86	12.15	12.38	12.33	12.42	15.02	14.99	16.61
cc-pCVTZ	UCCSD(T)	11.83	11.82	13.64	12.02	12.00	12.21	12.35	12.31	12.38	14.79	14.76	16.06
cc-pCVQZ	UCCSD(T)	12.02	12.00	13.86	12.19	12.17	12.39	12.54	12.50	12.57	15.00	14.97	16.30
cc-pCV5Z	UCCSD(T)	12.09	12.07	13.93	12.26	12.24	12.46	12.61	12.57	12.65	15.08	15.05	16.38
		$^2X O_3^+ \leftarrow ^3B_1 O_3$											
Basis	Method	2A_1			2B_2			2B_1			2A_2		
		T_e	T_0	T_v	T_e	T_0	T_v	T_e	T_0	T_v	T_e	T_0	T_v
cc-pCVTZ	CASSCF	9.13		9.43	9.27		9.90	10.13		11.04	10.03		10.32
cc-pCVQZ	CASSCF	9.10		9.40	9.25		9.88	10.12		11.02	10.00		10.29
cc-pCV5Z	CASSCF	9.10		9.40	9.24		9.87	10.11		11.02	10.00		10.28
cc-pCVTZ	UCCSD	11.25	11.31	11.61	11.53	11.54	12.62	11.77	11.75	13.35	11.73	11.70	12.21
cc-pCVQZ	UCCSD	11.36	11.41	11.71	11.65	11.65	12.75	11.91	11.90	13.49	11.84	11.81	12.33
cc-pCV5Z	UCCSD	11.40	11.46	11.76	11.70	11.70	12.80	11.95	11.94	13.55	11.89	11.86	12.37
cc-pCVTZ	UCCSD(T)	10.85	10.89	11.07	11.09	11.08	11.94	11.74	11.75	12.72	11.85	11.83	12.25
cc-pCVQZ	UCCSD(T)	10.98	11.02	11.20	11.22	11.22	12.09	11.89	11.78	12.88	11.99	11.97	12.40
cc-pCV5Z	UCCSD(T)	11.04	11.07	11.26	11.28	11.28	12.15	11.94	11.81	12.95	12.04	12.02	12.45
Experiment ^a		11.07			11.21								

^a $T_0 [^2X (X = A_1, B_2) O_3^+ \leftarrow ^1A_1 O_3] - T_0 [^3B_1 O_3 \leftarrow ^1A_1 O_3]$ See Table 8

Table A.5. Theoretical ionization potentials with respect to the 2A_1 and 2B_2 states of O_3^+ (in eV).

		${}^4X O_3^+ \leftarrow {}^2A_1 O_3^+$											
Basis	Method	4A_1			4A_2			4B_2			4B_1		
		T_e	T_0	T_v	T_e	T_0	T_v	T_e	T_0	T_v	T_e	T_0	T_v
cc-pCVTZ	CASSCF	1.29		3.87	1.38		1.94	1.72		2.14	4.05		6.38
cc-pCVQZ	CASSCF	1.31		3.90	1.39		1.96	1.74		2.16	4.08		6.43
cc-pCV5Z	CASSCF	1.30		3.90	1.39		1.96	1.74		2.16	4.07		6.43
cc-pCVTZ	UCCSD	0.39	0.34	4.06	0.44	0.35	1.32	0.89	0.80	1.54	3.49	3.41	6.70
cc-pCVQZ	UCCSD	0.46	0.40	4.17	0.49	0.40	1.38	0.96	0.86	1.61	3.59	3.51	6.83
cc-pCV5Z	UCCSD	0.47	0.41	4.19	0.50	0.41	1.40	0.97	0.88	1.62	3.62	3.53	6.86
cc-pCVTZ	UCCSD(T)	0.98	0.93	3.97	1.17	1.11	1.78	1.50	1.42	1.94	3.93	3.87	6.45
cc-pCVQZ	UCCSD(T)	1.04	0.98	4.08	1.22	1.15	1.84	1.56	1.48	2.01	4.02	3.96	6.59
cc-pCV5Z	UCCSD(T)	1.05	1.00	4.10	1.23	1.16	1.85	1.58	1.50	2.03	4.04	3.98	6.61
		${}^4X O_3^+ \leftarrow {}^2B_2 O_3^+$											
Basis	Method	4A_1			4B_2			4B_1			4A_2		
		T_e	T_0	T_v	T_e	T_0	T_v	T_e	T_0	T_v	T_e	T_0	T_v
cc-pCVTZ	CASSCF	1.15		1.66	1.58		2.40	3.91		5.10	1.24		1.49
cc-pCVQZ	CASSCF	1.16		1.68	1.60		2.42	3.93		5.13	1.25		1.50
cc-pCV5Z	CASSCF	1.16		1.68	1.60		2.42	3.93		5.13	1.25		1.50
cc-pCVTZ	UCCSD	0.11	0.10	0.82	0.61	0.56	1.76	3.21	3.18	4.66	0.16	0.12	0.58
cc-pCVQZ	UCCSD	0.16	0.16	0.88	0.67	0.62	1.81	3.30	3.27	4.75	0.19	0.15	0.61
cc-pCV5Z	UCCSD	0.18	0.17	0.89	0.68	0.63	1.83	3.32	3.28	4.76	0.20	0.16	0.62
cc-pCVTZ	UCCSD(T)	0.75	0.73	1.29	1.26	1.23	2.16	3.70	3.67	4.84	0.93	0.91	1.21
cc-pCVQZ	UCCSD(T)	0.79	0.78	1.34	1.32	1.28	2.22	3.78	3.76	4.93	0.97	0.95	1.25
cc-pCV5Z	UCCSD(T)	0.80	0.79	1.36	1.33	1.30	2.23	3.80	3.77	4.95	0.98	0.96	1.26

Table A.6. Theoretical ionization potentials with respect to the 1A_1 state of O_3 (in eV).

Basis	Method	$^4X O_3^+ \leftarrow ^1A_1 O_3$ (eV)											
		4A_1			4A_2			4B_2			4B_1		
		T_e	T_0	T_v	T_e	T_0	T_v	T_e	T_0	T_v	T_e	T_0	T_v
cc-pCVTZ	CASSCF	12.16		13.29	12.25		12.37	12.58		12.85	14.92		16.28
cc-pCVQZ	CASSCF	12.17		13.32	12.26		12.39	12.61		12.87	14.94		16.33
cc-pCV5Z	CASSCF	12.18		13.33	12.26		12.39	12.61		12.88	14.95		16.34
cc-pCVTZ	UCCSD	13.01	12.94	14.52	13.06	12.96	13.25	13.51	13.40	13.84	16.11	16.02	17.78
cc-pCVQZ	UCCSD	13.22	13.14	14.74	13.24	13.14	13.44	13.72	13.61	14.04	16.35	16.25	18.04
cc-pCV5Z	UCCSD	13.29	13.22	14.82	13.31	13.21	13.51	13.79	13.68	14.12	16.43	16.34	18.12
cc-pCVTZ	UCCSD(T)	13.32	13.25	14.58	13.51	13.43	13.62	13.84	13.75	14.09	16.27	16.19	17.64
cc-pCVQZ	UCCSD(T)	13.53	13.46	14.82	13.71	13.63	13.83	14.06	13.96	14.31	16.52	16.44	17.91
cc-pCV5Z	UCCSD(T)	13.61	13.54	14.90	13.79	13.71	13.91	14.14	14.05	14.39	16.60	16.53	18.00
	MRCI ^a			14.35			13.43			13.93			17.42

^a Reference 39.